Doppler Compensation Algorithms for DSP-based Implementation of OFDM Underwater Acoustic Communication Systems

Ammar Abdelkareem

Newcastle University

School of Electrical, Electronic, and Computer Engineering,

Newcastle upon Tyne, UK.

A thesis submitted for the degree of

Doctor of Philosophy

2012

To my loving parents and my wife

Science is organised knowledge. Wisdom is organised life.

-Immanuel Kant

Acknowledgements

Throughout my PhD research in this University, I was fortunate to have the opportunity to work with such a high quality supervision team. This team included Prof. Bayan Sharif who introduced me to working on an embedded system implementation for Doppler compensation algorithms. I would like to express my sincere gratitude and appreciation for his valuable comments, guidance and suggestions.

I wish to direct my special gratitude to Dr. Charalampos Tsimenidis for suggestions that contributed to the development of a research project of high quality and for his help during the PhD research journey. Thanks are also due to my third supervisor, Mr. Jeffrey Neasham.

I am grateful to my friends for their support and companionship. Additionally, I wish to express my thanks to Iterative Solutions Inc. for their CML toolbox.

I greatly appreciate the assistance provided in the form of a scholarship from the Iraqi Governments Ministry of Higher Education and Scientific Research. Without their funding and support, it would have been impossible to commence and successfully complete this research work.

Special thanks to my wife and my children, Yasir, Ali and Rahaf, for their support and patience during my study.

Finally, I would like to express my deep gratitude to my parents who have supported me throughout my education. Praise God, for all things that have happened to me in my life.

Declaration

I declare that this thesis is my own work and it has not been previously submitted, either by me or by anyone else, for a degree or diploma at any educational institute, school or university. To the best of my knowledge, this thesis does not contain any previously published work, except where another person's work used has been cited and included in the list of references.

Abstract

In recent years, orthogonal frequency division multiplexing (OFDM) has gained considerable attention in the development of underwater communication (UWC) systems for civilian and military applications. However, the wideband nature of the communication links necessitate robust algorithms to combat the consequences of severe channel conditions such as frequency selectivity, ambient noise, severe multipath and Doppler Effect due to velocity change between the transmitter and receiver. This velocity perturbation comprises two scenarios; the first induces constant time scale expansion/compression or zero acceleration during the transmitted packet time, and the second is time varying Doppler-shift. The latter is an increasingly important area in autonomous underwater vehicle (AUV) applications. The aim of this thesis is to design a low complexity OFDM-based receiver structure for underwater communication that tackles the inherent Doppler effect and is applicable for developing real-time systems on a digital signal processor (DSP). The proposed structure presents a paradigm in modem design from previous generations of single carrier receivers employing computationally expensive equalizers. The thesis demonstrates the issues related to designing a practical OFDM system, such as channel coding and peak-to-average power ratio (PAPR). In channel coding, the proposed algorithms employ convolutional bit-interleaved coded modulation with iterative decoding (BICM-ID) to obtain a higher degree of protection against power fading caused by the channel. A novel receiver structure that combines an adaptive Doppler-shift correction and BICM-ID for multi-carrier systems is presented. In addition, the selective mapping (SLM) technique has been utilized for PAPR. Due to their time varying and frequency selective channel nature, the proposed systems are investigated via both laboratory simulations and experiments conducted in the North Sea off

the UK's North East coast. The results of the study show that the proposed systems outperform block-based Doppler-shift compensation and are capable of tracking the Doppler-shift at acceleration up to 1m $/s^2$.

Contents

List of Figures

List of Tables

Nomenclature

Acronyms

ACS Add Compare Select

ADC Analogue to Digital Converter

AET Automatic Early Termination

APP A Posteriori Probabilities

AUV Autonomous Underwater Vehicle

$AWGN$ Additive White Gaussian Noise

$BBER$ Block Bit Error Rate

$BCJR$ Bahl Cocke Jelinek Raviv

BER Bit Error Rate

$BICM$ Bit Interleaved Coded Modulation

$BICM - ID$ BICM with Iterative Decoding

CC Convolutional Code

$CDMA$ Code Division Multiple Access

CE Channel Estimation

CFO Carrier Frequency Offset

CIR Channel Impulse Response

$COFDM$ Coded Orthogonal Frequency Division Multiplexing

CP Cyclic Prefix

CRC Cyclic Redundancy Check

CSI Channel State Information

DAC Digital to Analogue Converter

$DDWS$ Direct Digital Wave Synthesis

DEU Doppler Extraction Unit

DFE Decision Feedback Equalizer

DM Data Memory

$DPSK$ Differential Phase Shift Keying

DSP Digital Signal Processing

ECC Error Correction Coding

ER Expectation Range

FEC Forward Error Correction

FFT Fast Fourier Transform

FIR Finite Impulse Response

$FPGA$ Field Programmable Gate Array

FSK Frequency Shift Keying

$HTLS$ Hankel Total Least Square

ICI Intercarrier Interference

ISI Intersymbol Interference

LFM Linear Frequency Modulated

LLR Log Likelihood Ratio

LM Learning Mode

LMS Least Mean Square

LOS Line of Sight

LP Learning and Punishment

MAP Maximum a Posteriori

$MIMO$ Multiple Input Multiple Output

MLE Maximum Likelihood Estimator

$MLSE$ Maximum Likelihood Sequence Estimation

$MMLE$ Marginal Maximum Likelihood Estimation

$MMSE$ Minimum Mean Square Error

MSE Mean Square Error

NSC Non Systematic Code

$OFDM$ Orthogonal Frequency Division Multiplexing

$PAPR$ Peak to Average Power Ratio

PDP Power Delay Profile

PLL Phase Lock Loop

PM Punishment Mode

PSF Pulse Shaping Filter

QAM Quadrature Amplitude Modulation

$QPSK$ Quadrature Phase Shift Keying

RF Radio Frequency

RLS Recursive Least Square

$SICM$ Symbol Interleaved Coded Modulation

$SISO$ Soft-in Soft-out

SNR Signal to Noise Ratio

$SOVA$ Soft Output Viterbi Algorithm

SPI Serial Port Interface

$SRAM$ Static Random Access Memory

TCB Transfer Control Block

TCM Trellis Coded Modulation

TI Texas Instruments

TL Transmission Loss

UAC Underwater Acoustic Channel

UWC Underwater Communication

$VHDL$ Very high speed Hardware Description Language

WSS Wide Sense Stationary

ZFE Zero Forcing Equalizer

ZP Zero Padding

List of Symbols

$a(f)$	attenuation loss
a	Acceleration in m/s^2
a(t)	Time-varying acceleration in m/s^2
α'	The forward-state metric
B	Signal bandwidth in kHz
B_{coh}	Coherence bandwidth in Hz
b_i	Information bits
β	Roll-off factor
β'	The reverse-state metric
c	Propagation speed of acoustic signals
c_k	group of interleaved bits
$\mathbb{C}$	Set of complex numbers
Δ	Doppler shift
ϵ'_Δ	Doppler shift estimation error
$\Delta(t)$	Time varying Doppler shift
$\hat{\Delta}$	Doppler shift estimate
Υ	The anticipated observation window
$\hat{\epsilon}$	Residual Doppler shift estimate
δf	Sub-carrier bandwidth
f_c	Carrier frequency
f_n	Sub-carrier frequency
f_s	Sampling frequency
F_d	Doppler frequency shift
ϕ	Shift in OFDM samples
$\hat{\phi}$	Estimate shift in OFDM samples
$\hat{\phi}_p$	Previous estimation of fine symbol timing offset

$\hat{\phi}_c$	Current estimation of fine symbol timing offset
$\hat{\phi}_s$	Sampling frequency offset estimate at the leading edge
$\hat{\phi}_e$	Sampling frequency offset estimate at the trailing edge
ϕ_{step}	The tracking step
$\hat{\phi}_l$	The centroid-based 1st order moment estimate
$\hat{\phi}_x$	Correlation-based 1st order moment estimate over Υ
$\hat{\phi}_{yy}$	Correlation-based 1st order moment estimate over full CP samples
$\bar{\phi}_a$	Average shift in samples between $\hat{\phi}_c$ and $\hat{\phi}_p$
$\hat{\phi}_{CP}$	Expected control range (in samples) for positive a
$\hat{\phi}_{NP}$	Expected control range (in samples) for negative a
ϕ'	Fine tuned 1st order moment of the correlation lag
Γ_{th}	Threshold for the correlation peaks
γ	The branch metric
h_l	Path amplitude
$\hat{H}_p$	Estimated channel at pilot symbols
$\hat{\boldsymbol{H}}_{LS}[n]$	Least square channel estimate at each sub-carrier
K	Constraint length
K_d	Length of information bits
K_c	Length of coded bits
κ	Sampling frequency offset of one sample drift
L	Total number of paths
L_{int}	Interleaver length
L_a	A priori LLRs
L_e	Extrinsic LLRs
L_f	The transmitted passband samples' length
L'_f	The Doppler shifted received passband samples' length
$\Lambda(m,i)$	Timing function at window range m and i
M	Constellation size
m'	Slop of a linear equation
$\mu_{\mathbf{i}}$	Vector of maximum peak positions
N_c	Number of sub-carriers
N_d	Data bearing sub-carriers
N_p	Pilot sub-carriers

N_g	Guard samples
N_S	Number of samples per symbol
$\mathcal{N}$	Group of OFDM symbols
p_{rc}	Pulse shaping filter
$\hat{P}$	Position estimate of the maximum Doppler shift
Π	Interleaver
Π^{-1}	De-Interleave
$\hat{\Psi}$	Relative sampling frequency offset estimate
$\hat{\Psi}_{(\mathrm{I})}$	Integer relative sampling frequency offset estimate
$\hat{\Psi}_{(\mathrm{F})}$	Fractional relative sampling frequency offset estimate
R_c	Code rate
$\tilde{r}(t)$	Received signal in passband
ρ	Correlation vector
σ_w^2	Noise variance
T_s	Sampling time
T_{coh}	Coherence Time
T_g	Guard time
$\tau_l(t)$	Time varying path delay
τ_{max}	Maximum delay spread
$\mathbf{U}$	Sequence of phases for PAPR
$\mathbf{U}^{opt}$	Optimal sequence of PAPR phase
W	Weighting coefficients vector
$X(n)$	Transmitted frequency domain OFDM
$Y_i[n]$	Received frequency domain OFDM at index i
Y_p	The received pilot symbols after the FFT
ζ	Frame synchronization point
ζ'	Fine tuned synchronization point

Chapter 1

Introduction

Since 1919, when the first scientific paper on underwater sound was published by German scientists who presented a theoretical description of the bending of sound rays and their importance in determining sound ranges [2], remarkable interest has been shown in the exploitation of acoustic waves for both military and commercial purposes. In military applications for instance, they are employed extensively by submarines and for navigation; while as far as commercial applications are concerned, acoustic waves are utilised in offshore oil exploration, monitoring underwater pipelines, fish finding and as an aid to divers. The emergence of digital signal processors has made possible the development of complex methods of signal processing for underwater communication (UWC) systems applications. In recent years, researchers and engineers have devoted great efforts towards achieving high data rates and reliable wireless communication systems for data, video and voice without incurring any loss of information. However, wireless UWC systems have to overcome many physical obstacles such as temperature and pressure variations, salinity, ambient noise, multipath and the Doppler effect. The Doppler effect is caused by current and wave motions and is due to the relative motion between the transmitter/receiver. In order to attain reliable communication in such severe circumstances, as far as the underwater acoustic channel is concerned, it is necessary to take into account these obstacles. The characteristics of the underwater acoustic channel and the most notable accomplishments in underwater communication in recent years are presented in the following sections. In this thesis, practical Doppler shift compensation techniques for OFDM-based receivers are adopted. In addition, BICM-ID is employed to protect the data against the channel effects and it is considered as an

application for ADSP-21364 SHARC DSP.

1.1 Underwater Channel Characteristics

Although the interference and crosstalk properties from other users are stationary in a wired communications system, it fails to achieve mobility and flexibility in terms of maintenance, particularly in deep water; therefore, wireless communication is a more practical alternative. Underwater acoustic communications are preferred on radio frequency (RF) communications because electromagnetic waves do not propagate over long distances underwater, except at high power. This is a direct constraint which makes acoustic waveforms the best solution for transmitting data undersea. However, these waveforms present challenges as far as achieving reliable communication is concerned due to their special properties such as low propagation speed.

Dealing with underwater acoustic channels is a daunting challenge, but one which should be considered in order to achieve more reliable wireless communications. These channels are time-varying in nature and delay dispersive to the order of 100 symbol time. Furthermore, due to the low propagation speed of acoustic signals (c) of approximately 1500 m/s, the transmitted signal is more vulnerable to the Doppler effect when compared to other communication systems. Therefore, even a slow movement between the transmitter/receiver and/or the inherent current wave's motion can stretch or press the transmitted signal, depending on the direction of motion, and consequently destroy the synchronization. Many receiver structures have been proposed to deal with the time varying multipath that causes inter-symbol interference (ISI). All of them adopt channel estimation and equalization schemes, coding algorithms and spread spectrum systems. These receivers are based on a time-domain view of the channel and they require a highly complex structure. Recently, an alternative multi-carrier communication system in the form of OFDM has gained considerable interest for communication over frequency-selective channels, where the symbol duration is made much larger than the delay spread. Furthermore, the OFDM is also attractive due to its simplicity in terms of modulation/demodulation by means of fast Fourier transform (FFT). However, the relative Doppler shift in the channel, due to the transmitter/receiver motion (v) with the acoustic signal propagation and the sensitivity of the OFDM to the Doppler effect,

means that delicate synchronization algorithms are required.

The available bandwidth in UAC is restricted by the transmission loss and signal-to-noise ratio (SNR). The transmission loss is proportional to the range and SNR is limited by the noise level caused by the ambient such as the sound of ships' engines, bubbles and acceleration thrust. Thus, for the desired transmission range, this frequency susceptibility to transmission loss ultimately adds a constraint on the choice of the carrier frequency [3]. Consequently, underwater acoustic communication links can be divided into three types according to their range. Firstly, a long-range system, operating over several tens of kilometres, is limited to a few kHz of bandwidth. Secondly, a medium-range system, operating over several kilometres, has a bandwidth of the order of ten kHz. Thirdly, a short- range system, operating over several tens of metres, may have available bandwidths of more than a hundred kHz [3]. Additionally, multipath propagation is prevalent in UAC channels. These channels' characteristics vary with time [4] and hence they are also called *doubly selective channels*, as the transmitted signal undergoes dispersion in both the time and frequency domains. Furthermore, the multipath arrivals are highly dependent on the location of the transmitter and receiver in the given geometry and density of the medium. While the vertical channels exhibit little multipath, the horizontal channels may have extremely long multipath spreads. Establishing reliable communication and combating the underwater multipath is considered, without exception, to be a daunting task for any underwater acoustic communication system.

Two main problems are encountered when considering the underwater channel. The first one is multipath propagation due to reflection from the surface and the seabed; the second one is the Doppler effect [5], arising due to relative motion between the transmitter and receiver. In multipath propagation, each transmitted signal is received via multiple paths and delays and is accompanied by random fluctuations in phase and amplitudes. The multipath structure depends on the channel geometry. For instance, the multipath spread in a vertical channel is very small compared with its counterpart in a horizontal channel which attains a hundred times the multipath spreads experienced in radio channels. For example, a multipath spread of 10 ms in a shallow water channel causes the ISI to extend over 100 symbols, if the system is operating at a rate of 10 kilo-symbols per second (ksps) [6]. In single carrier transmission, the multipath effects are dealt with by adopting equalizers at the receiver, which has the effect of adding a burden to the complexity. An

alternative, with a lower degree of complexity, is the multi-carrier transmission in the form of OFDM. However, it is very sensitive to the Doppler shift [7] caused either by the sampling rate mismatch between the transmitter/receiver pair or their motion.

The time-varying multipath exhibits random fluctuations resulting in a spectral broadening of the received signal, known as Doppler spreading. Due to the motion of the transmitter-receiver pair relative to each other, in addition to the motion of waves, the Doppler spread is increased by an additional frequency shift in the signal. The Doppler effect due to motion on any given frequency can be modelled as [8]

$$f_c' = f_c\,(1 \pm \Delta)\,, \tag{1.1}$$

where f_c is the transmitted carrier frequency, Δ is the Doppler shift defined as a ratio of $\frac{v}{c}$ and f_c' is the received frequency. The (+) sign indicates an expansion situation where the distance between the transmitter-receiver pair increases, resulting in decreasing frequency and vice versa. For narrow-band signals, i.e. ($fc >> B$) [8], Doppler shift translates all OFDM sub-carriers by the same amount of carrier frequency and (1.1) is often used as an approximation; whereas in the case of wide-band signals ($\frac{B}{f_c} \sim 1$), each sub-carrier is shifted non-uniformly [7]. In such a case, the Doppler effect is modelled as a complete time scaling (expansion or compression) of the signal waveform [8]

$$r'(t) = x((1 \mp \Delta)t). \tag{1.2}$$

where $x(t)$ and $r'(t)$ are the source and Doppler shifted received signals, respectively. Here, (-) sign indicates decreasing distance between the transmitter and receiver, resulting in compression of the signal and vice versa. In this case, symbol synchronization is of equal importance to carrier synchronization. Furthermore, due to severe multipath distortion and fading, conventional synchronization techniques in single carrier transmission, such as phase-locked loop (PLL) [9], when coupled with equalization, are very unreliable in underwater acoustic communications [10]. In addition, receivers adopting PLL and equalizer are considered to be highly complex. The alternative OFDM-based receivers are less complex. If the normalized Doppler spread, defined as the ratio of the Doppler shift to sub-carrier spacing δf, is large, which is a typical scenario for most of the underwater channels [6], special care should be taken as far as the residual frequency offset is concerned, which

should be $<< \delta f$ [7] in order to mitigate inter-carrier interference (ICI), reserve the orthogonality and achieve reliable communication systems. To demonstrate how severe the Doppler effect can be in an underwater channel, an example comparing both a highly mobile radio system and an underwater communication system may be considered. Suppose a vehicle in the RF communication moving at a speed of 250 km/h, where c is 3×10^8 m/s, resulting in $\Delta = 2.3 \times 10^{-7}$; as opposed to this situation, consider a stationary acoustic system which may experience an unintentional motion of 0.5 m/s which is equivalent to 1 knot, resulting in $\Delta = 3.0 \times 10^{-4}$. Rapidly moving platforms, such as AUV, present a more serious problem where the factor Δ will be in the order of 10^{-3} [8]. Moreover, an acceleration in the order of (0.25 m $/s^2$) during the symbol time has a significant influence on how rapidly the channel changes with time. Therefore, it is evident that the effect of time expansion-dilation cannot be ignored in underwater communication. As the time varying multipath, combined with non-negligible Doppler effect, severely distorts the signal transmission, sophisticated signal processing algorithms are required to establish error free communication.

1.2 Advances in Doppler shift compensation for UWC systems

Several time-domain receivers which adopt coherent modulation with an emphasis on channel equalization to increase communication reliability have been suggested. However, the time-varying doubly-spread characteristic of the UAC requires a highly complex equalizer. An alternative low-complexity, high-speed communication scheme is the multi-carrier system in the form of OFDM in which fast Fourier transform (FFT) is used for modulation. This system resists the frequency selectivity of the channel by dividing the broadband data into parallel narrowband channels. Also, in a delay-dispersive environment, adopting CP of a length greater than the maximum delay spread provides an excellent way to assure the orthogonality of the carriers. However, the wireless propagation is considered time-varying, and thus time-selective due to the Doppler shift in which one sub-carrier may pose ICI with the adjacent sub-carriers. The Doppler shift sensitivity is inversely proportional to the OFDM symbol duration; therefore, slightly moving platforms can cause serious

synchronization impairments in long sub-carriers.

Previous studies on UWC have addressed several approaches for synchronization in the presence of Doppler distortion. For single carrier transmission, a block-based approach [8] has been used to estimate and compensate the Doppler shift. In this approach, two LFMs are used for coarse estimation of the time scaling factor and then an equalizer is used for residual Doppler shift compensation. Such an approach is well suited for constant speed. An alternative adaptive Doppler compensation technique has been suggested by [11] to accommodate AUV. This closed-loop Doppler correction necessitates high complexity when it is applied to OFDM systems because there is a demodulation requirement. For multi-carrier transmission, the authors in [12] utilized the principle in [8] and null sub-carriers for re-sampling factor estimation and residual Doppler compensation, respectively. Although these algorithms attain precise estimation by adopting preamble and post-amble, the bandwidth utilization factor is compromised.

A point estimate of the Doppler shift is adopted in [13], therefore it is suitable for situations where the Doppler shift stays constant or varies slowly during the packet time. The concept in [14] has been extended to work in UAC by [1], with an iterative cyclic prefix correlation. The author employs the symmetry of the guard interval with its replica in order to estimate the Doppler shift. This parameter is estimated iteratively depending on the peak location and its phase with respect to the new sampling interval and, for this reason, it is a computationally expensive search. Authors in [15] have examined iterative Doppler estimation, channel estimation and decoding.

The carrier frequency offset (CFO) is estimated using null sub-carriers as in [12]. Although re-sampling the signal removes the Doppler shift, a major problem with its residual is destruction of the orthogonality of the sub-carriers due to the resulting ICI. A considerable amount of literature has been published on the subject of combating ICI. These studies [16], [17] have presented the conclusion that successful communication will result in mitigating ICI.

A number of previous studies have based their criteria for Doppler shift and CFO estimation on utilizing signal space and statistics. For instance, the authors in [18] have used maximal likelihood estimation (MLE) and estimation of signal parameter via rotational invariance technique (ESPRIT) to estimate both CFO and Doppler shift in wideband OFDM, while in [19], HTLS *(Hankel)* Total Least Square has been

used for joint channel and Doppler estimation. The system requires no estimation of the CFO and there is no need to re-sample the signal. An extension to [13] has been suggested by [20] for symbol by symbol Doppler estimation. This method adopts marginal maximum likelihood estimation (MMLE) to track the Doppler variation between symbols. Despite its precise estimation, MLE has a number of associated problems in terms of hardware implementation, where it necessitates a high degree of complexity.

All the aforementioned researches assume the Doppler shift is constant during the symbol period and all paths have equal Doppler shift; hence re-sampling the signal with a unique time scaling factor is valid and therefore a symbol by symbol approach works satisfactorily. A recent study by [21] has highlighted the need to estimate the optimal time scaling factor in a multipath channel of different Doppler shift in each path. However, in our proposed method, it is assumed that the channel variation is mainly caused by the motion of both transmitter and receiver, leading to a significant time varying Doppler shift. This will consequently create acceleration that may exceed 1 m/s^2 due to speed alterations, and therefore ignoring this effect yields a significant ICI.

1.3 Contributions

This dissertation presents the algorithms that design low-complexity, high data rate OFDM-based receiver structures for underwater acoustic communication that compensate the inherent Doppler shift and are applicable in the development of real-time systems. Previous single-carrier receivers [22],[6], and [10] adopted beamforming to attain an acceptable performance; however, these receivers are considered costly.

Furthermore, this thesis provides remedies for a significant problem in the underwater acoustic channel (UAC) which is called time-varying Doppler shift. This problem is caused due to the acceleration that accompanies the applications of the autonomous vehicles. It should be stressed that this problem has not been discussed yet by other researchers, where most of the studies assume the speed is constant i.e., the acceleration is zero. However, we assume the acceleration is time-varying up to ± 1 m/s^2 during 5.5 seconds.

This thesis intends to determine the extent to which the multi-carriers modulation in the form of an OFDM and whether it can combat the channel impairments

with less complexity than single carrier receivers that employ equalizers. The application of an adaptive Doppler shift compensation with DFE and beamformer was presented in [11]. This approach accommodates AUV, moving at up to ±2.6 m/s. Instead of beamformers, the authors in [23] suggested BICM-ID and adaptive DFE in order to reduce the receiver complexity. For Doppler compensation, they combined an adaptive technique proposed by [11]. However, the complexity still exists due to the employment of RLS algorithm which demands extensive execution time and memory requirements. Multi-carrier communications, [12] and [13] adopt the block length-based technique in [8] to estimate the Doppler shift and, subsequently, fine tune the CFO.

The proposed OFDM-based techniques are of less complexity than single carrier receivers, and consider the acceleration within a packet duration, something which was not considered by all the aforementioned receivers [12], [13], and [20]. The proposed techniques were designed using the ZFE and BICM-ID for the channel equalization and decoding, respectively. Furthermore, this research presents a detailed comparison between the proposed techniques and the block length-based method at different channel conditions. Additionally, an adaptive iterative time varying Doppler shift compensation receiver is suggested and investigated under different scenarios and at various channel ranges. The results of the real-time implementation of the BICM-ID on the SHARC DSP are also presented. In summary, the following points indicate the contribution of the work:

1. Evaluate coded OFDM (COFDM) with velocity variation in AUV systems.

2. Design and development of a low-complexity compensation technique for inherent Doppler shift.

3. The performance of the receiver with time-varying Doppler shift is assessed.

4. The performance of an adaptive iterative receiver approach under the influence of time-varying acceleration is analysed.

5. The SHARC DSP in implementing a real-time system for the BICM-ID algorithm, which is the most challenging part in the system is applied.

1.4 Publications Arising From This Research

1. **A. E. Abdelkareem**, B. S. Sharif, C. C. Tsimenidis, and J. A. Neasham, "Compensation of Linear Multi-scale Doppler for OFDM-based Underwater Acoustic Communication Systems," *Journal of Electrical and Computer Engineering*, submitted (under reviews).

2. **A. E. Abdelkareem**, B. S. Sharif, C. C. Tsimenidis, and J. A. Neasham, "Adaptive Time-varying Doppler shift compensation for OFDM-Based Underwater Acoustic Communication Systems," (under preparation to submit to IEEE Journal of Ocean Engineering.).

3. **A. E. Abdelkareem**, B. S. Sharif, C. C. Tsimenidis, and J. A. Neasham, "Low-complexity Doppler compensation for OFDM-based Underwater Acoustic Communication Systems," in *Proc. IEEE Oceans*, Santander, Spain, 6-9 June 2011.

4. **A. E. Abdelkareem**, B. S. Sharif, C. C. Tsimenidis, and J. A. Neasham, "Adaptive Doppler-shift compensation for OFDM Underwater Acoustic Communications system," in *Proc. UAM*, Kos, Greece, 20-24 June 2011.

5. **A. E. Abdelkareem**, B. S. Sharif, C. C. Tsimenidis, and J. A. Neasham, "Time varying Doppler-shift compensation for OFDM-based shallow Underwater Acoustic Communication systems," in *Proc. IEEE MASS*, Valencia, Spain, 17-22 October 2011.

1.5 Thesis Outline

The thesis is organized as follows: Chapter 2 describes the background of the practical OFDM system that will be used throughout this thesis. It also surveys the research literature for the state of the art in UWC systems. Chapter 3 presents different Doppler compensation techniques that will serve as a base in developing and improving other techniques. In addition, it presents mainly a symbol by symbol approach to compensate the Doppler shift. Furthermore, this chapter suggests two approaches to dealing with the residual Doppler shift. Additionally, this chapter provides an application of the SHARC Digital signal processor for the real-time implementation of BICM-ID, which is the bottleneck of the proposed receiver.

Chapter 4 introduces a new approach that tackles a time varying Doppler shift due to the acceleration. This chapter addresses the main problems of such type of the Doppler shift. Chapter 5 focuses on the solutions to the problems outlined in chapter 4 due to the acceleration effects of broadband Doppler shift on the performance of the receiver. This chapter produces a model for the time varying Doppler shift under different scenarios in order to investigate the proposed system by extensive simulation to analyse the performance, in addition to the trial over different channel ranges. Finally, conclusions are drawn in Chapter 6 and the thesis ends with suggestions for future works.

Chapter 2

Background

The focus of this chapter is the provision of a background to the related fundamental materials that are used throughout this thesis such as CP-OFDM, PAPR, and pulse-shaping in the transmitter and BICM-ID on the receiver side. The chapter begins with an introduction to digital modulation schemes, which is followed by a literature survey to complement the survey discussed in chapter 1. In this chapter, the survey covers the advances in underwater communication, real-time implementation tools and channel coding. Details regarding some mathematical background of BICM-ID are also provided. In terms of hardware implementation, the aspects of the ADSP-21364 SHARC processor selection to implement the decoder are discussed.

2.1 Introduction to Digital Modulation

In a digital transmission, the information is either available in binary form or it is obtained by sampling an analogue signal. Particularly, a speech signal is first sampled and then quantized to appropriate signal levels to obtain binary information. In either case, it is not possible to transmit the information directly. Digital modulation is the process by which digital symbols are transformed into waveforms that are compatible with the characteristics of the channel. In the case of baseband modulation, these waveforms usually take the form of shaped pulses. However, in the case of bandpass modulation, these shaped pulses modulate a sinusoid known as a carrier wave. For radio transmission, the carrier is converted to an EM wave for propagation to the desired destination. The transmission of the EM wave through the space is accomplished by the use of antennas. The wavelength λ and the application govern the antenna size. For mobile communication, antennas are typically

$\lambda/4$ in size, where wavelength is equal to c/f, and c, the speed of light is 3×10^8 m/s. Let us consider a baseband signal where $f = 3$ kHz is coupled directly to an antenna without carrier modulation: in this case, the antenna size will be 2.5×10^4 m, which is not practical. However, if the baseband signal is first modulated onto a higher frequency carrier, e.g. a 900 MHz carrier wave, the antenna size will be 8 cm. For this reason, carrier wave or bandpass modulation is an essential step for all systems involving radio transmission. In the case of UWC, acoustic waves are transmitted as the EM waves cannot propagate through sea where the carrier frequency is in the range of 12 to 20 kHz and the speed of sound is 1500 m/s.

The choice of a modulation system is dependent upon many factors. This is because the signal is transmitted on an imperfect channel, aggravated by the addition of noise, and is subject to variations in the amplitude of the received signal, which is called fading due to the rapid change in the propagation conditions. The size of the constellation M is the main parameter that is associated with the modulation. When $M = 2$, which is binary phase shift keying (BPSK) in the M-ary phase shift keying (M-PSK) technique, each binary information bit is mapped to a polar format of ± 1. Another scheme, where $M = 4$, is known as quadrature phase shift keying (QPSK) which maps two consecutive bits to a symbol taken from the QPSK alphabet. The PSK modulation scheme offers only one degree of freedom as the amplitude of all the symbols is the same, whereas the quadrature amplitude modulation (QAM) offers two degrees of freedom as the symbols exhibit different amplitude and phase distribution. In the case of UWC, where the bandwidth is limited, it is desirable to use higher order modulation schemes such as 8-PSK or 16-QAM where more information bits can be packed into a symbol to increase the bit rate of the system. However, due to the limitations of the channel which exhibits severe multipath and low SNR, it is prohibitive to utilize such schemes as a higher data rate will lead to more ISI. The choice of the modulation system can therefore only result from a compromise adapted to a particular application. In UWC, QPSK or 4-QAM schemes are considered. The performance of the QPSK scheme under various channel conditions will be discussed later in the thesis.

2.2 Literature survey

2.2.1 Advances in Underwater Acoustic communications

It has been proven that phase coherent modulation techniques [24], such as PSK and QAM is the best technique to achieve high-speed data transmission over underwater acoustic channels (UAC) compared with non-coherent frequency shift keying (FSK) or differentially phase shift keying (DPSK) in term of performance; however it requires difficult carrier recovery. Phase-coherent communication systems are presented by the Woods Hole Oceanographic Institution (WHOI) in U.S.A. [25]. The modulation format is QPSK, and the signals are transmitted at 5kbps, using carrier frequency of 15 kHz. Its real-time operation contains 4 Texas instruments TMS320C40 DSPs. The effect of multipath is processed by a decision-feedback equalizer (DFE) operating under RLS algorithm.

An approach for multipath rejection at the receiver end was investigated at the University of Newcastle [22]. The researchers used adaptive beamforming with least mean square (LMS) type to steer the reflected wave. It was found that the beamformer encounter difficulties as the range increases relative to the depth because they used 64 point correlation sequence. The real time system was implemented using multiple DSPs. The system was tested in shallow water at 9.975kbps, and resulted bit error rate (BER) of 2.2×10^{-2} to less than 10^{-3}.

Spread spectrum is also involved as an attractive approach to mitigate the multipath effect in UWC [26], [27], and [28]. In [28], the authors adopt spread spectrum signals to suppress the multiple access interference, which utilize spreading codes to recognize between users and improve the performance against multipath effects. These techniques perform very well; however they come with the cost of reducing the throughput in a band-limited channel.

2.2.2 Tools and Algorithms for real-time implementation

Signal processing functions, such as Viterbi decoding, can be implemented using DSPs. Particularly, Analogue Devices [28], TigerSHARC ADSP-101S and SHARC ADSP-21065L can be used in the baseband modem implementation. The first of these manipulates the Viterbi Decoder in 0.86 MIPS and 1024-point complex FFT in 32.75 μs, and has been used as a multiprocessor structure by [29] with field

programmable gate array (FPGA) to implement an OFDM underwater acoustic communication system. The second manipulates 1024-point FFT in 0.274 ms. In addition, TMS320C6416 is designed for 3rd Generation Partnership Project (3GPP) turbo code and is capable of decoding up to 12 Mbps (6 Iterations) [30]. Furthermore, in [31] the transmitter has been implemented with multiple DSP's of type ADSP-TS101s and FPGA as the logical control. It has been proven from the experiment in the pool and lake that the signal transmitter satisfies requirements of signal transmission for OFDM in real-time in underwater multi-carrier acoustic communication, and the signal synthesis method, DDWS (Direct Digital Wave Synthesis) is adopted to realize producing OFDM. Furthermore, the authors in [32] have used optimized built-in code for turbo decoder implementation.

Other algorithms have been implemented using Texas Instruments (TI) platforms. The authors in [33] and [34] have implemented an OFDM acoustc modem with a 225 MHz TI TMS320C6713 DSP board and it has been successfully tested with in-air communication. In [35], TMS320C6713 and TMS320C6416 have been utilized to implement single-input single-output (SISO) and multi-input multi-output (MIMO) OFDM acoustic receivers. These receivers are coded and investigated with low-density parity-check (LDPC) and convolutional code (CC).

FPGA's can be used to implement COFDM in addition to DSP's in acoustic communications. For instance, they have been used in underwater communications to achieve reliable high rate data communication (1-10Kbps) in very shallow waters [36]. The researcher has implemented the transmitter and receiver of the suggested modem using VHDL on FPGA, and has employed differential PSK (DPSK) modulation to avoid channel estimation at the receiver, which results in reducing implementation complexity. DSP chips can be distinguished by their fixed-point or floating-point architectures. Currently, fixed-point processors are either 16-bit or 24-bit devices, while floating-point processors are 32-bit or 40-bit devices. The floating-point devices are dominant in the communications systems that have large dynamic range. The faster development cycle for a floating-point device may easily outweigh the extra cost of the DSP device itself [37].

2.2.3 Channel coding

To achieve reliable communication over acoustic channel, channel coding in the form of block or convolutional coding of the source bit stream should be involved to achieve reliable communication system [38]. In 1982, Ungerboeck introduced a trellis-coded modulation (TCM) system as a bandwidth-efficient signalling over an additive white Gaussian noise (AWGN) channel [39]. This study set out with the aim of assessing the importance of mapping. The most interesting finding was that coding reduces noise about 3-4 dB compared with uncoded with the same transmitted information. However these results were not very encouraging in undersea channel, thus for fading channels, the diversity order of the coded modulation system should be high; therefore the performance of TCM is degraded in such channels [40], but it can be improved by adding symbol interleaver. However, the limitation of the diversity order in symbol interleaved coded modulation and the cost of increasing the complexity of the code results in finding different approach called BICM. It was suggested by Zahavi [41] to improve the performance of coded modulation over fading channels. It was shown that the diversity order can be increased to a minimum number of distinct bits rather than symbols by using bitwise interleaving. It was shown in [42], [43], [44], [45], and [46] that with iterative decoding (ID), BICM can be used to provide excellent performance over any channel provided well designed signal mapping. In [47], the author has exploited the diversity that has been offered by the channel coding with convolutional BICM-ID to improve the reliability of the UWA channel.

2.3 OFDM system transmitter

2.3.1 Peak-to-average power ratio (PAPR)

One of the major obstacles in multicarrier transmission is the high PAPR of the transmit signal. There are many techniques [48], [49]have been used to avoid high PAPR signals based on computation complexity, BER, bandwidth expansion. The block diagram of SLM technique for PAPR reduction is predicted in Fig. (2.1). The input data $\boldsymbol{X} = [X[1], X[2], \cdots X[N_c]]$ is multiplied with $\boldsymbol{U}$ phase sequences $[e^{j\varphi_n^1}, ...e^{j\varphi_n^u}]$ where $\varphi_n \in [0, 2\pi]$ for $n = 1, 2, N_c$ and $u = 1, 2, \cdots, U$. An OFDM symbol data then contains a modified phase $\boldsymbol{X}^u = [X^u[1], X^u[2], \cdots X^u[N_c]]$ is ob-

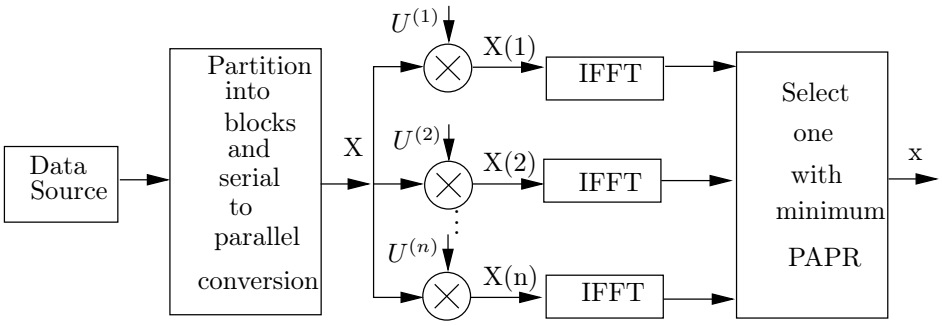

Figure 2.1: Block diagram of SLM method for PAPR reduction.

tained. Converting to the time domain at each sequence $\boldsymbol{U}$ by taking the IFFT results a corresponding sequences $\boldsymbol{x}^u = [x[1], x[2], \cdots, x[N_c]]$. In order to select the minimum PAPR for the transmission, each time domain OFDM symbol is produced according to its corresponding sequence, hence the discrete-time PAPR is calculated as

$$PAPR \triangleq \frac{max|x[n]|^2}{E_n[|x[n]|^2]}, \tag{2.1}$$

and the minimum phase is selected as shown [50]

$$\tilde{u} = \arg \min_{u=1,2,\cdots,U} (PAPR). \tag{2.2}$$

On the receiver, side information is transmitted to recover the optimal sequence. Considering the hardware implementation issue, our project buffers the optimal PAPR phase sequence as a vector and then provide this information to the receiver. It is worth to mention that this approach is useful when the transmitted message is knew, otherwise, side information is an alternative in the case of random message transmission. In this case, $\boldsymbol{U}$ IFFT operations are needed, whereas $\lfloor \log_2 U \rfloor$ bits are required as a side information.

2.3.2 Pulse shaping

The UAC is band limited, thus it constraints the transmitted signal and consequently an increase in the decoding error due to the ISI is most likely to occur at the receiver side. Therefore, these types of channels necessitate employing the pulse shaping in order to preserve the bandwidth and minimize the decoding errors.

The roll-off factor β govern the performance of the pulse shaping filter (PSF) [51]. In Fig. (2.2), when $\beta = 0$, it offers the most efficient use of bandwidth, but

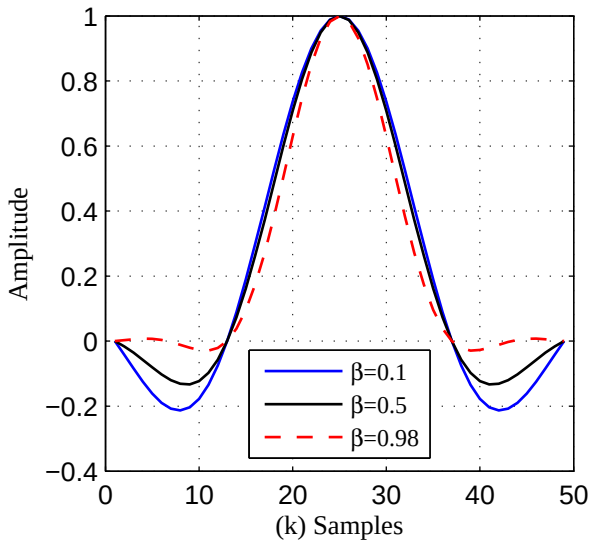

Figure 2.2: Time domain characteristics of raised-cosine function for different values of roll-off factor β.

comes with an increasing ripples relative to $\beta > 0$ in which there is an increase in the transmitted bandwidth on the cost of reducing the ripple magnitude. The pulse shaping $p_{rc}(t)$ which is realized as an up-sampled raised cosine FIR filter is defined in [52] as

$$p_{rc}(t) = \begin{cases} \frac{1}{T}, & 0 \leq |t| \leq \frac{T_s(1-\beta)}{2} \\ \frac{1}{2T_s}\left[1 + \cos\left(\frac{\pi}{\beta T_s}\left(|t| - \frac{T_s(1-\beta)}{2}\right]\right)\right], & \frac{T_s(1-\beta)}{2} \leq |t| \leq \frac{T_s(1+\beta)}{2} \\ 0, & \text{otherwise.} \end{cases} \tag{2.3}$$

2.3.3 Guard interval in the OFDM systems

There are two main approaches that can be used to insert the guard interval in OFDM systems. First is the zero padding (ZP) that pads zeros in the guard interval. The second approach is to preface the OFDM symbol by the last samples, this approach is called cyclic prefix (CP). Referring to [53] and calling that we aim to design a paradigm of a low complexity receiver that is applicable in the hardware implementation, selecting a CP approach is now feasible.

2.3.3.1 Cyclic prefix OFDM

Let $X(n)$ be the frequency domain OFDM symbol modulates the sub-carrier with a frequency of $f_n = n/T$, for $n = 0, 1, 2, \cdots, N_c$. The duration of this symbol $X(n)$

was originally T_s and its length has been extended to $T = N_c T_s$ by transmitting parallel N_c sub-carriers. This OFDM symbol comprises a signal corresponds to N_c sub-carriers that has a duration of T. Consider the ith OFDM signal

$$x_i(t) = \frac{1}{\sqrt{N_c}} \sum_{n=0}^{N_c-1} X_i(n) e^{j2\pi f_n (t-iT)}, \quad \text{for } iT \leq t < iT + kT_s. \tag{2.4}$$

For the channel with an impulse response of $h_i(t)$, the received signal is given as

$$y_i(t) = x_i(t) * h_i(t) + w_i(t) = \int_0^\infty h_i(\tau) x_i(t-\tau) dt + w_i(t), \quad iT \leq t < iT + kT_s, \tag{2.5}$$

where $w_i(n)$ is the additive white Gaussian noise. Sampling at $kT_s = kT_d/N_c$, (2.5) can be represented in a discrete time as follows

$$y_i(k) = x_i(k) * h_i(k) + w_i(k) = \sum_{m=0}^{\infty} h_i(m) x_i(k-m) + w_i(k). \tag{2.6}$$

Let T_d be the duration of the OFDM symbol without a guard interval. Then, $T_d = N_c T_s = 1/\delta f$, where $\delta f = 1/(N_c T_s) = B/N_c$ and $B = 1/T_s$. Due to the extension of the symbol duration by $N_c T_s$, the effect of the multipath is reduced on the OFDM symbol. However, there is a trade off between the symbol duration and the CFO. The longer duration means tight sub-carrier spacing and more effect of the Doppler shift. It is worth to mention that the impairments are still effective among the sub-carriers due to the ISI and thus inserting a CP as a guard between two consecutive OFDM is essential. By copying the last samples of the OFDM symbol into its front and thus extending the OFDM symbol is called CP. Hence, the OFDM symbol duration is changed to be $T = T_d + T_g$, where T_g represents the guard time. Once the length of the guard interval is selected longer than or equal τ_{max}, the ISI effect of the ith OFDM is limited within the guard interval, hence, the $i+1$th OFDM symbol is protected against the interference from the previous symbol. However, if the length of the guard interval is selected shorter than τ_{max}, the tail of the ith symbol affects the leading edge of the $i+1$th OFDM symbol and yields to an ISI. Now, assuming that the FFT window is completely synchronized, i.e., within the CP interval, then the received samples $y_i(k)$ of the ith symbol after FFT can be written as

$$
\begin{aligned}
Y_i[n] &= \sum_{k=0}^{N_c-1} y_i(k) e^{-j2\pi kn/N_c} \\
&= \sum_{k=0}^{N_c-1} \left\{ \sum_{m=0}^{\infty} h_i[m] x_i[k-m] + w_i[k] \right\} e^{-j2\pi kn/N_c} \\
&= \sum_{i=0}^{N_c-1} \left\{ \sum_{m=0}^{\infty} h_i[m] \left\{ \sum_{l=0}^{N_c-1} X_i[l] e^{j2\pi l(k-m)/N_c} \right\} \right\} e^{-j2\pi kn/N_c} + W_i[n] \\
&= \frac{1}{N_c} \sum_{l=0}^{N_c-1} \left\{ \left\{ \sum_{m=0}^{\infty} h_i[m] e^{-j2\pi lm/N_c} \right\} X_i[l] \sum_{k=0}^{\infty} e^{-j2\pi(n-l)k/N_c} \right\} e^{-j2\pi kn/N_c} + W_i[n] \\
&= H_i[n] X_i[n] + W_i[n],
\end{aligned}
\tag{2.7}
$$

where the transmitted symbol $X_i[n]$, the received symbol $Y_i[n]$, the channel response $H_i[n]$, and noise $W_i[n]$ are in frequency domain at the nth sub-carrier. Thus, it can be inferred that once the cyclic prefix is appended to the channel input, the convolution in time domain will be converted to a multiplication in frequency domain and a circular convolution is obtained. Therefore, taking the DFT of the channel output yields

$$
Y[n] = \mathrm{DFT}\left\{ y[k] = x[k] \circledast h[k] \right\} = H_i[n] X_i[n], \text{for } \; 0 \leqslant n \leqslant N_c - 1 \tag{2.8}
$$

as desired in the receiver to enable a single-tap equalizer by dividing the received symbol by the channel.

It should be stressed that increasing the CP length does not mean completely eliminate the ISI and/or ICI. Additionally, adding a CP comes with a cost. To be more specific, once the Doppler shift exist, the symbol time is expanded or compressed depending on the direction of the movement, hence, the FFT window start point is misaligned and therefore a synchronization impairments are occurred. That is, if the FFT window comes earlier than the lagged end of the previous symbol, ISI occurs; if the FFT window position is later than the beginning of a symbol, an ISI and ICI are the consequences [54]. Adding a CP comes with a cost of an overhead of N_g/N_c, where N_g is the CP length. Furthermore, the redundant data caused a loss in the transmitted power.

2.4 The Underwater Acoustic Channel

Unlike the existing communication channels, the UACs have not characterized yet as a standard channels. However, there are a main characteristics that should be considered in the case of establishing a reliable communication system for underwater acoustic. These characteristics are [2]:

1. Attenuation and ambient noise
2. Doppler effect
3. Time varying multipath channels

2.4.1 Attenuation and ambient noise

The acoustic signal experiences a power attenuation while travelling through its link. This attenuation is due to:

- Energy spreading, and
- Sound absorption loss.

Let r be the range from the source in km, then the attenuation of the signal is proportional to $\frac{1}{r^2}$ when the propagation is line-of-sight. This type of spreading is called spherical or inverse square law. When the acoustic wave is propagated via a reflection within a boundaries of the sea surface and the bottom, then the attenuation is proportional to $\frac{1}{r}$. This type of attenuation is called cylindrical spreading. For short-range < 1 km, spherical spreading is dominant while cylindrical spreading refers to the case of medium (1-10 km) and long-range (10-100 km) transmission.

Practically, it is interesting to formulate an equation as a function of the signal frequency that includes not only cylindrical but also spherical spreading and absorption loss, i.e., the total transmission loss (TL) is given by [55]:

$$TL(f) = k \log_{10}(r) + a(f)r \times 10^{-3}, \tag{2.9}$$

where k is 20 for spherical and 10 for cylindrical, $a(f)$ is the attenuation coefficient in dB/km. Several formulas for the absorption coefficients have been derived in [2]

out of which, one can be given as

$$a(f) = Af^2 + \frac{Bf_0}{1 + \left(\frac{f_0}{f}\right)^2} + \frac{Cf_1}{1 + \left(\frac{f_1}{f}\right)^2} \tag{2.10}$$

where the first term on the right hand side is fresh water attenuation, second term is magnesium sulphate relaxation and the third term is boric acid relaxation. Additionally,

$$A = 2.1 \times 10^{-10}(T - 38)^2 + 1.38 \times 10^{-7}, \tag{2.11}$$

$$B = 2S \times 10^{-5}, \tag{2.12}$$

$$C = 1.2 \times 10^{-4}, \tag{2.13}$$

$$f_0 = 50(T + 1), \tag{2.14}$$

$$f_1 = 10^{\frac{T-4}{100}}, \tag{2.15}$$

where S is the salinity in parts per thousand, T is the temperature in Celsius and f is the operating frequency in kHz. In practice, a useful design rule for determining at which point absorption losses become substantial is [56]

$$a(f)r < 10 \text{ dB}. \tag{2.16}$$

In the ocean, another factor that affects the received SNR is the noise. It can be classified into man-made noise and ambient noise. The latter comes from seismic events, marine life, ship's engine, rainfall, breaking waves [57] and so on. The majority of these types are approximated as Gaussian statistics. It should be stressed that the ambient noise is time-varying particularly in shallow water. Furthermore, the noise level is inversely proportional to the depth. Interested reader can refer to [57], (ch. 6) for more information.

2.4.2 Doppler effect

In general, the Doppler effect is inherent in the UAC due to the currents and wave motions. The movement of the receiver (Rx) and/or the transmitter (Tx) also yields to a shift of the received frequency, called Doppler frequency shift. This Doppler

shift can be represented as

$$F_d = f_c \frac{v}{c}. \tag{2.17}$$

The Doppler shift frequency is positive when the Tx and Rx move towards each other, where the transmitted signal will be compressed resulting in an escalated frequency. That is, the received frequency can be formulated as

$$f_c' = f_c[1 - \frac{v}{c}] = f_c - |\Delta|\,. \tag{2.18}$$

It is obvious that the frequency shift depends on the direction of the wave, and must lie in the range $f_c - \Delta_{max} \cdots f_c + \Delta_{min}$, where $\Delta_{max} = f_c v/c$. Furthermore, due to this movement, the path lengths are also affected, therefore, we assume here all paths have the same Doppler shift.

Since the propagation speed c is relatively small, as mentioned earlier, it seems the Doppler shift has a significant influences on the underwater link. This effect is arisen with an OFDM systems due to its sensitivity to Doppler shift. The sensitivity is proportional to the sub-carriers spacing which in turn depends on the symbol length. We assume the channel is quasi-static in this thesis. However, the Doppler shift is varying linearly within the OFDM symbol time as a result of the acceleration effect. This acceleration adds a burden on the receiver and needs a special signal processing such as an adaptive algorithm or iterative receiver to deal with this obstacle.

2.4.3 Time varying multipath channel

The time varying channel can be characterized by an impulse response $h(t, \tau)$ and in a frequency domain is characterized as $H(t, f)$. Furthermore, the time varying multipath channel is also characterized in terms of delay-Doppler spread $C(F_d, \tau)$. All aforementioned characteristics are related via a two-dimensional Fourier transforms. In particular, $H(t, f)$ and $C(F_d, \tau)$ are related to $h(t, \tau)$ as [58]

$$H(t,f) = \int_{-\infty}^{\infty} h(t,\tau) e^{-j2\pi f t} dt \quad , \quad C(F_d,\tau) = \int_{-\infty}^{\infty} h(t,\tau) e^{-j2\pi F_d t} dt \tag{2.19}$$

Let us assume that the channel is wide sense stationary (WSS) process in t and f, then the time-frequency correlation function

$$R_H(\Delta t, \Delta f) = \mathbb{E}\left\{H(t+\Delta t, f+\Delta f)H^*(t,f)\right\}. \tag{2.20}$$

In terms of signal distortion, $H(t,f)$ represents the effect of the channel in time and frequency. Considering this, there are a set of channel spread parameters T_{coh} and B_{coh} that can be used to identify the channel variations in time and frequency, respectively.

2.4.3.1 Doppler spread and coherence time

Although the maximum delay spread τ_{max} and coherence bandwidth B_{coh} do not provide information about the time-varying nature of the channel due to the relative motion between the transmitter and receiver, it can be considered as an indicator of the time dispersive nature of the channel. Practically, the channel is changing with time, therefore; it is very crucial to understand these time variations and how a digital communications system responds to it. In practice, the receiver is equipped with a mechanism to estimate the time variations due to the Doppler shift discussed in Chapter 4 in more detail.

The Doppler spread (F_d) of the channel is the range over which the Doppler spectrum is non-zero. The Doppler spread and coherence time are inversely proportional to each other. That is [9]

$$T_{coh} \triangleq \frac{1}{F_d}. \tag{2.21}$$

The amount of the spectral broadening depends on F_d which is relative to the velocity of the mobile.

The value of T_{coh} is actually a statistical measure of the time duration over which the channel impulse response can be considered invariant. In other words, coherence time means that the duration over which the channel is highly correlated. The channel variation in time is captured by the Doppler spread, therefore, this spreading factor is used to indicate the rapidity of the channel variation with time. Accordingly, a channel can be classified into a fast time-varying and a slow fading channel.

If T_{coh} is less than the OFDM symbol time T_d, the channel will change during

the transmission of a symbol and corrupt the source signal severely. This is called fast or time selective fading. However, if T_{coh} is longer than the symbol duration, the CIR will change very slowly compared to the symbol rate. This type of fading is called slow fading. If this is the case, the channel can be assumed to be constant over the signalling interval. Another way to characterise the channel is in terms of the product $F_{d_{max}}\tau_{max}$ which is known as the spread factor [59] of the channel. The channel requires to fulfil that the spread factor is $\ll 1$ to be considered as *underspread* in which case the channel can be measured without any ambiguity. However, if this condition is not fulfilled, i.e., the value of the spread factor is greater than 1, then, the channel is called *overspread* which makes it difficult to measure the CIR.

2.4.3.2 Delay spread and coherence bandwidth

While τ_{max} of the channel can be computed as the time difference between the latest to earliest arrival, the channel coherence bandwidth, B_{coh}, is derived from the delay spread. That is, τ_{max} is inversely related to the channel coherence bandwidth as [9]

$$B_{coh} \triangleq \frac{1}{\tau_{max}}. \tag{2.22}$$

The coherence bandwidth is a measure of the frequency selectivity in a multipath propagation. The frequency non selective fading is the range over which the channel remains almost constant in frequency. If the channel has a constant gain and phase over the transmitted signal bandwidth (B) which is less than the coherence bandwidth (B_{coh}), then the received signal will undergo flat fading. However, the received signal undergoes frequency selective fading when B is much greater than the B_{coh} of the channel, which means that all the transmitted frequency components will be similarly attenuated. This implies that the symbol duration is smaller than the maximum delay spread of the channel resulting in ISI in the received signal and the OFDM modulation technique is suitable for such case to mitigate these effects. In reality, the assumption of WSSUS does not hold for all the values t and τ. Therefore, the concept of a quasi-WSSUS channel is used which implies that the WSSUS assumptions hold for some values of t and τ observed by a communication system. In a simpler context, the channel remains constant for the duration of the transmitted signal but it can change for the next packet.

Fig. 2.3 and 2.4 illustrate typical normalized channel impulse responses for 500

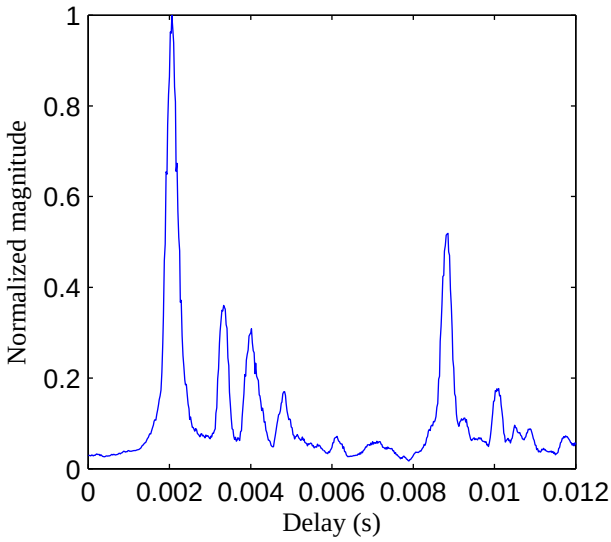

Figure 2.3: Normalized CIR of a 500 m range channel.

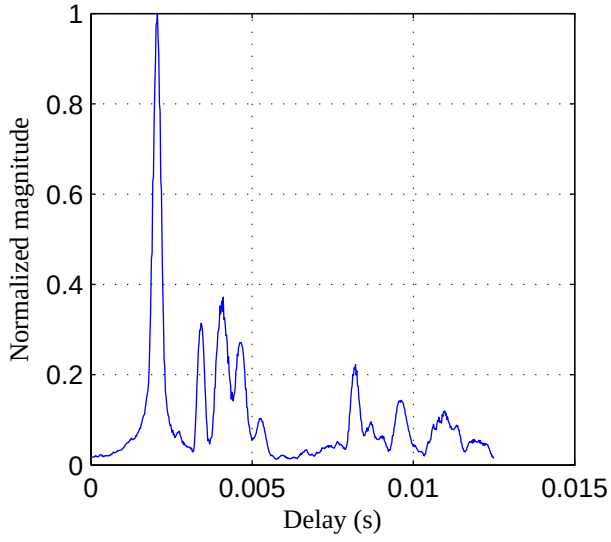

Figure 2.4: Normalized CIR of a 1000 m range channel.

and 1000 m range link set-ups, respectively. These CIRs were measured by means of the transmission of a linear frequency modulated (LFM) chirp signal and then correlation of the incoming chirp signal at the receiver end. The 500 m range channel exhibited a delay spread in the order of 10 ms which translates into 40 symbols of ISI at the data rate of 4 ksps. It was confirmed that the 1000 m range channel exhibited a delay spread of 5 ms, which is 2 times less than that of the 500 m range channel and translates into 20 symbols of ISI at the data rate of 4 ksps. There are many ways in which mitigation of channel impairments can be achieved; for example, by employing trellis based equalizers, a filter based equalizer, OFDM or beamforming. The problem is exacerbated when the channels vary rapidly within time. In such cases, it is necessary to employ a mechanism that is capable of estimating time variations at the receiver end. In this thesis, an OFDM technique is employed to address these time variations due to its low complexity as far as implementing the receiver is concerned.

2.5 BICM-ID OFDM system

In a multipath fading environment, the forward error correction (FEC) is used to reduce the error probability. However, this error performance comes with the cost of transmission bandwidth reduction and receiver complexity. An alternative spectral-efficient TCM is introduced by [39] which improves the performance of the band-limited communication systems by jointly optimizing the coding and modulation scheme. A reduction in the bandwidth expansion and significant coding gain are obtained from this approach.

Practically, a robust communication system should perform well not only in an AWGN such as TCM, but also in a fading channel. This is due to the burst of errors that accompanies the fading channel which is out of the capability of many FEC types in the case of long burst of errors. Hence, the emergence of interleaving has devised to reduce the effect of such type of error with a coded system in a multipath fading channels. The main effect of the interleaving with a coded modulation is to randomise the positions of the errors within a burst and ultimately convert this burst of errors into a random error that can be sorted by the FEC. This is the main task of the interleaver at the transmitter. The length of the interleaver L_{int} plays an important rule in making the fading independent and the longer is the best, however

the cost is the implementation complexity.

In order to achieve robust performance over a different channel conditions, interleaved coded modulation should exhibit both large Euclidean and Hamming distances [47]. Therefore, in a fading channels, maximizing the diversity order is the main target of designing an interleaved coded modulation scheme. Unlike block and convolutional codes, there are two options for interleaving in coded modulation. First is to interleave the bits and then map them to modulated symbols. This option is called BICM and it is now a dominant technique for coded modulation in fading channels. Alternatively, the modulation and coding can be done jointly as in coded modulation for AWGN channels and the resulting symbols interleaved prior to transmission. This technique is called symbol-interleaved coded modulation (SICM).

A major breakthrough in the design of coded modulation for fading channels was the discovery of BICM [41], [60]. In BICM the code diversity equals to the smallest number of distinct bits rather than channel symbols along any error event. This is achieved by bit-wise interleaving at the encoder output prior to symbol mapping, with an appropriate soft-decision bit metric as an input to the Viterbi decoder. While this breaks the coded modulation paradigm of joint modulation and coding, it provides much better performance than SICM. Moreover, analytical tools for evaluating the performance of BICM as well as design guidelines for good performance are provided in [60]. BICM is now the dominant technique for improving the performance of coded modulation in fading channels [61].

As mentioned earlier, the conventional BICM achieves good performance providing high diversity order. However, due to the randomization in the modulation caused by the bitwise interleaver, the Euclidean distance is reduced. Therefore, there is a degradation in the performance of the BICM in Gaussian channels compared to TCM [41]. To counter this problem, an iteratively decoded BICM with carefully selecting signal mapping, referred to as BICM-ID has been proposed in [62], [63], [64], and [65]. The idea behind BICM-ID is to increase the Euclidean distance of the BICM code and to exploit the full advantage of bit interleaving by performing soft iterative decoding technique [46]. BICM-ID was shown to be better than TCM and BICM in both AWGN and uncorrelated Rayleigh fading channels [66].

The system diagram of BICM-ID is illustrated in Fig. 2.5. The transmitter contains a serial concatenation of FEC, an interleaver Π and and signal mapping.

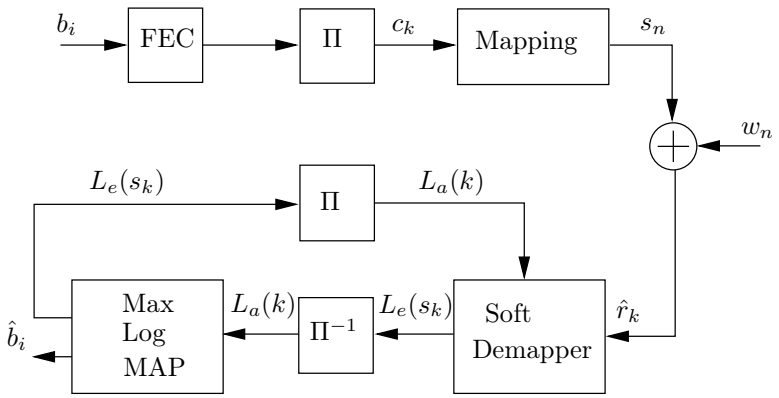

Figure 2.5: System diagram of BICM-ID.

The block diagram of a FEC that contains non-systematic convolutional (NSC) code is illustrated in Fig. 2.6. Unlike systematic code, NSC has a better error performance at large SNR. A sequence of K_d information bits, $\mathbf{b} = (b_0, \cdots, b_{K_d-1})$ are sent by the source. In order to protect this message, a convolutional code of rate $R_c \in (0, 1]$ is used to produce a sequence $\mathbf{c} = (c_0, \cdots, c_{K_c-1})$ of $K_c = (K_d + K_0)/R_c$ coded bits, where $K_0 \geq 0$ is the overhead introduced by the encoder, i.e. a termination sequence to set the final state of the encoder to zero.

An important characteristic of convolutional code is the constraint length K, which is defined as the number of stages that shift the message bits. In an encoder of M-stage shift register, then $M = K - 1$ flip-flops are required. This type of convolutional encoder thus contains 2^M states that denoted in binary or decimal form. Thus the state of an encoder shown in Fig. 2.6 contains two flip-flops can take 2^2 values. The interleaver is used to randomize the codeword and ultimately reduces the burst errors introduced in the transmission. The de-interleaver is an opposite procedure providing that the positions of the scrambling operations are known by the receiver.

The encoded bits are permuted by a random interleaver of length L_{int} and the output bit sequence, c_k, is grouped to form the sub-sequences $\mathbf{C}_n \triangleq [c_{n,1}, \cdots, c_{n,m}]$, where $m = \log_2 M$ represents the number of bits per symbol and M is the constellation size of the utilized modulation scheme. Subsequently, each $\mathbf{C}_n$ is mapped to M-ary symbols, s_n, taking values from the M-ary symbol alphabet $\Omega = \{\alpha_1, \cdots, \alpha_M\}$, where $\alpha_i \in \mathbb{C}$ and $\mathbb{C}$ denotes the set of complex number.

This chapter considers signal transmission on AWGN channel to simplify the receiver derivation. The application of BICM-ID in the case of frequency selective and Doppler shift channels is considered in next chapter. Therefore, the received

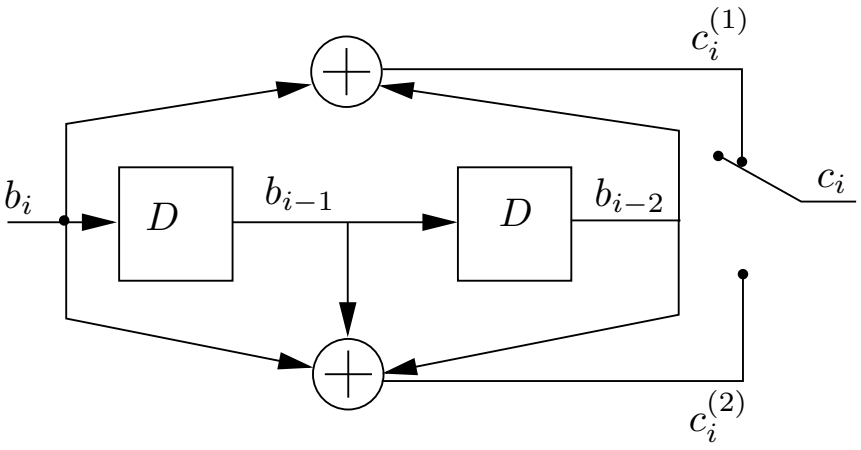

Figure 2.6: Convolutional encoder of rate R_c=1/2.

signal can be written as

$$\hat{r}_n = s_n + w_n, \tag{2.23}$$

where w_n is the complex zero mean Gaussian noise with variance σ_w^2 in each real dimension.

At the receiver, the demapper processes the received complex symbols $\hat{r}_n$, the corresponding *a priori* LLRs $L_a[C_{n,i}] = \log \dfrac{P[C_{n,i}=0]}{P[C_{n,i}=1]}$ of the coded bits and outputs extrinsic LLRs

$$L_e[C_{n,i}] = \log \frac{P[c_{n,i}=0|r_n, L_a(\mathbf{C}_n)]}{P[c_{n,i}=1|r_n, L_a(\mathbf{C}_n)]} - L_a(C_{n,i}), \tag{2.24}$$

where $C_{n,i}$ denotes the binary random variable with realizations $c_{n,i} \in \{0,1\}$.

Let Ω_b^i denote the subset of symbols $s_n \in \Omega$, whose bit labels have the value $b \in \{0,1\}$ in position $i \in \{1,2,..m\}$. Using Bayes' rule and taking the expectation of $p(\hat{r}_n|s_n)$ over $P[s_n|C_{n,i}=b]$, $s_n \in \Omega_b^i$ yields

$$L_e[C_{n,i}] = \log \frac{\sum_{x_n \in \Omega_0^i} p(\hat{r}_n|s_n) P[s_n|C_{n,i}=0]}{\sum_{s_n \in \Omega_1^i} p(\hat{r}_n|s_n) P[s_n|C_{n,i}=1]}. \tag{2.25}$$

The first term $p(\hat{r}_n|s_n)$ is computed according to the channel model assuming a Gaussian distribution [67]

$$p(\hat{r}_n|s_n) = \frac{1}{2\pi\sigma_w^2} e^{-\dfrac{|\hat{r}_n - s_n|^2}{2\sigma_w^2}}. \tag{2.26}$$

The second term $P[s_n|C_{n,i}=b]$ is computed from the *a priori* information of the

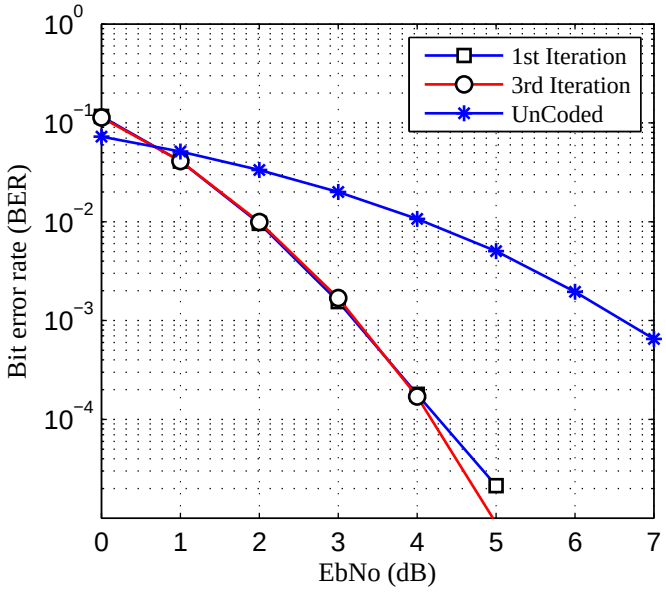

Figure 2.7: Performance comparison of BICM-ID OFDM and uncoded system.

individual bits [45]

$$P[s_n|C_{n,i}=b]=\prod_{j=1,j\neq i}^{m}\frac{1}{1+e^{-L_a(C_{n,j})}}e^{-L_a(C_{n,j})c_{n,j}}. \tag{2.27}$$

The extrinsic estimates $L_e[C_{n,i}]$ are deinterleaved and applied to the Log MAP channel decoder. Performing iterative decoding, extrinsic information about the coded bits from the decoder is fed back and regarded as a priori information $L_a[C_{n,i}]$ at the demapper. During the initial demapping step, the a priori LLRs are set to zero.

The MAP or BCJR [68] decoder is preferred in implementing such soft-in-soft-out (SISO) algorithm because it has better performance. In this algorithm, we need to compute the forward-state metric α', the reverse-state metric β', the branch metric γ. The forward state probabilities $\alpha'_k(s)$ can be calculated as [69]

$$\alpha'_k(s)=\sum_{\forall \acute{s}}\alpha'_{k-1}(\acute{s})\gamma_k(\acute{s},s). \tag{2.28}$$

Thus, once the $\gamma_k(\acute{s},s)$ values are known, the $\alpha'_k(s)$ values can be calculated recursively. Assuming that the trellis has the initial state $S_0=0$, the initial conditions for this recursion are

$$\alpha'_0(S_0=0)=1,$$

$$\alpha'_0(S_0=s)=0,\forall s\neq 0. \tag{2.29}$$

The backward state probabilities $\beta'_k(s)$ can similarly be calculated recursively as

$$\beta'_{k-1}(\acute{s}) = \sum_{\forall s} \beta'_k(s)\gamma_k(\acute{s}, s). \tag{2.30}$$

The initial conditions for this recursion are

$$\beta'_N(S_N = 0) = 1,$$

$$\beta'_N(S_N = s) = 0, \forall s \neq 0. \tag{2.31}$$

The transition probabilities $\gamma_k(\acute{s}, s)$ can be calculated using the received sequence and available a priori information, which can be written as

$$\gamma_k(\acute{s}, s) = P(\mathbf{y}_k|\mathbf{x}_k)P(u_k), \tag{2.32}$$

where u_k is an input bit necessary to cause the transition for state $S_{k-1} = \acute{s}$ to state $S_k = s$; $P(u_k)$ is a priori probability of this bit, $\mathbf{x}_k$ is the transmitted codeword associated with this transition, $\mathbf{y}_k$ is the received codeword associated with this transition and k is the time index.

However, it is complex in a real time environment. A sub-optimal version of MAP is max-log-MAP or linear approximation to log-MAP is adopted, which performs the max* operations (Jacobian logarithm) defined as [70]

$$\max^*(x, y) = \max(x, y) + \log(1 + e^{-|x-y|}), \tag{2.33}$$

where x and y represent the modulated encoded bits and received *intrinsic* information with noise, respectively. Sometimes, the expression $\log(1 + e^{-|x-y|})$ is approximated using a constant or ignored.

2.6 The Effects of the Interleaver

Due to the impairments of the signal transmission that are caused by the multipath fading channel, the received signal arrives at a different phase and with distortion. In addition, UWA channels suffer from ambient noise and other burst noise (e.g. ship engine noise, noise of fish and humans). All of these impairments result in a dependency among successive symbol transmission. That is, the disturbances cause

errors that occur in burst rather than individual events. This case is an example of the channel with memory which cannot be considered as a single random bit error and it causes degradation in error performance. Therefore, such burst errors of the channel are dealt with by the use of interleaving. The idea behind the employment of interleaving the coded bits before transmission and a corresponding deinterleaving after reception is to spread in time the burst errors caused by the deep fade of the channel, hence translating them into random errors, and thus enabling the FEC to work effectively in correcting burst errors [71].

In this thesis, the aim is to use a BICM-ID as a tool to mitigate bursts of channel error. The iterative decoding algorithms are derived assuming that all input LLRs to the SISO modules are reliable. However, the system performance degrades when the Doppler effect exists. When trying to detect a particular code bit and calculate its output LLR, a SISO module uses the input LLRs for the nearby code bits in the computations. This means that the correlation between nearby input LLRs will cause performance degradation and hence this scrambling operation is necessary between the SISO modules.

There has been much focus on interleaver design regarding BICM-ID and processing of the signals [72] and [73]. Considering BICM-ID for a time-varying channel is difficult because the inner code, i.e. the channel, cannot be considered as known when designing the interleaver. The interleaver should therefore be as random as possible. Since the focus of this work is to deal with the Doppler effect and tackling the channel by designing BICM-ID system as a tool, therefore it is considered that the bit redistribution pattern is known by the receiver for the purpose of deinterleaving before decoding. Furthermore, the proposed system uses a block interleaver, implying that the interleaver operates on a block of coded bits at a time. Unless otherwise stated, the length of the interleaver is assumed to be equal to the length of the codeword.

2.7 DSP platform selection issues

Selecting the most appropriate DSP processor and tackling a real-time signal is an important issue. Programmable DSP is more flexible, of a lower cost and a higher speed than other processors, so it has become the best solution for many communication, medical, and industrial products because traditional microprocessors are

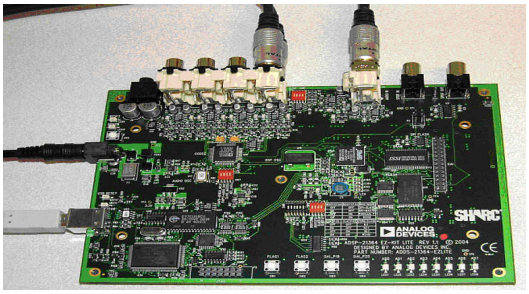

Figure 2.8: SHARC ADSP-21364.

inappropriate for such applications. The main aspects of selecting a DSP processor are as follows: data format, memory bandwidth, CPU architecture, and million integer operation per second (MIPS) or million floating point operations (MFLOPS) [74].

In terms of data format, fixed point DSPs are generally cheaper, but produce higher quantization noise. This will be added to the signal and lower the signal to noise ratio of the system. In addition, extra code has to be written to overcome the overflow or underflow and the programmer should be aware of what scaling needs to take place. In comparison, floating point devices have better precision, a higher dynamic range, and a shorter development cycle [74].

As there is iterative decoding in the suggested receiver and the algorithm spends most of the execution time, especially the SISO algorithm because of the add compare select (ACS), it is important to take advantage of some of the available architecture, such as super Harvard architecture (SHARC), as shown in Fig. (2.8), because it includes an instruction cache in the central processing unit (CPU) and has split instruction and data buses. This feature is important with regard to avoiding any conflict between data and instruction transfer during the fetch cycle, and to ensure the program memory does not have to be accessed for the instructions to be restored. Consequently, all of the memory for CPU information transfers can be accomplished in a single cycle, which results in a high memory access bandwidth. Additionally, on-chip memory is a key factor to be considered when deciding which DSP device to use, because the memory should be sufficient enough to hold the digitized samples.

The third aspect of selecting a DSP is the CPU architecture. For instance, traditional architecture uses single memory for both data and instruction, whereas some DSPs have very long instruction word (VLIW) core architectures; thus they execute

Table 2.1: DMA operation

Receive	Process	Transmit
Block A	-	-
Block B	Block A	-
Block C	Block B	Block A
Block A	Block C	Block B
Block B	Block A	Block C
Block C	Block B	Block A

multiple instructions in parallel, resulting in fast operations. However, these types of architectures [75] dissipate more power than conventional DSP architectures. In contrast, SHARC has been improved by using separate memories for data and instruction. In addition, it includes a high speed I/O controller to support direct memory access (DMA). Furthermore, SHARC utilises shadow registers for all the CPU's registers. They are used to accomplish the interrupt quickly by moving the entire register contents to these registers in a single clock cycle.

SHARC ADSP-21364 has been selected to use the direct memory access (DMA) chaining facility, which allows the DMA controller to auto-initialize itself between multiple DMA transfers. A section of internal memory, called the transfer control block (TCB), is where the DMA attributes are stored for each DMA operation. A chain pointer is also associated with each DMA operation. Basically, the chain pointer (an address to a TCB) links one DMA operation to the next. To properly set up and initiate a chained DMA, the TCBs should first be set up with the appropriate attribute information. To enable the chained DMA, the DMA enable and chain enable bits in the corresponding DMA control register should be set simultaneously. The DMA controller will auto-initialize itself with the first TCB, then start the first transfer. When this transfer is over, if the current chain pointer register is non-zero, it will be used as a pointer to a new TCB and the process will begin again as shown in Table 2.1.

The challenge of any floating point architecture for the purpose of real-time application is the number of operations that can be carried out simultaneously. A benchmark has been used to express the speed of a microprocessor as a number. For example, [74] has pointed out that floating point devices can be specified by MFLOPS and MIPS to specify fixed point devices. This gauge is useful only in terms

Table 2.2: Receiver operation

Receiver stages	Additions	Multiplications
BPF	49	50
Symbol likelihood	102	31
Decoding	4698	627

of a single, known, processor architecture; so MIPS and MFLOPS is misleading [76] because the amount of processing required by an instruction can vary depending on the instruction format of that processor. Also, it ignores subscripting, memory traffic and the countless other overheads associated with program execution. However, it is useful to determine the minimum specifications of the platform. Therefore, in the current application, efforts have been focused on how many operations are performed in the receiver, where it contains the most complex parts such as iterative ACS in the SISO decoder. Table 2.2 demonstrates the number of operations (add and multiply) required for each stage in the receiver. It is noticeable from this table that the minimum number of operations are in the band pass filter (BPF) and maximum number of operations in the decoding stage. Therefore, using available DSPs could help in calibrating the system and make a first estimation of the required specification of the proposed system.

2.8 Chapter Summary

This chapter provides a background of a coded CP-OFDM system with an overview of the channel characteristics for wireless communication systems. A feature of the OFDM BICM-ID system is provided with a comparison in terms of performance against an uncoded OFDM system. The main characteristics of a multipath channel are explained. The key points in selecting the DSP platform are discussed in detail. Based on these aspects, the selection of an ADSP-21364 SHARC processor is justified.

Chapter 3

Low-complexity symbol-by-symbol Doppler shift compensation

In this chapter, low-complexity Doppler shift compensation techniques for OFDM-based UWAC receivers are proposed. Three techniques are demonstrated in this chapter in order to establish a base for developing further Doppler shift compensation algorithms. The first method is based on a one-shot estimation that independently manipulates the Doppler shift for each OFDM symbol within the packet. The second approach presents an algorithm to cope with a time variation of the Doppler shift between each OFDM symbol, depending on its preceding neighbours' values. This algorithm relies on the concept of the nearest neighbour rule to facilitate smoothing between symbols, and a dynamic symbol synchronization point to update the time scaling factor. To accomplish this, an adaptation step is derived, involving the weight of the nearest neighbour's time scaling in estimating the integer part of the re-sampling factor. The fractional part of the Doppler frequency shift is considered as a CFO. Based on this, a proposed approach that accommodates a broadband Doppler shift is devised. This algorithm exploits the integer and the fractional part of the time expansion/compression measured within a fraction of a sample period in each OFDM to jointly estimate the Doppler shift and its residual.

All aforementioned methods, instead of utilizing the whole guard interval, have exploited a finite length window of the cyclic prefix for correlation in each OFDM symbol in order to estimate the Doppler shift frequently. No iterative computation is required for the interpolation factor estimation. Furthermore, the proposed algorithms need to only buffer one OFDM frame before data demodulation, instead

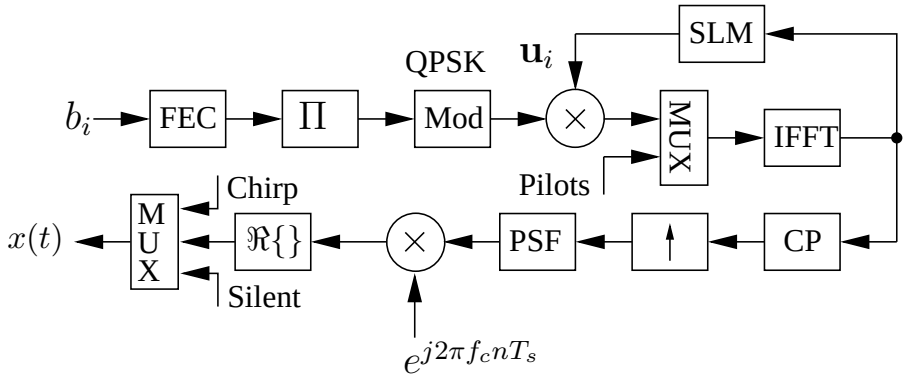

Figure 3.1: Proposed transmitter structure, where the operator $\Re$ represents the real part of the signal .

of buffering the whole data packet. Thus, it demands a lesser degree of complexity and memory requirements. Moreover, all proposed techniques rely on a single preamble of a packet consisting of multiple OFDM symbols to detect the start of the packet; hence, the throughput is increased. An experiment was conducted in the North Sea during 2009 and the algorithms were compared with the block Doppler compensation technique. Results revealed that there is variation in speed during the packet time; therefore, the proposed system surpasses the block technique. It was confirmed that the time scaling factor of the adaptive system was estimated for each OFDM symbol, whereas the block approach failed in estimating these variations.

3.1 OFDM system description

3.1.1 System and channel models

The proposed system to be investigated contains the transmitter depicted in Fig.3.1. At each instant i, the encoder receives a vector of information bits b_i of length K_d at its input to produce a binary code of length $K_c = K_d/R_c$ encoded bits, where $R_c \in (0, 1]$ is the coding rate of NSC code. The coded bits are permuted by a random interleaver, then converted in groups of m successive bits into alphabet symbols of constellation size $M = 2^m$. This mapping operation generates a sequence of $N_d = K_c/m : \mathbf{s} = \{s_0....s_{N_d-1}\}$, where $s_i \in \mathbb{C}$ and $\mathbb{C}$ denotes the set of complex symbols. Subsequently, in the OFDM symbol to be constructed, pilot symbols of phase shift keying (PSK) with unit amplitude are embedded with the data symbols in a comb method. These pilot symbols are used for the purpose of channel response estimation at the receiver. A PAPR reduction is introduced using the SLM technique [50]. To

implement this technique, a sequence of phases $\mathbf{U}$ are added in the transmitted signal to be multiplied by the input data sequences and the symbol sequence of minimum PAPR is selected for transmission. The resulting OFDM symbol, containing N_p pilots and N_d data-bearing sub-carriers, where $N_d + N_p = N_c$, is then modulated by an IFFT of size N_c and the last samples are copied and prefaced to the symbol to form the CP-OFDM frame. The guard interval of length N_g is chosen to be longer than the channel dispersion time in order to minimize the inter-symbol interference (ISI). The resulting frame is pulse shaped, using a pulse shape filter (PSF), and then up-converted using carrier modulation. Let T_d denote the OFDM symbol duration and T_g the guard interval. The total OFDM frame duration is $T = T_d + T_g$. Let $f_n = f_c + n\delta f$, being the carrier frequency corresponding to each of the sub-carriers of the OFDM spectrum, where $\delta f = 1/T_d$ is the frequency separation between alternate sub-carriers and f_c is the carrier frequency, so the bandwidth is $B = N_c \delta f$. The time-domain representation of the ith OFDM symbol is given by

$$x_i(t) = \frac{1}{\sqrt{N_{\mathrm{c}}}} \sum_{n \in \mathcal{I}} d_i(n) u_i^{opt}(n) e^{j2\pi \frac{n}{T_d}(t - T_g - iT)} p_{\mathrm{rc}}(t - iT), \quad \text{for } \; iT \leq t < (i+1)T, \tag{3.1}$$

where $d_i(n)$ is the symbol transmitted over the nth sub-carrier, $\mathbf{U}^{opt}$ is the optimum phase set $[u_i(1), u_i(2), ...u_i(n)]$ for lower PAPR with $u_i(n) = e^{j\varphi_n}$, $\varphi_n \in [0, 2\pi]$, $\mathcal{I}$ denotes the set of modulated sub-carriers and $p_{rc}(t - iT)$ is the pulse shaping filter, which is realized as an up-sampled raised cosine FIR filter. An equivalent passband model of (3.1) is

$$\begin{aligned} x(t) &= \Re \left\{ e^{j2\pi f_c t} \sum_{i=0}^{\infty} \frac{1}{\sqrt{N_{\mathrm{c}}}} \sum_{n \in \mathcal{I}} d_i(n) u_i^{opt}(n) e^{j2\pi \frac{n}{T_d}(t - T_g - iT)} p_{\mathrm{rc}}(t - iT) \right\}, \\ &= \Re \left\{ \sum_{i=0}^{\infty} \frac{1}{\sqrt{N_{\mathrm{c}}}} \sum_{n \in \mathcal{I}} d_i(n) u_i^{opt}(n) e^{j2\pi f_n (t - T_g - iT)} p_{\mathrm{rc}}(t - iT) \right\}, \end{aligned} \tag{3.2}$$

It is assumed that the signal is transmitted over a multipath fading channel characterized by

$$h(\tau, t) = \sum_{l=0}^{L-1} h_l(t) \delta[\tau - \tau_l(t)], \tag{3.3}$$

where $h_l(t)$ are the path amplitudes, $\tau_l(t)$ are the time-varying path delays and L is the total number of paths. As in [12], we assume the path delay τ_l and the gains h_l are constant over the frame duration T. For perfect OFDM synchronization, and providing that the maximum delay spread is within the guard interval, the received passband signal can be written as

$$\begin{aligned}\tilde{r}(t) =&\Re\left\{\frac{1}{\sqrt{N_c}}\sum_{n\in\mathcal{J}} d_i(n)u_i^{opt}(n)e^{j2\pi f_n t}\right.\\ &\left.\times\sum_{l=0}^{L-1} h_l\ p_{rc}(t-\tau_l)e^{-j2\pi f_n\tau_l}\right\}+\tilde{w}_i(t),\end{aligned} \tag{3.4}$$

where $w_i(t)$ is a white Gaussian noise with variance σ^2; hence down-conversion and removing the CP yields the received baseband signals which are thus expressed by

$$r(n)=\sum_{i=0}^{\infty}\sum_{n\in\mathcal{J}} H_i(n)x_i(n)+w_i(n), \tag{3.5}$$

3.1.2 Doppler shift in wideband communication

When the Doppler is present, a transmitted signal is received as:

$$r(t)=x[(1\pm\frac{v}{c})t-\tau_l], \tag{3.6}$$

where the (+) sign indicates an expansion of the signal since the distance is increased and vice versa. The magnitude of the spectrum of $r(t)$ can be written as

$$|R(f)|=|X[\frac{f}{(1\pm v/c)}]|. \tag{3.7}$$

Sampling at an integer multiple of the carrier frequency assuming zero Doppler and replacing the time index with k gives

$$r(k)=x(\frac{k}{f_s}-\tau_l). \tag{3.8}$$

With Doppler, the received signal is then given by

$$r(k)=x[\frac{k(1\pm\frac{v}{c})}{f_s}-\tau_l], \tag{3.9}$$

Adjusting the sampling frequency by the same Doppler shift gives a new sampling frequency of

$$f_s' = f_s(1 \pm \frac{v}{c}), \tag{3.10}$$

which forms a new received signal

$$r'(k) = x[\frac{k(1 \pm \frac{v}{c})}{f_s'} - \tau_l], \tag{3.11}$$

Substituting (3.10) in (3.11) yields,

$$r'(k) = x(\frac{k}{f_s} - \tau_l) = r(k). \tag{3.12}$$

At this point the results are identical and processing of the data can proceed as in the zero Doppler case.

For narrow-band signals, $(i.e, fc >> B)$, Doppler shift translates all OFDM sub-carriers by the same amount of carrier frequency, whereas in the case of wide-band signals, $(fc = 1.5B)$, Doppler shift translates each sub-carrier by a different amount. Let T_s be the sampling period: in such a case, the Doppler effect is modelled in discrete time as a complete sampling period scaling (interpolation or decimation) of the signal waveform [8]

$$r[kT_s] = x[k(1 \pm \Delta)T_s], \tag{3.13}$$

where, k is an integer, and $x(kT_s)$, $r(kT_s)$, are the sampled signals transmitted and Doppler shifted received sampled signals, respectively. This wide-band model results in an inevitable symbol timing error and CFO. Equivalent to (3.13), the Doppler shifted received frame is modelled by

$$L_f' = (L_f \pm \phi), \tag{3.14}$$

where $L_f = \frac{N_c}{B \cdot T_s}$ represents the transmitted passband samples' length and L_f' is the Doppler shifted received passband samples' length. To remove both CFO and symbol shift, an inverse time scaling of the received (compressed/expanded) signal should be achieved, providing that the amount of Doppler shift Δ is known. This is equivalent to changing the sampling rate of the passband signal by $1 + \Delta$ in discrete-

time processing. From (3.14), it can be inferred that increasing or decreasing the length of samples is equivalent to re-sampling the sampling frequency f_s by $1 + \Delta$; thus an equivalent to (3.13) is rewritten as

$$f_s = f_s'/(1 \mp \Delta). \tag{3.15}$$

We assume that all paths have a similar Δ, therefore the received signal in (3.4) can be rewritten as

$$\begin{aligned} \tilde{r}(t) =& \Re \left\{ \frac{1}{\sqrt{N_c}} \sum_{n \in \mathcal{J}} d_i(n) u_i^{opt}(n) e^{j2\pi f_n (1+\Delta) t} \right. \\ & \left. \cdot \sum_{l=0}^{L-1} h_l \; p_{rc}((1+\Delta)t - \tau_l) e^{-j2\pi f_n \tau_l} \right\} + \tilde{w}_i(t), \end{aligned} \tag{3.16}$$

The passband signal model in (3.16) is modulated at f_c, thus the corresponding baseband model $r(t)$ such that $\tilde{r}(t) = \Re\left\{r(t) \cdot e^{j2\pi f_c t}\right\}$ can be written as

$$\begin{aligned} r(t) =& \sum_{n \in \mathcal{J}} d_i(n) u_i^{opt}(n) e^{j2\pi n \delta f t} \; e^{j2\pi \Delta f_n t} \\ & \cdot \sum_{l=0}^{L-1} h_l \; p_{rc}[(1+\Delta)t - \tau_l] \; e^{-j2\pi f_n \tau_l} + w_i(t) \\ =& \sum_{i=0}^{\infty} \sum_{n \in \mathcal{J}} H_i(n) d_i(n) u_i^{opt}(n) e^{j2\pi n \delta f t} e^{j2\pi \Delta f_n t} + w_i(t), \end{aligned} \tag{3.17}$$

where $H_i(n)$ is the channel transfer function of the ith symbol at nth sub-carrier and can be written as

$$H_i(n) = \sum_{l=0}^{L-1} h_l \; e^{-j2\pi f_n \tau_l} \; p_{rc}\left[(1+\Delta)t - \tau_l)\right]. \tag{3.18}$$

3.2 Doppler compensation techniques

3.2.1 Block length-based Doppler compensation

In order to compensate the Doppler shift on a received signal, it is necessary to adopt a method that is capable of estimating the interpolation factor and then apply its

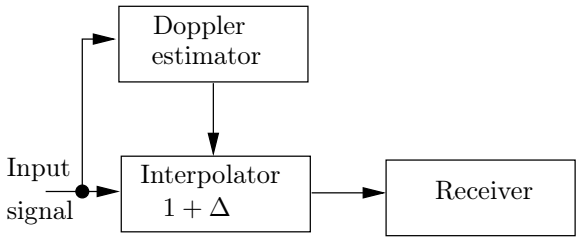

Figure 3.2: Open loop Doppler correction.

inverse on the received signal. This system is shown in Fig. (3.2) [8]. This approach provides a generic preprocessor that can be used with wide-band receiver structures. The interpolator structure can be used either on bandpass or baseband signals. For a complex baseband interpolator structure, the carrier frequency offset must be removed prior to demodulation. Baseband interpolation offers a considerable computational saving for relatively narrow-band signals; however, for an underwater communication system, which is inherently broadband, this saving is not significant.

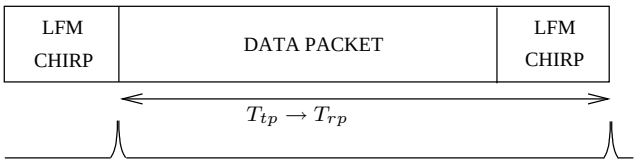

Figure 3.3: Packet length measurement using chirp correlation.

Therefore, the target is to estimate the interpolation factor Δ precisely. In [8], a novel block length-based approach was presented in order to estimate the Doppler shift for single carrier transmission by comparing a prior knowledge of the transmitted data packet duration (T_{tp}) with the received Doppler shifted packet (T_{rp}), as shown in Fig. (3.3). The Doppler shift estimate $\hat{\Delta}$ can be written as

$$\hat{\Delta} = \frac{T_{rp}}{T_{tp}} - 1. \tag{3.19}$$

This equation can be considered as a coarse estimation of the Doppler shift for both single and multi-carriers transmission.

Block length-based algorithm can be summarised for an OFDM system as follows:

1. Design a chirp signal of duration $\geq$ 50 ms with a bandwidth in the range $[f_c - B/2, f_c + B/2]$.

2. Formulate a packet that contains 10 OFDM symbols with a chirp at the pre and post-amble. A silent period of the same LFM duration is set after and

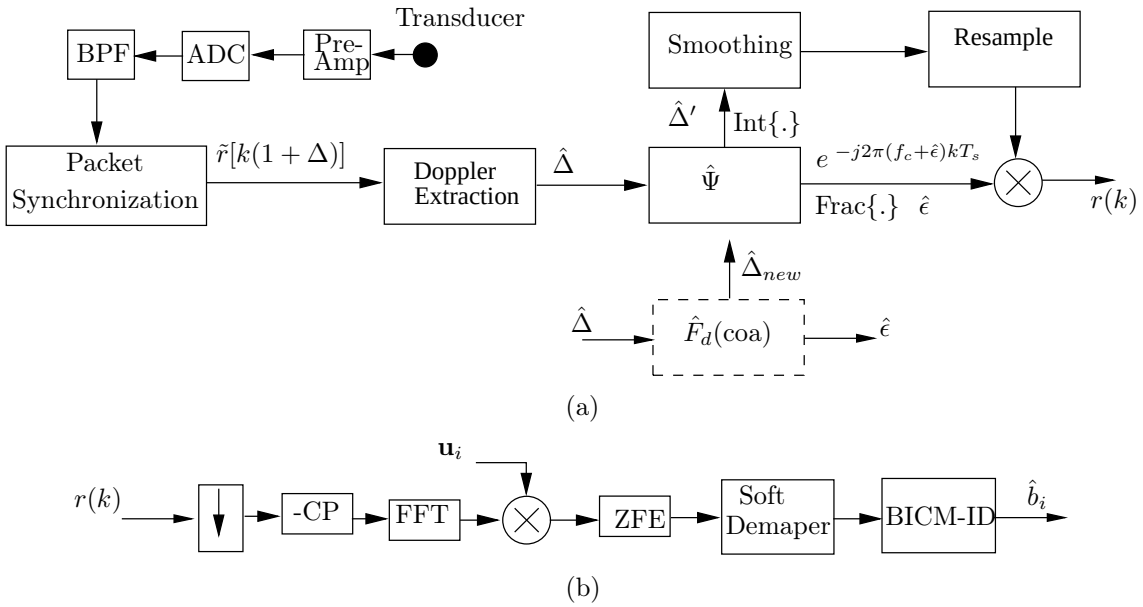

Figure 3.4: Receiver structure of the proposed system.

before the pre-amble and post-amble, respectively.

3. For simulation purposes, set an array of different speeds in accordance with each OFDM symbol in the transmitted packet.

4. FIR correlate the received signal with the LFM signal to detect the maximum peaks that associate the pre-amble and post-amble chirps.

5. Apply (3.19) to estimate the interpolation factor.

In the block length based approach, the resolution of the Doppler shift estimation is proportionate to the packet duration. It is worth mentioning that this approach is very accurate for a fixed speed situation, in which the estimated speed represents the average or the mid-point of the packet. However, this case is not pragmatic, particularly in a medium range, where the Doppler spreads are already found undersea, regardless of the system's mobility [4]. Additionally, in the OFDM systems, as the sub-carriers' bandwidths are mostly tight, such a method is not considered due to the residual Doppler shift or CFO impairments. Therefore, all suggested techniques in this thesis consider the CFO to achieve reliable communication.

3.2.2 One-shot Doppler shift compensation

The receiver structure of the suggested technique is depicted in Fig. (3.4). In the preprocessing stage, a bandpass filter 8-16 kHz is designed to remove unwanted

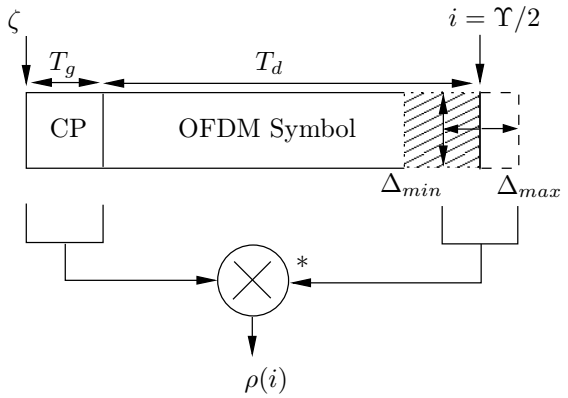

Figure 3.5: Correlation operation in (3.21), ζ and $i = (\frac{\Upsilon}{2})$ represent the leading and trailing edge of the OFDM frame, respectively.

sidelobes. After bandpass filtering, the received samples are passed through a FIR-correlator to detect the start of the packet. The resulting Doppler shifted samples $\tilde{r}[k(1+\Delta)]$ are then given as input to the Doppler extraction unit (DEU).

In one-shot algorithm, the Doppler shift is estimated on symbol-by-symbol basis and independently. This method estimates the Doppler shift and its CFO based on the estimated Doppler shift $\hat{\Delta}$ of the current OFDM symbol only, regardless of a change in the speed from symbol to symbol during the packet time. In order to estimate the re-sampling parameter $\hat{\Delta}$, the DEU mentioned earlier is designed to comprise two main stages that are employed as a preprocessor for all techniques in this chapter. These stages will be explained in detail in the following sections.

3.2.2.1 Coarse Doppler estimation

Due to the Doppler effect, errors in the symbol timing will be increased or decreased proportionally to Δ. To align the symbol within its period, samples should be removed, if $(\Delta > 0)$, or added, if $(\Delta < 0)$, at regular intervals [77]. For an OFDM symbol with N_c =1024 sub-carriers and Δ =0.0013, the OFDM symbol drift will be $\pm$15.97 samples per OFDM symbol, which is equivalent to a Doppler shift of 15.6 Hz. Therefore, with these samples' drift, there is no need to consider the whole CP window; hence a massive reduction in complexity is obtained.

Accordingly, the redundancy introduced by the guard interval is exploited and the drift in the received passband samples is measured by correlating the first N_g samples with the anticipated observation window denoted by Υ. Let $\tilde{r}_g = [r[0]...r[N_g]]$ be a vector of N_g received samples, known as guard vector, $\tilde{r}_\phi$ be a vector of the received samples within the observation window and ζ denote the

frame *synchronization point*, as shown in Fig. (3.5), therefore

$$r_D = [\zeta + N_c - (\frac{\Upsilon}{2}) + i, \zeta + N_c + N_g - (\frac{\Upsilon}{2}) + i], \tag{3.20}$$

is the search range of the useful block, where Υ is an even integer and $\forall i \in \Upsilon$. In (3.20), it is apparent that when $i = (\frac{\Upsilon}{2})$, the OFDM symbol is received within its period; otherwise the frame length drifts by ϕ samples. In the proposed estimator, the covariance between $\tilde{r}_g$ and $\tilde{r}_\phi$ is exploited through the observation window to detect the peaks ρ as

$$\rho(i) = |\sum_{n=0}^{N_g-1} \tilde{r_g}(n)\tilde{r_\phi}^*(\zeta + n + N_c + i)|, \tag{3.21}$$

where both $\tilde{r}_g$ and $\tilde{r}_\phi$ are real samples. It should be noted that the envelope of the correlation must be smoothed in order to improve detection.

3.2.2.2 Peak localization

Undesired correlation sidelobes are produced due to the inhomogeneities of the signal fragment window r_D with the guard interval. These inhomogeneities occur due to the correlation of different data symbols which are affected by the existence of ISI. Consequently, the correlation produces uncertainty in the peak location, depending on the channel conditions. This time position uncertainty in the maximum peak will pose significant fluctuation in estimating the symbol timing offset. To tackle this random process, the proposed algorithm adopts a threshold and utilizes a weighted centroid algorithm [78]. It is assumed that Γ_{th} represents this threshold. Due to the difficulty of determining Γ_{th} analytically, it has been chosen empirically,

$$\Gamma_{\text{th}} = \frac{\max\{\rho\}}{2}. \tag{3.22}$$

Thus, all peaks that exceed this threshold are accumulated in a temporary buffer w_i. This will enable the positional approximation of the weights within the split-buffer to be determined. Let μ_i be a vector of these time positions; hence the coordinates of all peaks that attain Γ_{th} can be formulated as

$$\mu_{\mathbf{i}} = \arg\{\rho(i) > \Gamma_{\text{th}}\}, i = 1 \ldots n. \tag{3.23}$$

After the peak's locations have been gathered, along with its corresponding weight, the goal is to estimate the unknown position $\hat{P}(\mu_i, y_i)$ of the maximum Doppler shift which is equivalent to the time expansion/compression in the OFDM frame. Let y_i denote the weights w_i (amplitude) reserved in a split-buffer which corresponds to each location; it follows that the time position of the maximum Doppler shift can be approximated as

$$\hat{P}(\mu, w) = \frac{\sum_{i=1}^{n} w_i \mu_i}{\sum_{i=1}^{n} w_i}, \tag{3.24}$$

and this correlational behaviour is called *localization* [79]. It should be stressed that the estimation error of $\hat{P}(\mu, y)$ results in timing misalignment and, consequently, it degrades the FFT demodulation.

In order to estimate the time scaling factor, it is necessary to estimate the timing offset of the OFDM block $\hat{\phi}$, which can be derived based on (3.24) as

$$\hat{\phi} = (\frac{\Upsilon}{2}) - \hat{P}(\mu, w). \tag{3.25}$$

This timing metric is estimated independently on a symbol-by-symbol basis. In the case of no gradient, a unique Doppler shift estimation for each symbol, based on the estimated timing offset, is a feasible solution. However, in a worse case such as velocity acceleration, this approach does not hold because the timing offset changes over time. The next section will present this situation.

The Doppler shift manifests itself as a complete time expansion/compression, therefore it can be estimated using (3.25)

$$\hat{\Delta} = \frac{L_f}{L_f \pm \hat{\phi}}, \tag{3.26}$$

where the transmitted frame length L_f is known. For the sake of simplicity, only the sign (+) will be considered in this chapter. The parameter in (3.26) represents the Doppler shift based on a one shot estimation that can be divided into an integer part in order to re-sample the received signal and a fractional part for CFO.

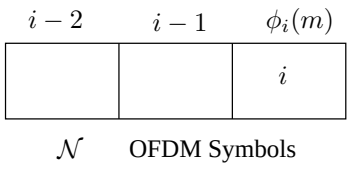

Figure 3.6: A set of OFDM symbols showing the closed and far neighbour to symbol i. At time n, symbol i estimates $\phi_i(n)$

3.2.3 Adaptive Doppler compensation

So far, the timing metric and its associated Doppler shift, have been estimated on a symbol-by-symbol basis and assumed to be independent; thus it was called one-shot algorithm. An alternative adaptive system is suggested in order to estimate these parameters in accordance with their preceding neighbours' values. This approach aims to design a basis that can accommodate a more realistic situation than one-shot algorithm by considering the speed change between OFDM symbols. As in the preceding scheme, the coarse Doppler shift is estimated using (3.26). On the other hand, by utilizing the concept of the nearest neighbour rule [80], this Doppler shift is further performed to deal with a slow Doppler variation during the OFDM symbol. To formulate the adaptation step, the following assumption is adopted:

Assumption 1: Due to the Doppler shift, the OFDM symbol could be expanded towards the *far edge* or compressed in the opposite direction. That means estimating the average Doppler shift (i.e., at the middle) as in the block length-based approach is not hold.

In both cases, the edge between the current symbol and its nearest neighbour should be smoothed to mitigate both the channel and the noise effects. After taking into consideration a set of $\mathcal{N}$ OFDM symbols, the adaptation equation for the symbol timing is

$$\hat{\phi}(n) = \sum_{p=0}^{p-1} W(n-p)\hat{\phi}(n-p), \tag{3.27}$$

where $W(n-p)$ is a weighting coefficients vector of $p \in \mathcal{N}$ symbols. The first symbol, which is estimated in (3.25), excludes this equation as it contributed to the initialization process. Thus, start initializing $\hat{\phi}(n-1)$=0, $\hat{\phi}(n-2)$=0, and for each OFDM symbol repeat

$$\hat{\phi}(n-2) = \hat{\phi}(n-1);\ \hat{\phi}(n-1) = \hat{\phi}(n). \tag{3.28}$$

3.2.3.1 Weighting coefficients

Although there are many possible choices of *weights* W in the literature [81], the weighting coefficients in this approach have been chosen in accordance with the concept of *nearest neighbour rule* [80] and the premised acceleration. To be more specific, the following assumption should be taken into consideration:

Assumption 2: If the OFDM symbol time T_d is 256 ms, then it needs approximately $4T_d$ to accelerate the speed to (1 m/s), providing the initial speed is zero and the acceleration is (1 m $/s^2$).

From this assumption, we can infer that the maximum speed in each OFDM symbol is approximately ± 0.25 m/s, i.e., within the symbol time. This leads to the use of the concept of *nearest neighbour rule* [80], where the cardinality [81] is proportional to how close the neighbour symbol is to the current one. This is practically true and therefore assigning the nearest symbol $\phi(n-1)$ higher weight, means that its reliability is high on the assumption that the Doppler shift is variable from symbol to symbol, while the weight decreases with time. All of these assumptions are made because the change of the Doppler shift, or the symbol timing offset between previous OFDM symbols, will contribute to predicting the subsequent values; hence, resorting to involve preceding symbols in order to reinforce the estimation accuracy of the current parameters. Consequently, each OFDM symbol can be assigned a weight; however, this is inexpedient due to the convergence speed. Alternatively, a dedicated group of symbols from the transmitted packet is considered as shown in Fig. (3.6). This group consists of only the information related to the two previous symbols' timing metric with their weights to be involved in estimating the new timing metric. This weighting vector of tripartite coefficients should satisfy

$$0 < W_i < 1, \sum_{i=1}^{p} W_i = 1 \ \forall i \in n, W(n-p) = 0 \text{ if } p \notin \mathcal{N}, \tag{3.29}$$

where, p represents the number of symbols in the group. Therefore, smoothing $\hat{\phi}$ in (3.27) by using the coefficients in (3.29) contributes to improvements in the Doppler shift estimation. It is worth mentioning that these weighting coefficients can also be utilized to smooth the Doppler shift and the following sections will discuss this case.

3.2.3.2 Fractional CFO Estimation

Thus far, only the time scaling factor has been estimated. Based on this factor, the coarse estimation of the Doppler frequency shift, as shown in Fig. (3.4), is then approximated as

$$\hat{F}_{d\ (\mathrm{coa})} = (1 - \hat{\Delta}) f_c. \tag{3.30}$$

This parameter represents the integer part of the Doppler shift obtained by the adaptive algorithm as shown in Fig. (3.4)(a), where it is assigned a dashed square. In order to only re-sample the integer part, this coarse estimate is quantized. Let $\lfloor . \rfloor$ denote rounding toward the lower integer, then $F_{d\ (\mathrm{quant})} = \lfloor \hat{F}_{d\ (\mathrm{coa})} + 0.5 \rfloor$, and

$$\hat{\Delta}_{\mathrm{new}} = \frac{f_c - \hat{F}_{d\ (\mathrm{quant})}}{f_c}. \tag{3.31}$$

An efficient sample-by-sample linear interpolation method is used in the receiver to re-sample the OFDM block with a re-sampling factor $\hat{\Delta}_{\mathrm{new}}$. r'_k can be expressed mathematically as

$$r'(k) = (\Delta_n - 1)\, \tilde{r}_{m'+1} + \Delta_n\, \tilde{r}_{m'}, \tag{3.32}$$

where $m' \in \{1, 3, 5...\}$, $k \in \{1, 2, 3...\}$ and $\Delta_n = 1$ for $n = 1$.

The subsequent stage is to compute the residual Doppler shift $\hat{\epsilon}$ based on the coarse frequency estimation.

$$\hat{\epsilon} = \hat{F}_{d\ (\mathrm{coa})} - F_{d\ (\mathrm{quant})}. \tag{3.33}$$

After re-sampling and CFO compensation, the channel estimation was implemented using the least square (LS) method.

It is obvious from (3.30) and (3.33) that the carrier frequency contributes in the estimation of the Doppler shift and then in the estimation of its residual. However, involving the carrier frequency in estimating such parameters for a channel of a broadband nature results in an inaccurate approximation of these parameters; therefore, an ICI is produced and, consequently, it is necessary to resort to exploiting the sample time expansion/compression in order to increase the accuracy and ultimately improve performance.

3.2.4 Proposed Doppler shift compensation

Unlike preceding schemes, the proposed technique derives the Doppler shift based on a sampling frequency estimate.

As the Doppler shift is evidenced by a frame time expansion/compression [8], it can be inferred that the rate of sampling frequency will be changed. Accordingly, joining the samples' drift, in estimating the Doppler shift and CFO, is now feasible. To accomplish this, let κ be the sampling frequency offset of one sample drift caused by an expansion, which can be formulated as

$$\kappa = f_s(\frac{L_f + 1}{L_f}) - f_s, \tag{3.34}$$

therefore, the relative sampling frequency offset $\hat{\Psi}$ is given by

$$\hat{\Psi} = \frac{(1 - \hat{\Delta})f_s}{\kappa}, \tag{3.35}$$

where the coarse Doppler shift is approximated as in (3.26). Clearly, a $\Delta \neq 1$ causes a sampling frequency error; hence a drift in the symbol timing. Therefore, the relative offset in (3.35) represents the samples' drift which causes the timing error. To perform Doppler shift compensation, the samples' drift is exploited and divided into an integer part and a fractional part. The integer part, $\hat{\Psi}_{(\mathrm{I})}$ is used to estimate a new interpolation factor and is given by

$$\hat{\Delta}' = \frac{L_f - \hat{\Psi}_{(\mathrm{I})}}{L_f}, \tag{3.36}$$

where $\hat{\Psi}_{(\mathrm{I})} = \lfloor \hat{\Psi} \rfloor$ is rounded toward the lower integer.

At the same time, the fractional part $\hat{\Psi}_{(\mathrm{F})}$ is exploited to estimate the CFO, where the fractional deviation of the samples' drift is approximated as

$$\hat{\Psi}_{(\mathrm{F})} = (\hat{\Psi} - \hat{\Psi}_{(\mathrm{I})}), \tag{3.37}$$

It can be noticed that the main factor which destroys the orthogonality is the fractional drift of the sub-carrier spacing δf. This is based on the misalignment of the symbol which degrades the FFT demodulation and consequently an inter-carrier interference (ICI) will result.

Hence, estimating the fractional drift in (3.37) is crucial to the approximation of

the CFO, where

$$\hat{\epsilon} = \hat{\Psi}_{(\mathrm{F})} \cdot \kappa \cdot (\frac{f_c}{f_s}), \tag{3.38}$$

is the residual Doppler shift. Subsequently, compensating for $\hat{\epsilon}$ in (3.16) after re-sampling, we obtain

$$\tilde{r}(t) = \tilde{r}(t)e^{-j2\pi\hat{\epsilon}}, \tag{3.39}$$

where in this case, the orthogonality is preserved. It should be stressed that this is an approximation of the ICI free received signal.

3.2.4.1 Doppler shift variation adjustment

Due to the wideband nature of the UA channels, each sub-carrier will be shifted non-uniformly [12]. Furthermore, if the relative velocity between the innermost and the outermost edge of the symbol were not constant (i.e., with acceleration) over the symbol duration, then an error in Doppler estimation will result and will need to be considered. Hence, adjusting this velocity perturbation necessitates frequent estimations of the re-sampling factor or reduction of the symbol length. However, in OFDM signal design there is a trade-off between the number of sub-carriers, carrier frequency, scaling factor resolution and complexity. In such cases, reducing the symbol length does not only cause a reduction in the bandwidth efficiency, but also mitigates the immunity against the ISI. In this method, there is a compromise between these system specifications. These circumstances of speed variations are dealt with by employing weighting coefficients to smooth the edges between symbols. These coefficients are chosen based on the principle of the nearest neighbour rule, discussed earlier. Consider a set of $\mathcal{N}$ OFDM symbols; the adaptation equation for the Doppler shift is

$$\hat{\Delta}(n) = \sum_{p=0}^{p-1} W(n-p)\hat{\Delta}(n-p), \tag{3.40}$$

where $W(n-p)$ is a weighting coefficients vector of $p \in \mathcal{N}$ symbols. The Doppler shift of the first symbol, which is estimated in (3.36), excludes this equation as it contributes to the initialization process. Thus, start initializing $\hat{\Delta}(n-1)$=0, $\hat{\Delta}(n-2)$=0, and for each OFDM symbol time n repeat Algorithm 1. The receiver then re-samples the OFDM symbol with a re-sampling factor obtained after smoothing.

input : Set weighting coefficients W_1, W_2, W_3 such that $\sum W_i = 1$
output: A smoothed Doppler shift $\hat{\Delta}'_{\mathrm{n}}$

$Temp \leftarrow \hat{\Delta}'_n$// <*Temp* is a temporary buffer>
if $Flag > 1$ **then** // <*Flag* represents the symbol index>
  $\hat{\Delta}'_n \leftarrow \hat{\Delta}'_n W_1 + \hat{\Delta}'_{n-1} W_2 + \hat{\Delta}'_{n-2} \cdot W_3$
  else
  if $Flag = 1$ **then**
    $\hat{\Delta}'_n \leftarrow \hat{\Delta}'_n W_1 + \hat{\Delta}'_{n-1} W_2$
  end
end
$\hat{\Delta}'_{n-2} \leftarrow \hat{\Delta}'_{n-1}$; $\hat{\Delta}'_{n-1} \leftarrow Temp$

Algorithm 1: Smothing algorithm

Algorithm 1 is also applied to smooth the timing offset $\hat{\phi}$. It is worth pointing out that the weighting coefficients W_1, W_2 and W_3 are empirically obtained.

3.2.4.2 Fine timing estimation

There is a noticeable degradation in the FFT demodulation due to the fractional part ψ which accompanies $\hat{\phi}$ in (3.9). Accordingly, this part is considered for the purpose of updating the *synchronization point* ζ. Therefore, starting with $\hat{\psi}_m^{[0]}$=0, and then for each OFDM symbol m in the packet, repeat

$$\hat{\phi}_m = \hat{\phi}_m + \hat{\psi}_m, \tag{3.41a}$$

$$\hat{\zeta}_{m+1} = \hat{\zeta}_m + \lfloor \hat{\phi}_m \rfloor + L_f, \tag{3.41b}$$

$$\hat{\psi}_m = \hat{\phi}_m - \lfloor \hat{\phi}_m \rfloor, \tag{3.41c}$$

where the operator $\lfloor . \rfloor$ denotes truncation to the nearest integer.

3.2.4.3 Channel estimation and decoding

After re-sampling and CFO compensation, the channel estimation is implemented using the least square (LS) method.

$$\hat{H}_p(n) = D[X_p(n)]^{-1} Y_p(n),\ n = 0 \ldots N_p - 1, \tag{3.42}$$

where $\hat{H}_p(n)$ are the estimated pilot channel values, $D[X_p(n)]$ is a diagonal matrix constructed using the known transmitted pilot symbols, and $Y_p(n)$ are the received

Table 3.1: Correlation complexity estimates.

Operation	Proposed
Add	$8 \times \Upsilon$
Multiply	$N_g \times \Upsilon$

pilot symbols after the FFT operation. After removing the channel effect, the signal is then passed through the soft de-mapper to produce the extrinsic estimates to be deinterleaved and then applied to the BCJR algorithm in order to decode convolutional codes. The output of the BCJR in the first iteration is fed to the cyclic-redundancy-check (CRC). Accordingly, the symbols with errors can be corrected by re-encoding the detected information from the first iteration. This procedure is called BICM-ID.

3.2.4.4 Complexity analysis

It is now appropriate to consider the computational complexity of (3.20) and (3.21) for the proposed method in estimating the Doppler shift. In this analysis, a conventional approach is followed where the number of operations, such as addition and multiplication, are counted as a benchmark for this purpose. It is worth pointing out that the proposed algorithm is implemented in passband, and therefore the benchmark for real operations only. Furthermore, the proposed method requires no iteration to estimate the Doppler shift. Table 3.1 shows the complexity estimation of the proposed technique.

3.3 Simulation Results

The performance of the proposed system was tested over a multipath channel impulse response, $h(n) = 0.6708\delta(n) + 0.5\delta(n-1) + 0.3873\delta(n-2) + 0.3162\delta(n-3) + 0.2236\delta(n-4)$, and the corresponding delays at time n to $n-4$ were $0, 2.5, 5, 7.5, 10$ ms. In these simulations, transmission was organized in packets of equal duration, each containing single 50 ms LFM followed by a 12.5 ms silent period, and then 10 CP-OFDM frames as shown in Fig (3.7). A total of 8920 information bits were transmitted in each setting. The carrier frequency was set to 12 kHz, whereas the sampling frequency was $f_s = 4f_c$. N_c =1024 sub-carriers were used along with

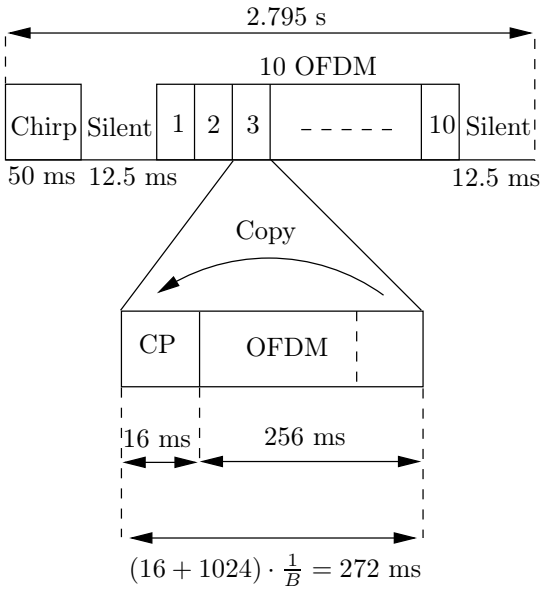

Figure 3.7: Packet structure for $N_c = 1024$.

bandwidth B =4 kHz, which led to a sub-carrier spacing of 3.90625 Hz. The guard interval was set as T_g =16 ms. A rate 1/2 NSC code and interleaver was adopted in this simulation to map 892 data bits to 1792 interleaved bits. The achieved data rate [82] was 3.2794 kb/s

$$R = \frac{R_c N_d \log_2 M}{T_g + T_d}, \tag{3.43}$$

and the bandwidth utilization factor was 0.8198 bits/sec/Hz for the QPSK modulation scheme.

$$\varrho = \frac{R}{B} \quad \text{bits/sec/Hz.} \tag{3.44}$$

Fig. (3.8) shows the performance comparison of the CP-based Doppler shift compensation between one-shot and the algorithm in [1]. The channel frequency and phase responses are depicted in Fig. (3.8)(a) and used for both algorithms to unify the comparison. It can be shown that the centroid-based normalization of the CP-based correlation in estimating the Doppler shift outperforms the estimation algorithm in [1]. In addition, due to the computational unlimited search on the angle of the correlation, it can be inferred that the proposed scheme reduces complexity and is more pragmatic than [1]. Fig. (3.9) shows the CP-correlation output in the proposed scheme and its smoothing to improve the detection of the maximum peaks. However, these correlation peaks are affected by the ISI and the Doppler shift variation between symbols.

A comparison between the proposed system and the block Doppler technique

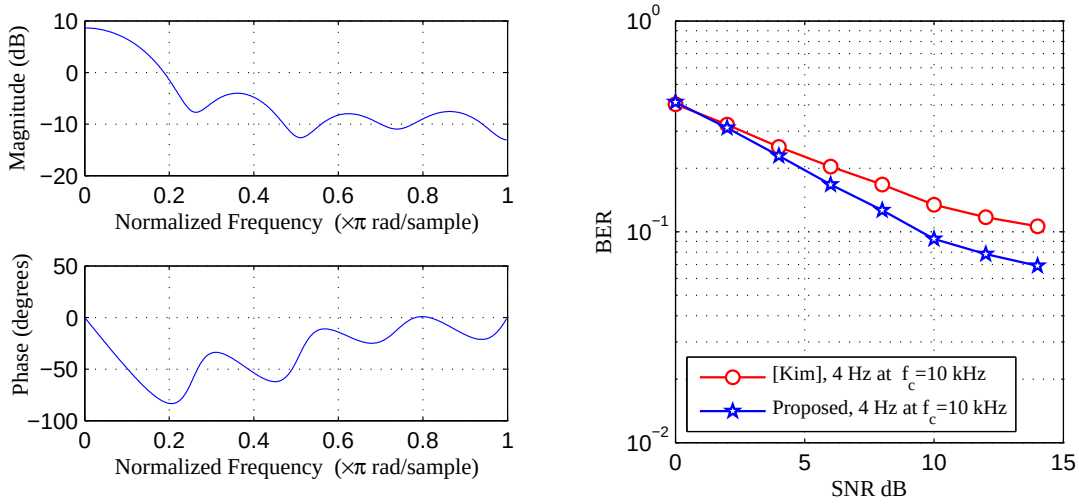

(a) CIR. (b) BER

Figure 3.8: Performance comparison between one-shot algorithm and the algorithm proposed by Kim in [1].

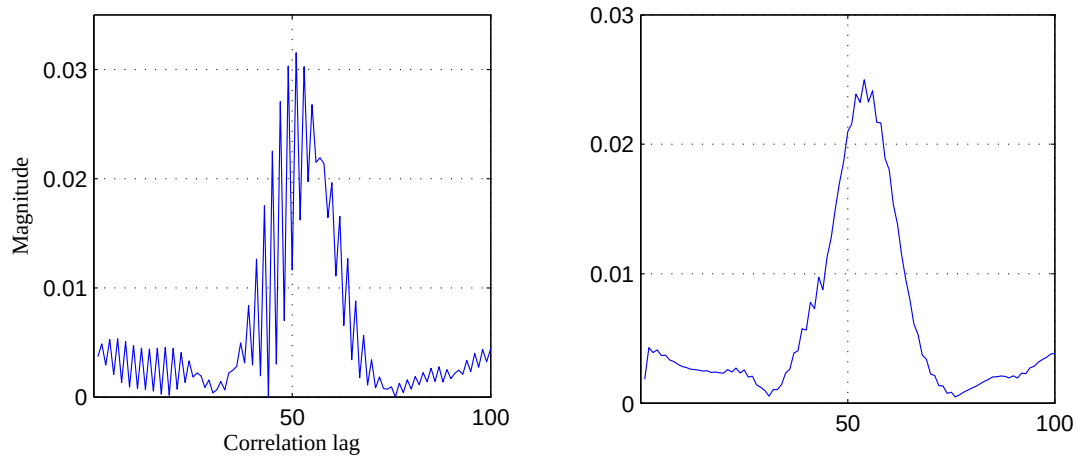

(a) Before smoothing. (b) After smoothing

Figure 3.9: Anticipated correlation window before and after smoothing for packet 1, symbol 3 at speed -0.25 m/s from the experiment.

was made using variable and fixed speeds during the packet time. To investigate each OFDM symbol, an array of speeds was set to equal [1 1 1 2 2 2 0.5 0 1 1] and [1 1 1 1 1 1 1 1 1 1] m/s for both variable and fixed speeds, respectively.

The BERs of the simulation are plotted in Fig.3.10, which indicates that the block Doppler compensation technique outperforms adaptive approach by about 2 dB in a fixed speed and moderate SNR. This is because the length of time left between two LFMs increases the resolution of the average scaling factor estimate; hence,

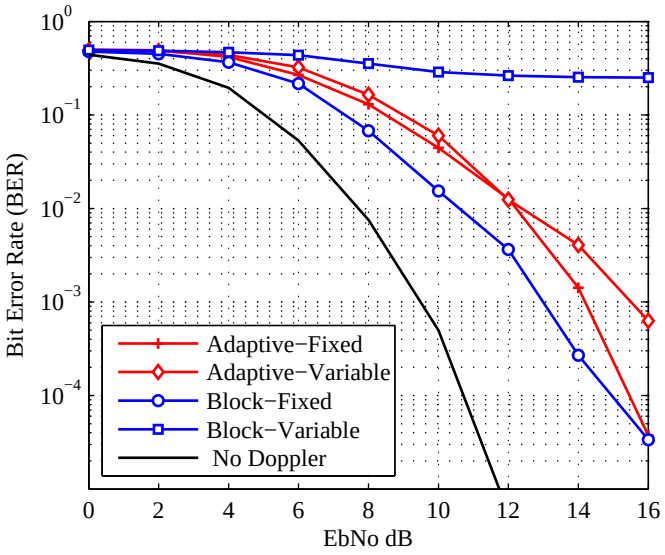

Figure 3.10: Performance comparison between the adaptive scheme and block Doppler compensation for fixed and variable speeds.

the Doppler shift estimate at the mid-point is approximately equal to the actual speed. Furthermore, since the bandwidth is comparable to the carrier frequency in a broadband Doppler shift, it follows that employing this frequency in estimating the CFO cannot be accounted by the receiver. On the other hand, the block technique fails to track the Doppler variation from symbol to symbol because the average estimate is no longer capable of tracking the variation between each OFDM symbol.

3.4 Experimental Results

3.4.1 Experiment setup

During the summer of 2009, an experiment was conducted in the North Sea to evaluate the system performance. The trial setup is illustrated in Fig. (3.11). The transmitter and receiver were set at 10 and 5 m from the sea surface, respectively. The transmitter power was set to 180 dB re 1μPa. There was a rapid time varying multipath channel in that area due to the hard surface of the seabed. In the trial, transmission was organized in packets of equal duration, each containing one 50 ms LFM followed by a 12.5 ms silent period, and then 10 CP-OFDM frames. A total of 8920 information bits were transmitted in each setting. A total of 20 packets of 2.795 s were sent. The carrier frequency was set to 12 kHz, whereas the sampling frequency was $4f_c$. 1024 sub-carriers were employed and the system bandwidth was

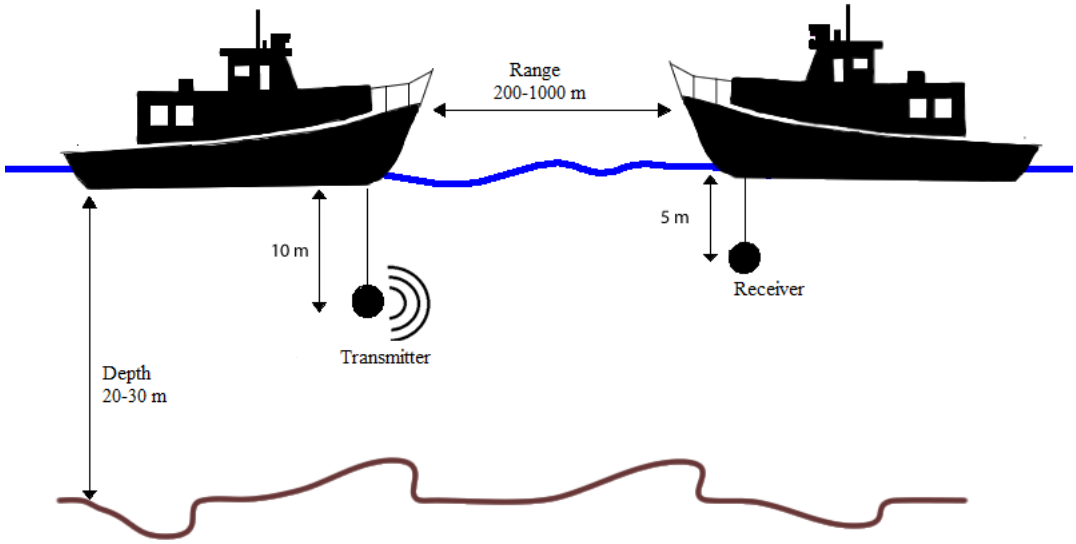

Figure 3.11: Configuration of the experiment in the North Sea.

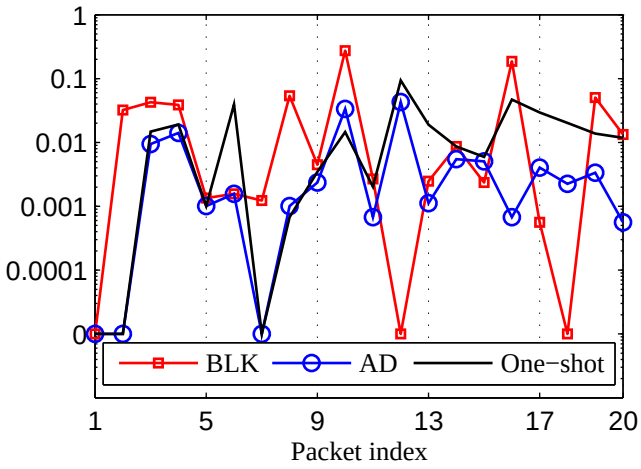

Figure 3.12: Bit error rate over each packet of 8920 bits.

4 kHz, which led to a sub-carrier spacing of 3.90625 Hz. The guard interval was set as T_g =16 ms.

3.4.2 Performance evaluation

Fig. (3.12) shows the BERs performance comparisons of the block, one-shot and adaptive techniques. It is obvious from this figure and clarified in Table 3.3 that the adaptive algorithm which employs the weighting coefficients outperforms block length-based and one-shot methods by 83.6383, 63.9932 %, respectively. At the

same time, Table 3.3 shows that one-shot algorithm surpasses block length-based approach by 54.5594 %. It can be seen from Fig. (3.12) that only the packets (12, 18) have high decoding errors and no significant reduction in the bit error rate was found with the adaptive technique compared with the block method. This is due to an error in estimating the time scaling factor due to the noise and the channel which caused an ambiguity in estimating the Doppler shift at a fixed speed. Looking at Fig. 3.13, it is apparent that the speed of packet (P12) was fixed; thus, estimation of the average Doppler shift during a long packet time is approximately equal to the actual value, and consequently the block technique outperforms our adaptive algorithm. Fig. 3.15 presents, however, evidence that there was a variation in the speed during the packet time; therefore, the adaptive technique surpasses the block method. This is evidenced by Fig. 3.13, where the time scaling factor of the adaptive technique in packet 2 (P2-AD) has been estimated for each OFDM symbol; whereas in the same packet, the block approach (P2-BLK) fails in estimating this variation. Furthermore, compared with a one-shot approach which processes symbol-by-symbol independently, it is shown in Fig. 3.13 that there is an improvement in the performance due to the adoption of the weighting coefficients that smooth the estimated parameters. Locking at Fig. 3.14, in the uppermost graph, it is apparent that the scaling factors for packets (P6, P12) were changing in one direction at what can be considered semi-fixed speeds, thus, estimation of the average speed during long packet time indicates that the block technique is outperforming our proposed system. Furthermore, it is obvious from this figure, in the lower graph, that the scaling factors of (P16, P10) have been changed from compression to expansion or vice versa during the packet time. In packet 5, it is clear that the Doppler shift is very small; therefore the algorithms have similar performances.

Turning now to the experimental evidence on the performance of the proposed technique, the technique combines the measuring of the time expansion/compression of the sample period and utilization of the weighting coefficients in estimating and smoothing the Doppler shift, respectively. To evaluate the performance, a comparison of the proposed algorithm and the block method are depicted in Fig. (3.16)(a). It is apparent that the suggested method surpasses the block technique in 18 out of 20 packets. In the proposed scheme, it can be seen that only in packets (6, 12) are the BERs high compared with the block technique. This is a synchronization issue, where the proposed algorithm is based on the assumption that the Doppler shift

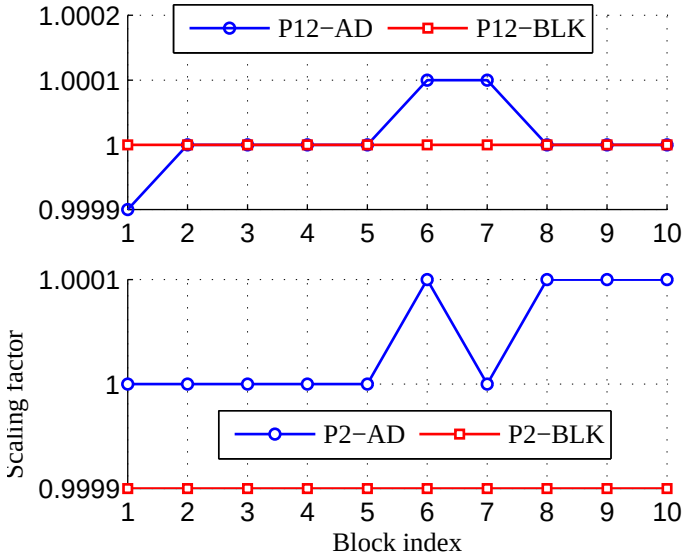

Figure 3.13: Estimation of the Doppler scaling factor over each block for packets (2, 12) of the adaptive algorithm.

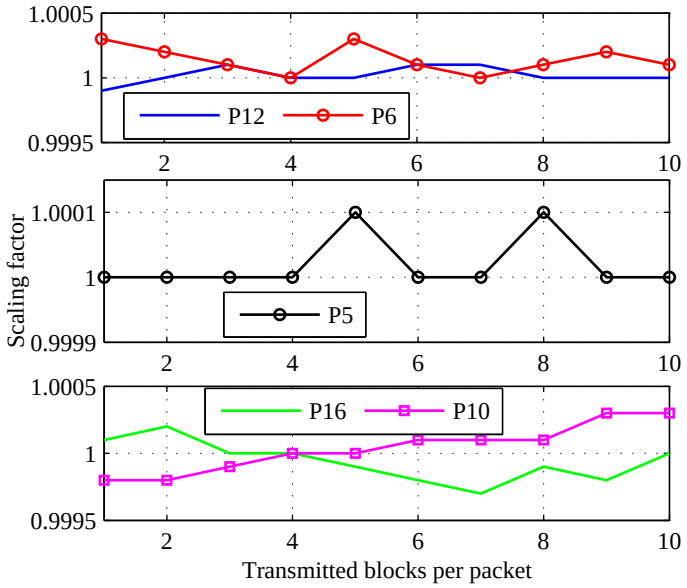

Figure 3.14: Estimation of the Doppler scaling factor over each block for packets (5, 6, 10, 16) of one-shot algorithm.

varies during the symbol time and consequently during the packet time; therefore, this variation degrades the receiver performance if it is not taken into consideration. Hence, the last symbol in the packet should also be involved in the smoothing algorithm. This case is evidenced in Fig. (3.16)(b), where it is apparent that the error in the OFDM symbol of index 1 comes from the Doppler variation of the last symbol in the previous packet. In symbols of indices (7, 8), the case is different, where there is an error in estimating the Doppler shift during the OFDM symbol. As shown in

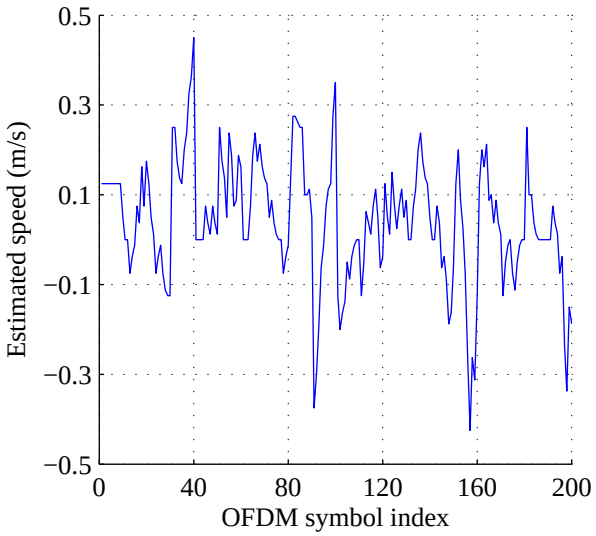

Figure 3.15: Changing of speed through the packets' time.

Fig. 3.16(c), the speed at the end of OFDM symbol index 7 starts changing its direction and this necessitates considering the slope variation. In addition, it is shown in Fig. 3.16(c) that the average speed of the packet is approximately constant; hence, estimating the average Doppler (i.e., at the mid-point) outperforms the proposed method. The BER results of the proposed method in Fig. (3.16)(a) were obtained with two iterations, whereas in the block method the iterations were 10. This figure, in conjunction with the summarized results in Tables 3.2 and Tables 3.3, confirms the improvements of the proposed technique over counterpart techniques. The improvement ratio was 93 % between the proposed and the block technique, whereas this ratio was 57.2363 % between the proposed and the adaptive algorithm. The underlying reason for this improvement is due to the broadband nature of the channel in conjunction with a tight sub-carrier spacing; the receiver becomes very sensitive to the Doppler shift and, consequently, it is not capable of accounting for a shift in a carrier frequency. Therefore, adopting the complete sample time of the transmitted frame to compensate for the integer and the fractional part of the Doppler shift was the main contribution in this improvement.

3.5 Real-time implementation of BICM-ID

As mentioned earlier, the proposed system adopts iterative decoding at the receiver. This iterative decoding is computationally expensive and requires long execution time therefore, it is interested to benchmark the BICM-ID implementation. The

Table 3.2: Performance results of the experiment

Packet index	1	2	3	4	5	6	7	8	9	10
Block	0	119	423	347	3	44	11	505	39	2443
one shot	0	0	132	170	9	344	0	6	31	90
Adaptive	0	0	84	91	9	14	0	9	21	245
Proposed	0	0	3	2	0	32	0	4	22	210
Packet index	11	12	13	14	15	16	17	18	1 9	20
Block	24	0	33	178	21	1702	21	0	471	119
one shot	18	802	169	77	53	383	267	176	123	105
Adaptive	6	384	10	49	45	6	36	20	30	5
proposed	3	141	9	3	0	11	3	0	7	5

Table 3.3: Average BER and error statistics comparison of the experimental results for different Doppler shift compensation techniques

Method	Error statistics		Improvement ratio
	Errors/178400	Average BER	
Block	6503	0.0365	
One-shot	2955	0.0165	54.5594 %
Adaptive	1064	0.0059	63.9932, 83.6383 %
Proposed	455	0.0025	57.2368, 93 %

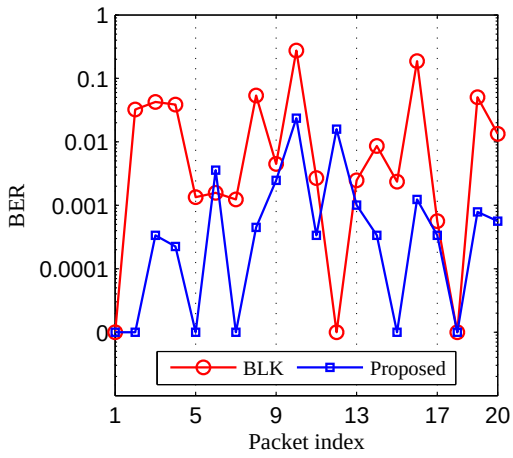

(a) BER performance.

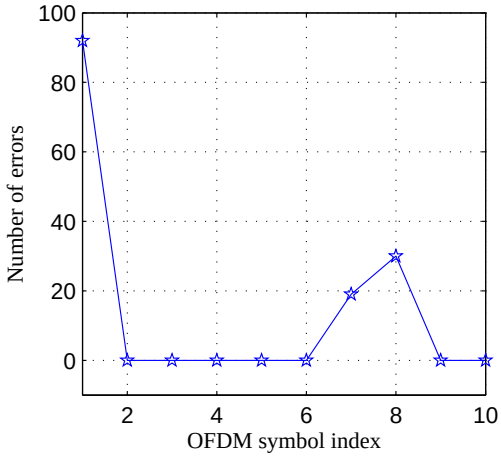

(b) Error statistics of packet 12.

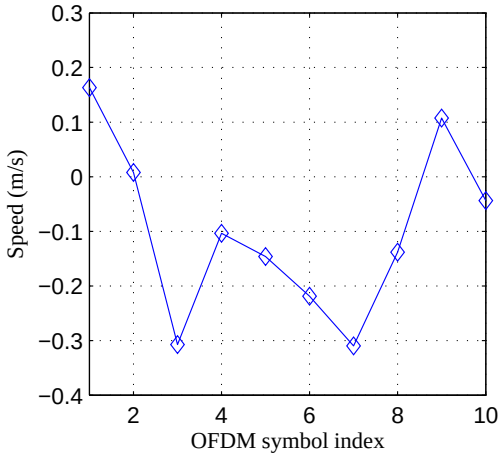

(c) Estimated speed of packet 12.

Figure 3.16: Performance of the proposed system from the experiment.

general system compromises a single DSP in transmitter (Tx) and receiver (Rx) as shown in Fig. 3.17. Data streams of length $b_i = 2047$ bits are generated to form the input of the encoder. It is composed of FEC with convolution NSC, which has a code rate of 1/2 and $K = 5$, then passes to an interleaver. In this interleaver, $L_{int} = 4120$ bits is used to permute the encoder output and consequently randomize error. The digital modulation technique is QPSK mapped to Gray mapping. The encoded data are transmitted with the carrier frequency of $fc = 10$ kHz and the symbol rate of 4 ksps. On the receiver side, ADC data, in 24-bit unsigned integer format, must first be converted to floating point representation. Additionally, signal amplitude should be scaled from the ADC values to a normalized +/- 1.0 range for the subsequent signal processing stages. After bandpass FIR filter and

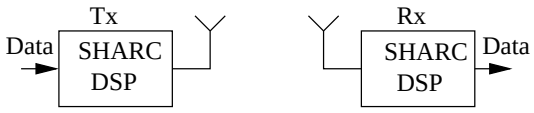

Figure 3.17: General System Specification.

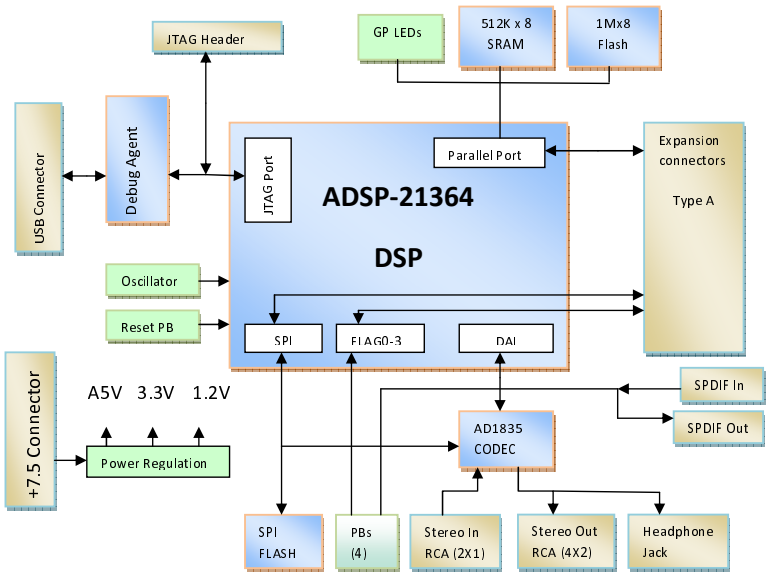

Figure 3.18: SHARC ADSP-21364 system architecture block diagram.

frame synchronization, soft demodulation is required. These soft information are de-interleaved and then decoded with a BICM-ID.

3.6 Hardware platform description

Fig. 3.18 shows the platform ADSP-21364-EZLITE Kit SHARC family from Analog Devices. In this section, we will describe some features that have been actually used in the implementation, the readers are referred to [83] for more details information. ADSP-21364 SHARC is a 32/40-bit floating point processor optimized for high performance automotive audio applications with large on chip SRAM (3M bit) and ROM (4M bit), multiple internal buses to eliminate input-output (I/O) bottlenecks, and an innovative digital audio interface (DAI). This interface is crucial for the processor to communicate with the DAC/ADC or sometimes called CODEC.

One of the key components of the acoustic modem is the audio signal input/output module. The ADSP-21364 development board used has a built-in module for sampling audio signal. The task is handled by the integrated Analog Device AD183x CODEC family [83]. Data transfer word lengths of 16, 20, 24, and 32 bits, with sampling rates from 8 kHz to 96 kHz, are supported. The operation mode of AD183x

can be programmed with a set of control registers. For sampling rate of 48 kHz, if the processor's buffer holds 1024 samples, then it has a frame acquisition interval of 21.33 ms (i.e., $1024 \times 20.833\mu$s). Here the DSP has 21.33 ms to complete all the required processing tasks for that frame of data. Three buffers of size 1024 have been used to exchange these samples between CODEC, DMA and serial ports as shown in Table 2.1, so data sampling and processing can be done simultaneously and no incoming signals are missed even if the DSP is processing previously received data.

Serial peripheral interface (SPI) is an industry standard synchronous serial data link named by Motorola. It provides full-duplex synchronous serial interface to communicate with DAI and the core processor. This processor achieves an instruction cycle time of 3.0 ns at 333 MHz.

3.6.1 Processing time optimization

In a simulation environment, we can process a whole communication packet in one simulation time instance regardless of its size. In addition, the time synchronization between transmitter and receiver can be assumed to be perfect. However, in a real-time system, we have to process the communication signals in frames rather than packets due to the limitation of the internal memory of DSP systems and stringent real-time constraints. Frames of length $N_f = 2060$ of coded and modulated symbols are utilized. The transmitter sends a block of 1024 samples at each interrupt time to a DAC of sampling rate 48 kHz. As the processor is running at 333 MHz, then the number of clock cycles the processor can perform before an interrupt are 7104000 cycles for a block of 1024 samples. On the receiver side, soft de-mapping, log-MAP decoder, and de-interleaver are complex algorithms, particularly with iterations, therefore, they require more processing time to be run by the DSP than the frame duration allows, which is 515 ms. These algorithms should convene the DSP real-time requirements. This constraint can be relaxed in twofold. Firstly, by setting the silent period time between two consecutive frames equal to the decoding time and greater than frame duration; however this reduces bandwidth. Alternatively, design a silent period of minimum length according to the required time to empty the bandpass filter taps and introducing one frame duration delay (first frame) during reception. In this mode, the DSP collects the received samples in data memory

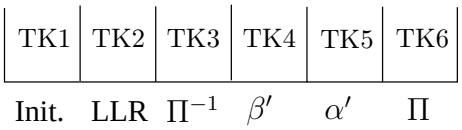

Figure 3.19: Receiver tasks.

instead of processing them immediately. Each symbol time in the frame duration was exploited to manipulate a specific task of previous frame duration as shown in Fig. (3.19).

That is, optimization of the processing time is dealt with based on the disposition of the frame time according to the processing time of each stage in the outer receiver. Moreover, this structure adopts pipelining the analysis and processing phases of incoming frames and relies on the internal memory only. In this figure, the time of task1 (TK1) is set in accordance with the measured decoding cycles in the DSP board. Particularly, to infer how many symbol times need to be set for TK1, we need to know the maximum cycles of each task. Thus, it is apparent that the maximum cycles spent in TK5 are 28250768, in order to process N_f symbols from start to end through all 16 states of BCJR. The details of this decoder, which is denoted relative to its authors, are mentioned in [68].

Based on the time of each task in the decoder, we can find a relation for each repetition as shown below. This relationship includes all stages of the data symbols during the SISO decoding. We can also note that, in (3.45), the number of iterations I, has an influential role in determining the number of necessary symbols that can be exploited at every stage. Except the first phase, I has no effect because this phase is used for the purpose of array initialization,

$$Step[I] = (686, 20I, 158I, (8I) - 1, 2I, 158I), \tag{3.45}$$

where I=1,. . . , 3. In the second phase (soft de-mapper), a period of twenty-symbols has been exploited in the iteration to be done. We can infer that, a period of forty and sixty symbols has been exploited in the second and third iterations, respectively, to accomplish it. In our system, the time required for 20 symbols is 5 ms for the case of $I = 1$, therefore in each symbol time of the current incoming symbol, we

process 103 symbols of the previous frame in the second stage.

$$N_p(i) = \frac{N_f}{Step(i)}, \tag{3.46}$$

where i=2,. . . ,6, and N_p is the number of symbols per stage.

By applying (3.46) to all stages of the decoder, we can find the maximum symbols, in the iteration from the previous frame as below:

$$N_I = N_i + I \sum_{i=2}^{6} N_p(i), \tag{3.47}$$

where N_I, is the maximum symbol length in the iteration after processing time optimization. For N_i=4, the maximum symbol length in iterations 1, 2 and 3 are 1423, 1424 and 1429 symbols, respectively.

From (3.46), we can find also that, in TK5 or $Step(5)$, the maximum symbol length is 1030 symbols. This result leads to determining the maximum cycles which can be stolen from each symbol in one iteration, as below:

$$MAX_S = \frac{MAX_c}{Ns_\alpha}. \tag{3.48}$$

$$= \frac{28250768}{1030} = 27428 \text{ cycles}, \tag{3.49}$$

where MAX_S , MAX_C , Ns_α is the maximum stealing for each symbol, the maximum cycles and the maximum symbol length in stage TK5, respectively.

For the purpose of determining the stealing ratio, the total cycles were measured. By applying the relation below, we can calculate how many cycles have been stolen by each iteration:

$$C_{Stol} = \frac{C_{tot}}{N_T} \tag{3.50}$$

$$= \frac{38679420}{1423} = 27181 \text{ stolen cycles}, \tag{3.51}$$

where C_{Stol} , C_{tot} and N_T are the cycle stolen, the total cycles and the total symbols in iteration one, respectively. Therefore, the stealing ratio of the iteration is:

$$S_R = \frac{C_{Stol}}{S_C}, \tag{3.52}$$

$$= \frac{27181}{83250} = 32.65\%, \tag{3.53}$$

where S_C is the symbol cycles.

Table 3.4: Total Cycles

Iteration 1	Iteration 2	Iteration 3
3,8679,420	7,7238,370	11,5857,252

3.6.2 Memory allocation

The 3Mbit onchip static random access memory (SRAM) of the DSP is split into 4 blocks, of different sizes. For 32 bit words, these blocks are allocated as the following: 32K (0x8000) of data memory (DM) space in memory block1, 16K (0x4000) of program memory (PM) space in memory block2, 8K (0x2000) of heap space in memory block3, 8K (0x2000) of stack space in memory block4. In this system, the challenge is to process N_f symbols in the β' stage. All symbols, from start to end in this stage should be processed through all 16 states. Therefore, a size of more than 32k of DM should be available. To tackle insufficient memory space, β stage memory has been buffered into both DM and heap. In addition, overwriting technique has been used for the sake of memory optimization, especially to buffer the whole frame in the case of block interleaver and deinterleaver.

3.6.3 Real-time experimental results

The performance of the proposed BICM-ID receiver is investigated real-time in tank with 3-iterations only as shown in Fig.3.20. This scatter diagram is used to present the experimental output of the iterative decoding. A evidence can be inferred from this figure that the system met the real time requirements and the iterative receiver suited the underwater channel. What is interesting in these requirements is that, the RAM has been determined (including interleaver), which is $21N_f$. Comparisons between these memory requirements and [84] results our system outperform their system in one block memory requirement, where they used $22N_f$.

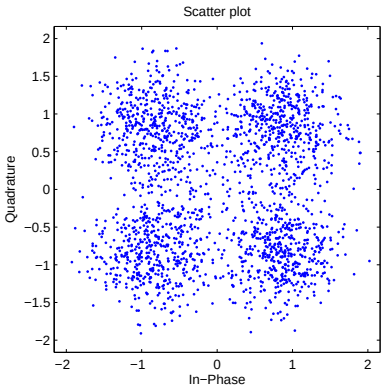

Figure 3.20: Output of real-time BICM-ID 3 Iterations.

3.7 Chapter summary

The following key points have been discussed in this chapter:

- Three low-complexity Doppler compensation techniques are presented.
- Comparison of the CP-correlation is demonstrated by simulation.
- Re-sample with unique Doppler shift in each OFDM, but variable between symbols within the packet is adopted in all suggested algorithms.
- Real-time implementation requirements of the most computionally extensive part of the proposed BCJR decoder has been presented with SHARC ADSP-21364 processor.
- In one-shot technique, it has been shown it cannot account for the Doppler shift and CFO based on the carrier frequency due to the wideband nature of the channel.
- It has been proven through the experimental results that the weighting coefficients improve the Doppler shift estimation and accommodate the change in speed between the OFDM symbols.
- A proposed system which combines the using of the weighting coefficients and adopting the sample time expansion/compression is devised among all previous schemes to establish a basis for other techniques.
- The conclusion is the Doppler shift cannot be considered constant and it needs an algorithm that is capable of tracking the speed variation within the OFDM symbol time. The next chapter addresses the frequency estimation.

Chapter 4

Time varying Doppler shift compensation

Traditional techniques employed in order to compensate for the Doppler shift in conventional receivers are based on the assumption that there is a common Doppler shift during the OFDM symbol time. In particular cases, such as acceleration, it is difficult to ignore the time-varying Doppler scale during the packet time, a factor which necessitates the use of a tracking algorithm to enable frequent estimation of this multi-scale parameter. Therefore, this chapter aims to design a receiver structure that is capable of accomplishing such time-varying Doppler compensation. In this chapter, two approaches are taken into consideration in order to estimate the symbol timing offset parameter. The first method employed to achieve an estimate of this particular parameter is based upon centroid localization mentioned in chapter 3 and this prediction is reinforced by a second technique which utilises linear prediction, based on the assumption that the speed changes linearly during the OFDM symbol time. Subsequently, the two estimations of the symbol timing offset parameter are smoothed in order to obtain a fine tuned approximation of the Doppler scale. Additionally, the effects of weighting coefficients discussed in chapter 3 on smoothing the Doppler scale and on the performance of the receiver are also investigated. The proposed receiver is investigated, incorporating an improvement that includes fine tuning of the coarse timing synchronization in order to accommodate the time-varying Doppler. Based on this fine-tuned timing synchronization, an extension to the improved receiver is presented to assess the performance of two point correlations. The proposed algorithms' performances were investigated using

real data obtained from an experiment that took place in the North Sea in 2009.

4.1 Time varying Doppler shift model

Based on the assumption that the speed of the motion changes linearly during the ith OFDM symbol interval $t \in [iT, T(i+1))$, the Doppler shift is varied with time, therefore the constant Δ does not hold to accommodate this variation and it should be replaced by $\Delta(t)$. Thus, the time varying Doppler shift can be modelled as

$$\Delta(t) = \frac{v(t)}{c}, \tag{4.1}$$

where $v(t)$ represents the speed variation during the symbol time. Therefore, the received passband signal in (3.16) can be rewritten as

$$\begin{aligned} \tilde{r}(t) =& \Re \left\{ \frac{1}{\sqrt{N_{\mathrm{c}}}} \sum_{n \in \mathcal{J}} d_i(n) u_i^{opt}(n) e^{j2\pi f_n (1+\Delta(t))t} \right. \\ & \left. \cdot \sum_{l=0}^{L-1} h_l \; p_{rc}[(1+\Delta(t))t - \tau_l] e^{-j2\pi f_n \tau_l} \right\} + \tilde{w}_i(t), \end{aligned} \tag{4.2}$$

and its corresponding complex baseband signal model in (3.17) can be written as

$$r(t) = \sum_{i=0}^{\infty} \sum_{n \in \mathcal{J}} H_i(n) d_i(n) u_i^{opt}(n) e^{j2\pi n \delta f t} e^{j2\pi \Delta(t) f_n t} + w_i(t), \tag{4.3}$$

where $H_i(n)$ is the channel transfer function of the ith symbol at nth sub-carrier with a time varying Doppler shift that can be written as

$$H_i(n) = \sum_{l=0}^{L-1} h_l \; e^{-j2\pi f_n \tau_l} \; p_{rc}\left[1 + \Delta(t)t - \tau_l\right]. \tag{4.4}$$

As referred to in [85], it is obvious in (4.3) that the effect of the Doppler shift on the received signal is twofold. First, it scales the received OFDM frame duration T by a factor of $1 + \Delta(t)$, yielding sampling frequency errors that result in symbol timing error [86]. Second, there is a time varying CFO.

4.1.1 Sampling frequency errors

In discrete time, the sampled transmitted signal $x[kT_s]$ in (3.13) is equivalent to a scaling of the sampling period (interpolation or decimation)

$$\tilde{r}[kT_s] = x[k(1 \mp \Delta(t))T_s], \tag{4.5}$$

where k is an integer, and T_s and $\tilde{r}(kT_s)$ are the sampling period and Doppler-shifted received sampled signals respectively. The bidirectional effect of the Doppler shift causes symbol timing errors, which will be increased or decreased proportionally to $\Delta(t)$. To align the symbol within its period, samples should be removed if $(\Delta > 0)$ or added if $(\Delta < 0)$ at regular intervals [77]. Let $\pm\phi$ be the deviation of samples of the received sequence for each OFDM symbol due to the speed change. The sampling period results in expansion or compression of the samples' length, hence the Doppler-shifted received frame's length is modelled by

$$L'_f = (L_f \mp \phi), \tag{4.6}$$

where $L_f = \frac{N_c}{B \cdot T_s}$ represents the transmitted passband samples' length. It is apparent that L_f is only affected by T_s and any expansion/compression in the timescale will result in ϕ. Therefore, (4.6) is implicitly equivalent to (4.5). To remove both CFO and symbol shift, an inverse time scaling of the received (compressed/expanded) signal should be achieved providing that the amount of Doppler shift $\Delta(t)$ is known. This is equivalent to changing the sampling rate of the passband signal by $1 + \Delta(t)$ in discrete-time processing. From (4.6), we can infer that increasing or decreasing the length of samples is equivalent to adjusting the sampling frequency f_s by the same Doppler shift $1 + \Delta(t)$; thus (4.5) is rewritten as

$$\tilde{r}[k] = x[\frac{k(1 \mp \Delta(t))}{f'_s}], \tag{4.7}$$

where $f'_s = f_s(1 \mp \Delta(t))$. By substituting f'_s in (4.7), $\tilde{r}[k] = x[k]$, i.e. the signal received is then in conformity with the transmitted signal.

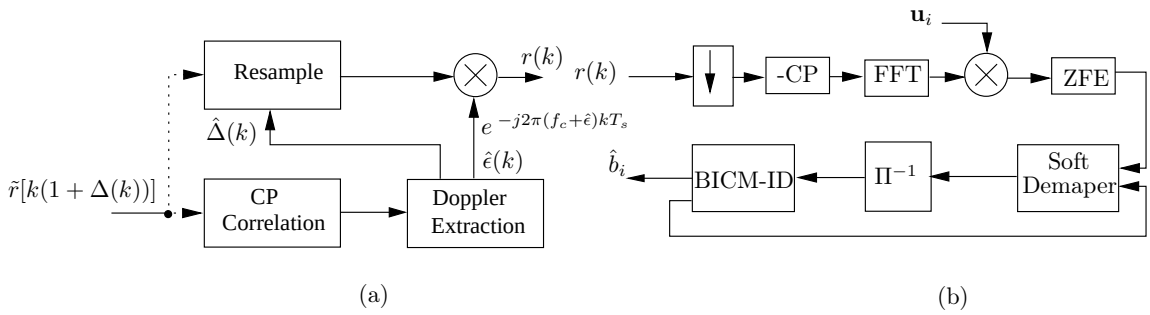

Figure 4.1: Proposed receiver structure

4.1.2 Carrier frequency offset errors

The factor $e^{j2\pi\Delta(t)f_n t}$ in the received signal in (4.3) represents a time varying CFO, where $\Delta(t)f_n = \Delta(t)f_c + \Delta(t)n\delta f$. The CFO ($\epsilon$) is due to the residual Doppler shift. It is destructive because it deviates the sub-carrier spacing δf and introduces ICI, which must be removed prior to the FFT to design an optimum receiver [86]. The re-sampling process removes the Doppler shift and converts the wideband system into narrowband. However, the residual Doppler shift produced by the fractional part of the time expansion/compression degrades the receiver.

4.2 Signal processing in the proposed receiver

To utilize the available bandwidth efficiently, the algorithm employs a low-complexity blind technique to estimate the Doppler shift based on estimating the coarse timing metric for each OFDM symbol by exploiting the inherent periodicity of the CP. Centroid-based localization has been used to refine the maximum amplitude of the timing metric; i.e. the timing offset, as explained in chapter (3). Using this coarse timing metric, the Doppler shift and its residual are frequently estimated by deriving a tracking step in the Doppler extraction unit (DEU). This unit comprises linear expectation of the timing offset, fine tuning of the estimated parameters, tracking the Doppler shift, and CFO estimation. In this technique, the fractional deviation of the sub-carrier spacing, which is the source of ICI, is estimated by exploiting the fractional part of the normalized sampling frequency offset; whereas the integer part of this offset is used to estimate the integer Doppler shift.

4.2.1 Coarse timing metric estimation

The receiver structure of the proposed system is depicted in Fig. 4.1. The received signal $\tilde{r}(t)$ in (4.2) is fed through the transducer, pre-amplifier and analogue-to-digital converter, and then filtered in the frequency band $[f_c - B/2, f_c + B/2]$. The resultant Doppler shifted passband signal $\tilde{r}[k(1 + \Delta(k))]$ is correlated with the Doppler tolerant-training (chirp) to detect the start of the packet ζ that contains several OFDM symbols. Based on the existing guard interval, the drift in the received Doppler-shifted signal $\tilde{r}[k(1 + \Delta(k))]$ is measured by correlating the guard samples $(N_g \cdot N_s)$ with an anticipated observation window in order to estimate the coarse timing metric for each OFDM symbol within the packet, as in chapter 3. In the case of time varying Doppler shift, i.e. multi time scaling factor, the resulting timing metric is affected by the velocity perturbation. Consequently, there is a demand on estimating this timing metric of the same OFDM symbol, but using an alternative approach to increase the accuracy of the Doppler shift estimation. Therefore, in Fig. 4.1(a), linear prediction is adopted to extract the Doppler shift for the purpose of reinforcing the symbol timing offset parameter that was estimated using CP correlation.

4.2.2 Time varying Doppler shift estimation

Thus far, the timing metric has only been considered for the case of a common Doppler shift during the OFDM symbol time. A worst case scenario may occur when there is a velocity that accelerates or de-accelerates within the symbol period. This situation can be explained in Fig. (4.2). This figure shows that the start of the OFDM symbol undergoes a different speed relative to the speed at the end of the symbol due to the acceleration, in which the speed is changing linearly with time. As a result, a linear multi Doppler shift during the OFDM symbol period is produced. In addition, the acceleration is a useful indication of how fast the change is, where in Fig. (4.2)(a) the Doppler frequency shift is 1.12 Hz at OFDM symbol 1 and it increases to 11.2 at OFDM symbol 10. The same case is demonstrated in Fig. (4.2)(b), where the acceleration is 1 m/s^2 and the Doppler frequency at OFDM symbol 10 is 22.4 Hz, in terms of time-selectivity measurement which is given as:

$$T_d F_d > 1, \tag{4.8}$$

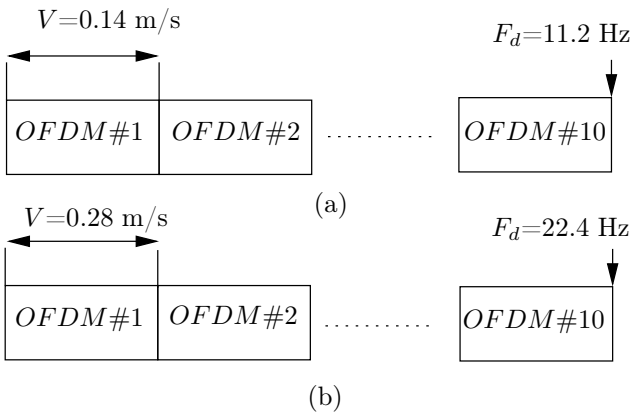

Figure 4.2: Acceleration effect over Doppler frequency change during each symbol time at f_c =12 kHz. (a) a=0.5 m/s^2, (b) a=1 m/s^2

This rapid change within the symbol duration gives an indicator of the amount of distortion caused by the channel on the signal.

Alternatively, frequent estimation of the Doppler shift within the OFDM symbol or reducing the frame length are viable solutions. However, in OFDM signal design, there is a trade-off between the number of sub-carriers, Doppler estimation resolution and sensitivity to the CFO. Hence, frequent estimation of the interpolation factor is more feasible than shortening the OFDM symbol length.

When the channel has a velocity that accelerates or de-accelerates in both directions (up or down) within the symbol period, the following assumption is considered: *Assumption* : If T_d is 256 ms and the maximum acceleration 1 m/s^2 starting from initial speed v_0, then the symbol needs approximately $4T_d$ to attain the maximum speed v_0+1 m/s. From this assumption, it can be inferred that the maximum speed change in each OFDM symbol is approximately 0.25 m/s.

For a system of 12 kHz carrier frequency, 48 kHz sampling frequency and a symbol time of 0.256 seconds, such speed variation causes a Doppler frequency shift F_d to increase by 2 Hz within each symbol up to 20 Hz by symbol number 10. In such circumstances, estimating a common timing metric may not hold to attain acceptable performance. Alternatively, a better solution and more accurate Doppler compensation can be realized by adopting a frequent estimation of the Doppler shift within the OFDM symbol.

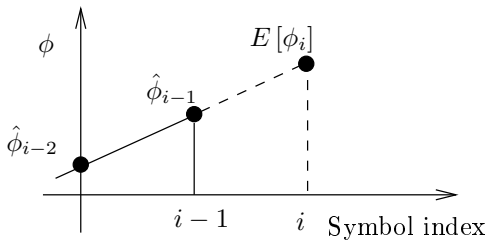

Figure 4.3: Estimation of timing offset during the packet time.

4.3 Doppler extraction

The Doppler extraction unit in Fig. (4.1)(a) comprises linear prediction of the symbol timing offset, fine symbol timing offset, tracking the Doppler shift and CFO or residual Doppler shift estimation.

4.3.1 Linear prediction of the symbol timing offset

As the transmission structure contains multiple OFDM frames within a packet, the synchronization between these frames is paramount to reduce both the ISI and ICI on the receiver side. In the proposed technique, an improvement is obtained by involving the estimated timing offset at time $i-1$ in predicting the timing offset at time i. To accomplish this, it is assumed that due to the first order Doppler shift, the OFDM frame could be expanded towards the *leading edge* or compressed towards the *trailing edge* in the range $[T(1+\Delta(t))+\tau_{\max}, T(1-\Delta(t))+\tau_{\max}]$, respectively. Therefore, the linear part of the speed variation can be formulated by the first order equation

$$y = m'i + b, \tag{4.9}$$

where $m' = \frac{\hat{\phi}_i - \hat{\phi}_{i-1}}{x_i - x_{i-1}}$ denotes the slope and x_i is the OFDM symbol at index i, as shown in Fig. 4.3. Accordingly, the gradient will vary gradually in accordance with the speed change and, subsequently, the output value y_i is obtained. The slope here is determined based on the previous two OFDM symbols estimated in (4.11) and subsequently used to predict the timing offset ϕ for the next OFDM symbol. Therefore the first order predicted timing offset of the current OFDM symbol can be formulated as:

$$E[\phi_i] = 2\hat{\phi}_{i-1} - \hat{\phi}_{i-2}. \tag{4.10}$$

4.3.2 Fine symbol timing offset and synchronization

Thus far, two estimations of the same parameter $\hat{\phi}$ have been obtained. It should be stressed that attaining accurate timing offset estimation may be difficult in the presence of noise and/or ISI, especially with a short observation window. Therefore, for the purpose of increasing the reliability of estimation, smoothing the timing offset is adopted. This yields the following fine tuned estimated timing offset

$$\hat{\phi}_i = \hat{\phi}_i W_1 + E\left[\phi_i\right] W_2, \tag{4.11}$$

where the coefficients W_1 and W_2 are empirically obtained and satisfy the condition of $0 < W_1 + W_2 \leq 1$. These coefficients are designed to attain a trade-off between estimation accuracy and tracking capabilities. It is crucial to mention that these coefficients have an effect on adapting the slope variation, where $W_1 = 1, W_2 = 0$ indicates fast slop variation and the linear expectation does not hold. At the same time, $W_1 = 0, W_2 = 1$ accommodates a constant gradient between symbols. The estimated fine timing offset $\hat{\phi}$ in (4.11) still represents the average. Assuming the change in the time scale is linear within the OFDM symbol, the change in the speed is considered unidirectional. This will enable tracking of the Doppler shift caused by speed variation within the OFDM symbol time. Performing such tracking demands knowledge of the timing offset at both edges of the symbol in order to determine the tracking step. By involving previous estimation of fine symbol timing offset $\hat{\phi}_p$ and current fine symbol timing offset $\hat{\phi}_c$, the offset at the leading edge can be formulated as

$$\hat{\phi}_s = \frac{\phi_p + \phi_c}{2}. \tag{4.12}$$

At the same time, the sampling frequency offset at the trailing edge $\hat{\phi}_e$ is determined as

$$\hat{\phi}_e = 2\hat{\phi}_c - \hat{\phi}_s, \tag{4.13}$$

where $\hat{\phi}_p$ and $\hat{\phi}_c$ represent the average fine timing offset estimate from (4.11). It should be stressed that the estimation accuracy of these two parameters plays an important role in increasing the ability to compensate for the Doppler shift and its residual effects in the subsequent stages.

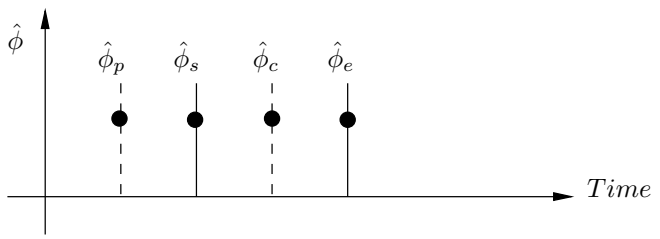

Figure 4.4: Tracking the Doppler within the OFDM symbol.

4.3.3 Tracking the Doppler shift

If the relative velocity between the transmitter and receiver during the packet time is constant, i.e. for zero acceleration, then the Doppler shift estimate computed can be used to compensate for the entire OFDM symbol. In time varying Doppler shift, however, a unique interpolation factor for the whole symbol does not hold due to the resulting non-negligible sampling frequency errors which must be tracked. Therefore, the sampling frequency offset affects channel estimation, which is computed over pilot sub-carriers, due to the different delays of the positions of these pilots. By searching for the delay in the 1st significant arrival of the estimated CIR [87], an approach to tracking the fractional sampling clock frequency offset due to a symbol timing error is possible. However, in the case of time varying Doppler shift, it is necessary to estimate the sampling frequency offset frequently.

An alternative realistic Doppler shift estimator, which can be realized by adopting frequent estimation of this parameter during the symbol time in the time-domain, is proposed here. In order to track the Doppler shift, it is necessary to derive a tracking step that corresponds to the sampling frequency offset change over $\hat{\phi}_s < \hat{\phi}_s + T_s < \hat{\phi}_e$. In such a case, the tracking step is given as

$$\phi_{step} = \frac{\hat{\phi}_e - \hat{\phi}_s}{L_f}, \tag{4.14}$$

where L_f represents the up-sampled sub-carriers. As shown in Fig. (4.4), each OFDM symbol is identified by the two parameters of sampling frequency offset $\hat{\phi}_s$ and $\hat{\phi}_e$, based on the assumption that the speed changes linearly. Accordingly, the estimated timing offset at the leading edge is updated at each sample time k, based on the step in (4.14). At the same time, the integer Doppler shift can be computed as

$$\hat{\Delta}(k) = \frac{L_f - \hat{\Psi}(k)_{(\mathrm{I})}}{L_f}, \tag{4.15}$$

where Ψ is the sampling frequency offset initialized with $\hat{\phi}_s$, and then updated at each sample as:

$$\Psi(k) = \Psi(k-1) + \hat{\phi}_{step}, \tag{4.16}$$

and $\hat{\Psi}_{(\mathrm{I})} = \lceil \hat{\Psi} \rfloor$ is rounded towards the nearest integer, respectively. This integer re-sampling factor is delivered to the sample-by-sample Lagrange Quadratic interpolation unit, as shown in Fig. 4.1(b), and the fractional part is dealt with as a carrier frequency offset. It should be stressed that the resolution of the interpolation factor in (4.15) is entirely dependent on the transmitted frame length.

4.3.4 Residual Doppler shift estimation

Efficient Doppler shift compensation relies on how accurately the re-sampling factor estimation reduces the residual Doppler. This residual Doppler has a direct impact on the performance of the receiver. Taking this effect into account involves finding the amount of the fractional part of the estimated samples that shifts the sub-carrier spacing fractionally. This deviation can be modelled as $(\hat{\Psi}(k) - \hat{\Psi}_{(\mathrm{I})})$, and therefore

$$\hat{\epsilon}(k) = [\hat{\Psi}(k) - \hat{\Psi}_{(\mathrm{I})}]\delta f \frac{f_c}{f_s}, \tag{4.17}$$

is the residual frequency estimate. The residual Doppler shift is not constant at each sample within the OFDM symbol and thus it is dealt with by determining the standard deviation across the fractional part of the estimated Doppler shift. Once the Doppler shift and its residual have been estimated and compensated, the output signal $r(k)$ is delivered to the outer receiver in Fig. 4.1(b). This signal is firstly down sampled and then its cyclic prefix is discarded. The PAPR phases $\mathbf{u_i}$ are removed prior to FFT demodulation. The zero forcing equalizer (ZFE) and least square (LS) method for channel estimation purposes are adopted by utilizing pilots which are embedded in a comb method. After removing the channel effect, the subsequent stage is BICM-ID.

4.4 Pilot-based channel estimation

In the channel estimation of the OFDM symbol, a comb type arrangement of the training sequence (pilot) is adopted. In this scheme, specific tone indices are allo-

cated on all transmitted OFDM symbols and the rest for data transmission. Unlike a block-based training sequence, the comb type is quite convenient for fast fading channels. Additionally, with the comb type, all pilots and data are transmitted simultaneously on all symbols. It is worth pointing out that in order to increase the accuracy of the channel estimation, the residual Doppler shift should be eliminated [88]. This is due to an induced ICI which destroys the orthogonality among sub-carrier frequency components and ultimately the diagonal of the channel matrix. In OFDM systems, the advantage of increasing the symbol duration in reducing the ISI effect can conflict with increasing the ICI impact, as a consequence of sub-carrier spacing reduction. Therefore, after re-sampling and CFO compensation, all sub-carriers are orthogonal (i.e. ICI free). Then the training symbols for N_c sub-carriers can be represented by the following diagonal matrix:

$$\boldsymbol{X} = \begin{bmatrix} X_p[0] & 0 & \cdots & 0 \\ 0 & X_p[1] & & \\ \vdots & & \ddots & 0 \\ 0 & \cdots & 0 & X_p[N_p-1] \end{bmatrix}, \tag{4.18}$$

where $X_p(n)$ represents pilot tones at the nth sub-carrier. This diagonal representation of $\boldsymbol{X}$ is based on the assumption that the sub-carriers are orthogonal. Let $Y_p(n)$ be the received pilot symbols after the FFT operation, then

$$\begin{aligned} \boldsymbol{Y} &= \begin{bmatrix} Y[0] \\ Y[1] \\ \vdots \\ Y[N_p-1] \end{bmatrix} = \begin{bmatrix} X_p[0] & 0 & \cdots & 0 \\ 0 & X_p[1] & & \vdots \\ \vdots & & \ddots & 0 \\ 0 & \cdots & 0 & X_p[N_p-1] \end{bmatrix} \begin{bmatrix} H_p[0] \\ H_p[1] \\ \vdots \\ H_p[N_p-1] \end{bmatrix} + \begin{bmatrix} W[0] \\ W[1] \\ \vdots \\ W[N_p-1] \end{bmatrix} \\ &= \boldsymbol{X}\boldsymbol{H} + \boldsymbol{W}, \end{aligned} \tag{4.19}$$

where $\boldsymbol{H_p} = [H_p[0], H_p[1], \cdots, H[N_p-1]]^T$ is a channel vector and $\boldsymbol{W}$ denotes the noise vector which is given as $\boldsymbol{W} = [W[0], W[1], \cdots, W[N_p-1]]^T$. $\hat{H}_p(n)$ are the estimated pilot channel values, $D[X_p(n)]$ is a diagonal matrix constructed using the known transmitted pilot symbols. This zero forcing estimator [89] is simple; however, it has a high mean square error. The channel estimation was implemented

using the least square (LS) method. [90]

$$\begin{aligned} X(n) =& X(mL+l) \\ =& \begin{cases} X_p(m), & l=0 \\ X_d(m), & l=1\cdots,L-1, \end{cases} \end{aligned} \tag{4.20}$$

where $L = \frac{N_c}{N_p}$ and $X_p(n)$ is the nth pilot sub-carrier value. Let $H_p(n)$ be the frequency response of the channel for $n = 0 \cdots N_p - 1$ at pilot sub-carriers. The estimate of the channel at pilot sub-carriers $\hat{H}_p(n)$ is given as

$$\hat{H}_p(n) = D[X_p(n)]^{-1} Y_p(n),\ n = 0 \ldots N_p - 1. \tag{4.21}$$

In the least square estimation, the channel $\hat{\boldsymbol{H}}$ is estimated by minimizing the following cost function

$$\begin{aligned} J &= \left\| \boldsymbol{Y} - \boldsymbol{X}\hat{\boldsymbol{H}} \right\|^2 \\ &= (\boldsymbol{Y} - \boldsymbol{X}\hat{\boldsymbol{H}})^H (\boldsymbol{Y} - \boldsymbol{X}\hat{\boldsymbol{H}}) \\ &= \boldsymbol{Y}^H\boldsymbol{Y} - \boldsymbol{Y}^H\boldsymbol{X}\hat{\boldsymbol{H}} - \boldsymbol{X}^H\boldsymbol{Y}\hat{\boldsymbol{H}}^H + \boldsymbol{X}^H\hat{\boldsymbol{H}}^H\boldsymbol{X}\hat{\boldsymbol{H}}, \end{aligned} \tag{4.22}$$

where H denotes conjugate transpose. For minimization of J in (4.22), let $\frac{\partial J}{\partial \hat{\boldsymbol{H}}^H} = 0$, then

$$\begin{aligned} \frac{\partial J}{\partial \hat{\boldsymbol{H}}^H} &= -\frac{\partial J}{\partial \hat{\boldsymbol{H}}^H}(\boldsymbol{X}^H\boldsymbol{Y}\hat{\boldsymbol{H}}^H) + \frac{\partial J}{\partial \hat{\boldsymbol{H}}}(\boldsymbol{X}^H\hat{\boldsymbol{H}}^H\boldsymbol{X}\hat{\boldsymbol{H}}) \\ &= -\boldsymbol{X}^H\boldsymbol{Y} + \boldsymbol{X}^H\boldsymbol{X}\hat{\boldsymbol{H}} \\ &= 0, \end{aligned} \tag{4.23}$$

we have $\boldsymbol{X}^H\boldsymbol{X}\hat{\boldsymbol{H}} = \boldsymbol{X}^H\boldsymbol{Y}$, therefore the LS estimation is written as:

$$\hat{\boldsymbol{H}}_{LS} = (\boldsymbol{X}^H\boldsymbol{X})^{-1}\boldsymbol{X}^H\boldsymbol{Y} = \boldsymbol{X}^{-1}\boldsymbol{Y}. \tag{4.24}$$

For sub-carriers $n = 0, 1, 2, \cdots, N_c - 1$, LS channel estimation $\hat{\boldsymbol{H}}_{LS}$ is written as:

$$\hat{\boldsymbol{H}}_{LS}[n] = \frac{\boldsymbol{Y}[\boldsymbol{n}]}{\boldsymbol{X}[\boldsymbol{n}]}. \tag{4.25}$$

The mean square error of the LS channel estimation is considered high when

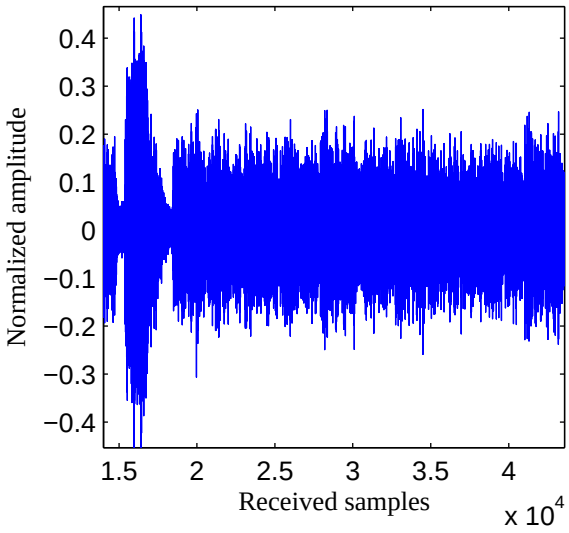

Figure 4.5: Received signal

compared with the minimum mean-square error (MMSE) estimate [91]. However, LS is attractive in implementing real-time systems due to its simplicity. In order to increase the reliability of the channel estimation, an interpolation in frequency domain between each pilot and data sub-carriers is adopted. It is well known that the LS is the first step of the channel frequency response estimation for the known pilots and should be followed by interpolation to obtain a non-pilot sub-carriers frequency response.

4.5 Experimental results

The setting of this experiment was mentioned in chapter 3. Fig. (4.5) and Fig. (4.6) show the channel measurements over a range of 1000 m. These figures show a received frame structure and the normalized CIR of a packet that exhibits maximum delay spread of the order of 6 ms, respectively. This multipath delay is equivalent to an ISI of 24 symbols for a system bandwidth of 4 kHz and this delay spread is inversely proportional to the range. In addition to the silent period shown in Fig. (4.5), the CP guard time also contributes towards reducing the ISI effect.

4.5.1 Proposed receiver performance

To evaluate the performance of the proposed system, the experimental results for both block-based and proposed techniques are depicted in Fig. 4.7(a). The performances of both receivers are presented in terms of bit error rate (BER). It can

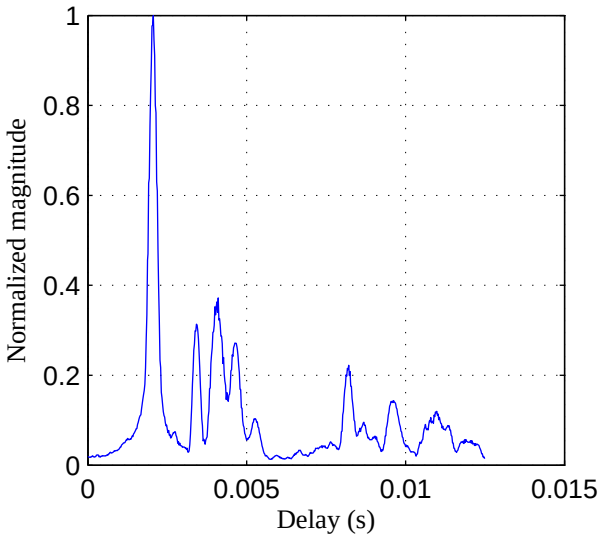

Figure 4.6: Sample of normalized channel impulse response for 1000 m channel range.

Table 4.1: Average BER comparison of the experimental results at different settings of weighting coefficients between the proposed and block-based Doppler shift techniques for N_c=1024

Method	**Error statistics**	
	Errors	BER
Block	6503	0.0365
Proposed-set1	772	0.004
Proposed-set2	105	0.0006

be seen that for all packets the proposed technique outperforms the block based method. Error statistics for both schemes are presented in Table 4.1. It can be seen that compensating the time-varying Doppler scale and its residual leads to a reduction in the BER from 0.0365 to 0.0006, which is equivalent to 98.4%. This is further clarified in Table 4.2 which shows that the proposed technique achieves acceptable performance in reducing errors in all packets compared with the block technique. However, Fig. 4.7 shows high decoding error in packet 6.

In Fig. 4.7, the bit errors are high only in two blocks within packet 6, as shown in Fig. 4.7(b). This is due to the noise effect which affects the Doppler scale estimation when estimating the timing offset. Evidence for this is shown in Figs. 4.8(b) and (d) where in packet 6, there is a mismatch in estimating the speed at the end of symbol

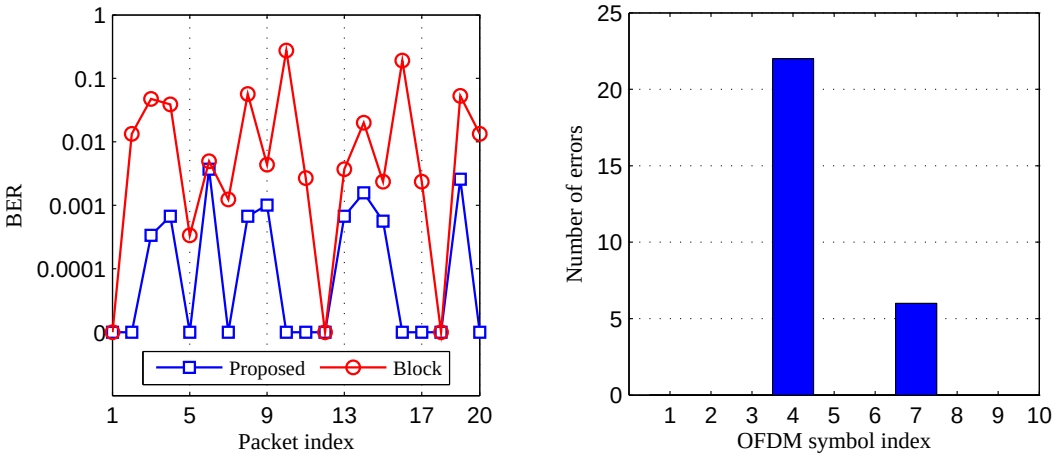

(a) BER for each packer over 1000 m range.

(b) Error statistics for packet 6; 2 out of 10 have decoding errors

Figure 4.7: Performance of the proposed system at 1024 sub-carriers.

3 and at the start of symbol 4. Therefore, a decoding error results in symbol 4. Furthermore, it can be seen from Fig. 4.8(a) that there is a relatively high deceleration of ~ 0.9 m/s^2 during the symbol time, which adds an error in approximating the correlation-based Doppler scale estimation. This result shows that there is a limitation on the acceleration that can be adopted in this algorithm.

Fig. 4.8 demonstrates that the adopted system is capable of precisely tracking the speed variation in each symbol. Particularly, in Fig. 4.8(a), the speed in symbol 3 of packet 6 has been changed three times during 0.256 s, whereas in (c) the speed is constant. However, changing the direction of velocity within the packet period, along with higher acceleration, can produce higher noise levels in the system. The source of this noise is the mismatch introduced by the transition from acceleration to deceleration, or vice versa. The proposed system detects this critical point through the CP correlation-based Doppler scale estimation and the linear expectation has no effect on this scenario. However, linear expectation reduces the channel and/or noise effect on the CP correlation. Consequently, accurate Doppler scale estimation is obtained.

Fig. (4.9) shows the performance of BICM-ID and ZFE in the experiment. In terms of (b), the figure shows that the ZFE delivers reliable information to the decoder. The reliability depends on how accurate the Doppler shift compensation is. It was mentioned earlier that the channel estimation is affected by the presence of residual Doppler shift which can cause ICI and, as a result, the orthogonality is

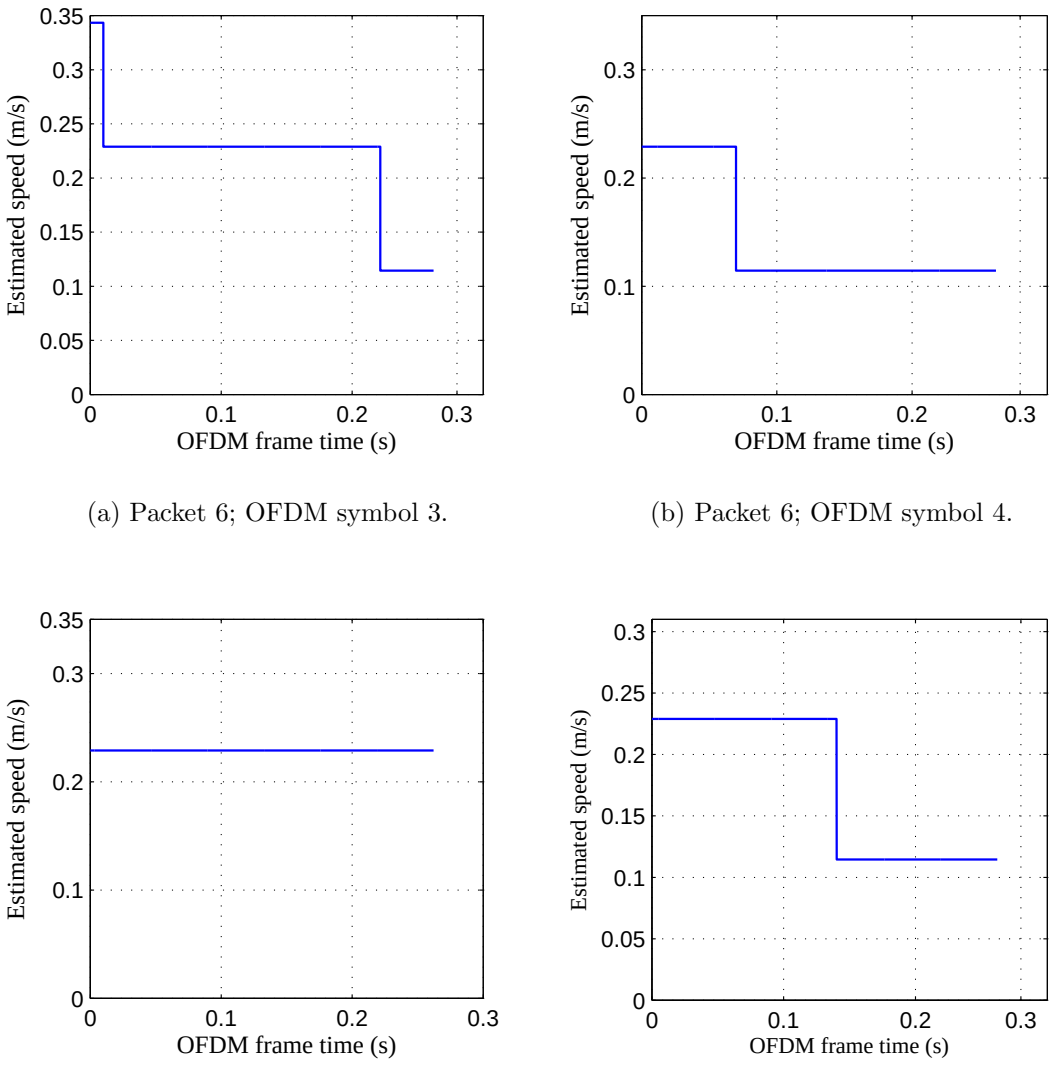

(a) Packet 6; OFDM symbol 3.

(b) Packet 6; OFDM symbol 4.

(c) Packet 6; OFDM symbol 6.

(d) Packet 6; OFDM symbol 7.

Figure 4.8: Estimated speed variation during OFDM symbol.

destroyed. Consequently, the iterative decoding stage can generate unreliable LLRs [92]. Thus, it can be seen that there is an improvement in the second iteration (d) compared with the first iteration in (c). At this stage, further iterations are pointless and no more gain is expected.

4.5.2 Effect of weighting coefficients

As mentioned in chapter 3, the weighting coefficients play an important role in the accuracy of the Doppler scale estimation. For this reason, special settings of these parameters are required in order to achieve acceptable performance. It can be shown that there is a trade-off between the value of the weighting coefficients

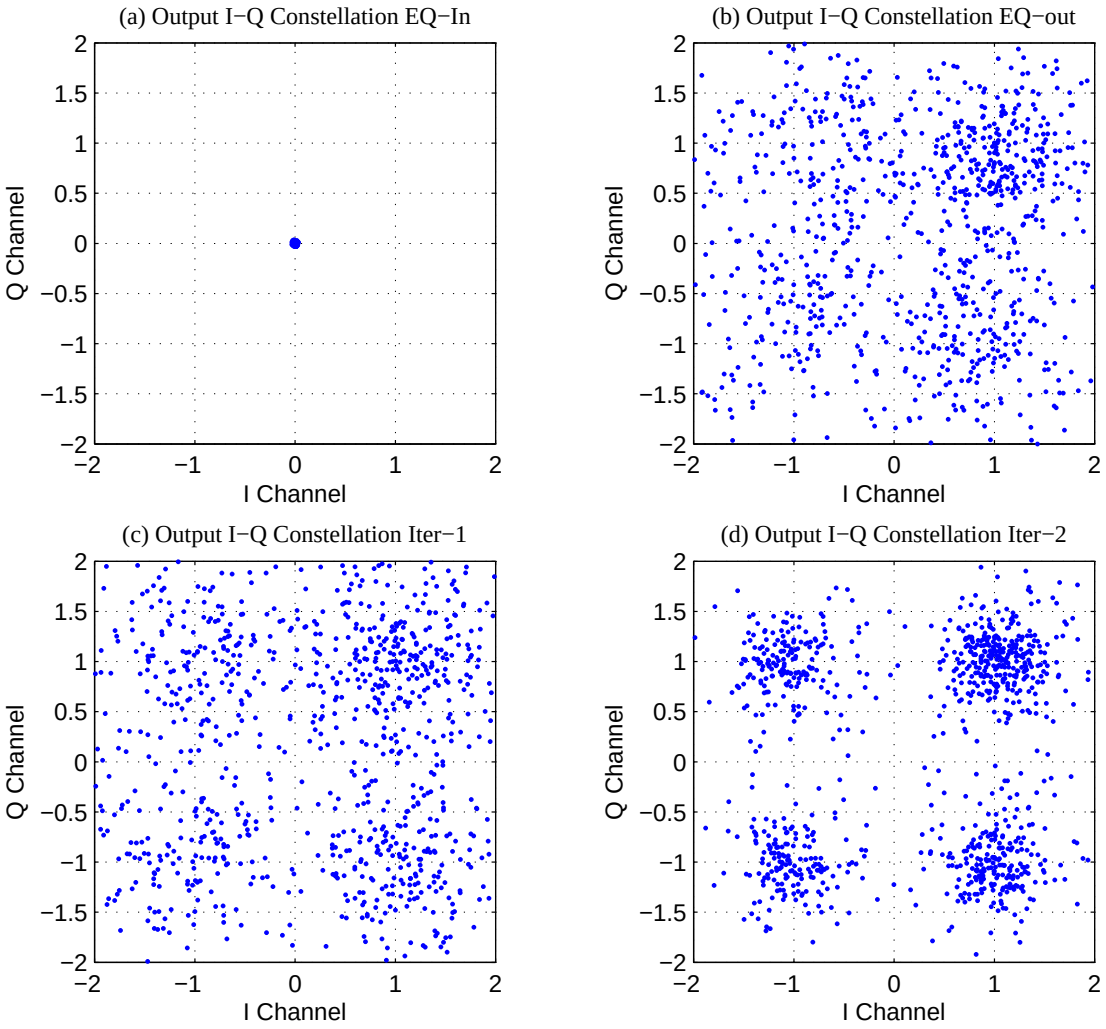

Figure 4.9: Constellation output from equalizer and iterative receiver.

and the receiver performance. To be more specific, by appointing the symbol timing offset, estimated by linear expectation, a lower weighting coefficient than correlation-based symbol timing offset estimation means there is a constant acceleration or deceleration between symbols, and vice versa. As shown in (4.11) and (4.14), the Doppler scale is approximated based on estimating the fine symbol timing offset and its tracking step is derived based on the sampling frequency offset at the start and end of the OFDM symbol. This means that the weighting coefficients have a direct effect on the estimation of the time varying Doppler scale $\Delta(t)$.

Fig. (4.10) shows two settings of these parameters and their effect on the performance of the receiver. In set 1, where $W_1 = 0.5$ and $W_2 = 0.5$, it can be seen that the receiver performance is poor. In Fig. (4.10) (a), it is obvious that packets 5 and 6 in set 1 exhibit a high BER of 271/8920 and 71/8920, receptively. The reason for this degradation is that increasing the weight of the linear expectation in a channel leads to significant acceleration that can cause maladjustment of the interpolation

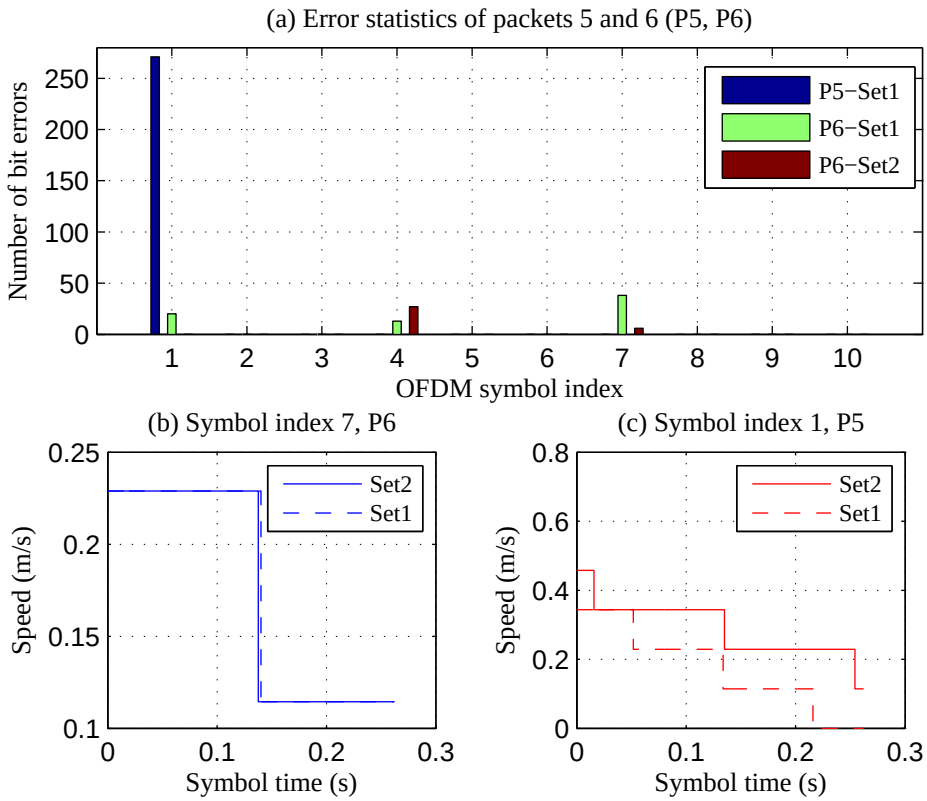

Figure 4.10: Effect of weighting coefficients on estimation.

factor and make the tracking of the Doppler scale change coarsely. This is shown in Fig. (4.10) (c). Although both sets have the same slope, there is a mismatch between them at the start and end of speed estimation. In set 2, on the other hand, $W_1 = 0.85$ and $W_2 = 0.15$, there is a great improvement in the performance as shown in Fig. (4.10) (a), with 0 errors in packet 5 and 33 bits in packet 6. Table 4.1 shows the performance of the receiver for the sub-carriers 1024 over a range of 1000 m using two different settings of the weighting coefficients. In set 2, it can be observed that the error decreases by about 86.4 % compared with set 1.

4.5.3 Performance evaluation with improved coarse timing estimation

As mentioned earlier, the impairments in the channel estimation due to synchronization failure will result in unreliable LLRs as a consequence of the Doppler effect. In contrast, estimating and compensating the Doppler scale precisely causes the received OFDM symbol to coincide with its transmitted period; thus improving the channel estimation and delivering reliable symbols to the decoder. Therefore, the

target is to improve the Doppler scale estimation and ultimately reduce the burden on the channel estimation. In order to extract the Doppler scale successfully, it is important to increase the reliability of estimating the symbol timing.

Considering the effect of acceleration on the chirp correlation is small, in the case of multiple OFDM symbols within a packet, the symbol timing error in each OFDM block is accumulated with acceleration during the packet time. Hence, adopting a single estimation of ζ for the whole packet is no longer accurate. Therefore, in order to mitigate the acceleration effect on the symbol timing error, ζ needs to be fine tuned. Performing the fine tuning necessitates updating the position of ζ after each symbol time. Let m, i denote the range of the timing offset around the leading and the trailing edge during the OFDM symbol, respectively. It follows that a two dimensional timing function is written as

$$\begin{aligned} \Lambda(m,i) &\triangleq \left| \sum_{n=0}^{N_g-1} r(\zeta+m+n)\; r(\zeta+n+N+i) \right| \\ m &\in \{-W/2 \cdots W/2\}\,;\; i \in \{-\Upsilon'/2 \cdots \Upsilon'/2\}\,, \end{aligned} \tag{4.26}$$

then, $\hat{\theta}_{m,i}$ can be estimated from obtaining the maximum peak of the multiplication and it can be written as

$$\begin{aligned} \hat{\theta}_{m,i} &= \arg\max\, (\max_{m,i}\, \Lambda(m,i)^T) \\ m &\in \{-W/2 \cdots W/2\}\,;\; i \in \{-\Upsilon'/2 \cdots \Upsilon'/2\}\,, \end{aligned} \tag{4.27}$$

and the fine tuned ζ' is obtained. The implementation of this fine tuning algorithm of the coarse packet synchronization can be summarized as follows:

1. compute the coarse packet synchronization point ζ which represents the time position of the maximum peak of the chirp correlation,
2. compute the timing function $\Lambda(m,i)$ for $m \in [-W/2, W/2]\,, i \in [-\Upsilon'/2, \Upsilon'/2]$,
3. choose the maximum of $\Lambda(m,i)$ as the estimated packet timing offset,
4. update ζ to be fine tuned which is given as

$$\zeta' = \zeta + \hat{\theta}. \tag{4.28}$$

It should be noted that a two dimensional search (i.e. m and i) is included in the proposed timing function $\Lambda(m, i)$. This is the main difference from the single synchronization point estimation in [93], where only coarse estimation of the packet synchronization point is adopted. The first search parameter is m, corresponding to the first search region in the range around the coarse synchronization point ζ. Meanwhile, the second search parameter is i, corresponding to the range in the region around the tail of the OFDM symbol which yields the expected Doppler shift. Once the fine tuned ζ' is obtained, the subsequent stage is the estimation of the first order moment $\hat{\phi}$. In existing techniques, [14] and [94], due to the acceleration and the inherent ISI, there is a fluctuation in the maximum of the timing function and the channel conditions have a direct effect on this maximum. Therefore, centroid-based localization is adopted to estimate $\hat{\phi}$, because it reduces the position uncertainty caused by the fading channel, and the search range is built on the fine tuned ζ', which can be written as

$$r_D \in [\zeta' + N_g + N - (\frac{\Upsilon}{2}) + i, \zeta' + N - (\frac{\Upsilon}{2}) + i], \tag{4.29}$$

and the centroid-based first order moment $\hat{\phi}_l$ is given as in chapter 3. Fig. (4.11) shows that fine tuning this parameter results in reducing the BER. It can be inferred from this figure that adjusting the misalignments of the symbol timing due to the time varying Doppler scale results in an improvement in the reliability of the re-sampling factor estimation, which in turn reduces the noise that accompanies accumulated errors from symbol to symbol within each packet and ultimately a reduction in BER is obtained.

4.5.4 Performance evaluation based on two point correlation

Fine tuning of the coarse symbol timing facilitates an alternative approach to estimating the first order moment of the correlation lag. The suggested approach here aims to increase the confidence of estimation by considering the first order moment that results from two correlation lags. The first correlation lag is estimated by means of centroid-based localization, in accordance with the anticipated window mentioned earlier. This type of correlation gives an accurate indication of the fractional part

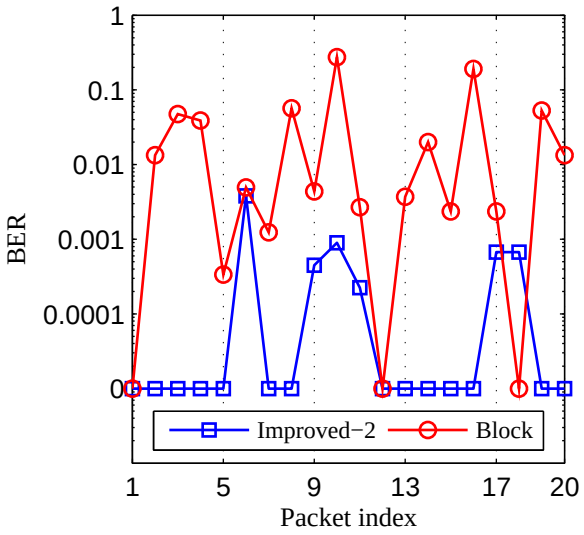

Figure 4.11: Performance of the proposed system with improved coarse timing estimation.

of the time-scale expansion/compression. However, the centroid-based localization is severely affected due to the velocity perturbation. This perturbation degrades the estimation performance of the timing function and ultimately $\hat{\phi}_l$. Therefore, an alternative approach has been adopted by involving another estimation point based upon full cross correlation of the CP with its replica. The addition of this correlation is based on the idea of increasing the certainty of the first order moment estimation. This correlation is based on the assumption that the OFDM timing is approximately aligned due to the fine tuning of the packet synchronization ζ'. By definition, the cross correlation between a pair of energy signals, $x[n]$ and $y[n]$, is given by [95]

$$r_{xy} = \sum_{n=-\infty}^{\infty} x[n]\, y[n-\chi], \qquad \chi = 0, \pm 1, \pm 2, \cdots, \tag{4.30}$$

where the parameter χ is called *lag* and it indicates the time-shift between the pair. Based on this theory, the time-shift in samples for either expansion or compression can be measured with respect to a reference sequence length of the guard interval N_g. In the case of the existence of Doppler shift, the received samples are shifted to the right in expansion or left for compression with respect to the reference. To be more specific, once the start of the packet ζ is identified, it can be deemed that the symbol timing identification is reliable and the correlation between the received CP

and its replica is computed to measure the time-shift in the samples

$$\begin{aligned} \Lambda_c &\triangleq \left| \sum_{n=0}^{N_g-1} r(\zeta' + n)\ r(\zeta' + n + N - \chi) \right|, \\ \chi &= 0, \pm 1, \pm 2, \cdots . \end{aligned} \tag{4.31}$$

Considering that the reference sequence of the transmitted CP is $N_{cp}N_s$, the first order moment of the Doppler shift ϕ_x can be approximated as

$$\begin{aligned} \hat{\phi}_x &= \arg\ \max\ \Lambda_c - N_{cp}N_s, \\ \chi &= 0, \pm 1, \pm 2, \cdots . \end{aligned} \tag{4.32}$$

Adopting such a scenario requires extraction of a fine tuned correlation lag. This necessitates involvement of two parameters of weighting coefficients to perform such a smoothing approach, as mentioned earlier. The coefficients W_1 and W_2 are empirically obtained from the experiment to accommodate the measured channel condition. Therefore, ϕ', which represents the fine tuned first order moment of the correlation lag, is given as

$$\phi' = \hat{\phi}_x W_1 + \hat{\phi}_l W_2. \tag{4.33}$$

This fine tuned parameter is then delivered to the Doppler extraction in Fig. 4.1(b) in order to estimate the Doppler shift. Accordingly, the estimated Doppler shift, which comprises both an integer and fractional part, is considered and utilized for compensation. Therefore, the estimated re-sampling factor requires no extraction of the fractional part to estimate the residual Doppler shift, as shown in Fig. 4.1(b); hence the CFO is approximated as

$$\hat{\epsilon} \simeq 0.5 f_c \delta f / f_s \simeq \frac{\delta f}{8}, \tag{4.34}$$

where $f_s = 4f_c$. For sub-carrier spacing of 3.90625, as in the case of 1024 sub-carriers, $\hat{\epsilon}$ is 0.4883 Hz. These two-point estimations of $\hat{\phi}_l$ and $\hat{\phi}_x$, in conjunction with ϕ', contribute towards improving the Doppler shift estimation and thus eliminate the need to determine the CFO.

Fig. (4.12) demonstrates the implications of improving the Doppler shift estimation. It is obvious in this figure that there are two estimations that show the deceleration in velocities over the symbol time. With respect to the improved sys-

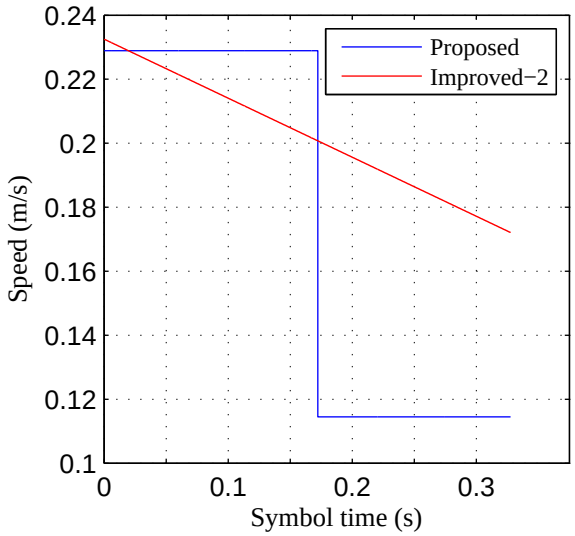

Figure 4.12: Improved time-varying speed estimation during OFDM symbol 7 of packet 6.

tem, the gradient is estimated smoothly. This confirms that an accurate estimation of the drift in samples results in an accurate estimation and tracking of the time varying Doppler shift. On the other hand, this figure illustrates that perturbations in estimating the variation of speed within the OFDM symbol can lead to inaccurate re-sampling factor estimation. In particular, it can be inferred from this figure that there is a time varying Doppler shift during the symbol time which decelerates in the order of 0.25 m/s^2. This deceleration is estimated by smoothing ζ estimation. However, in the proposed system, the deceleration is approximated to 0.48 m/s^2 over the same symbol. For the sake of clarity, the proposed system refers to the system before the improvements and the improved system refers to the proposed system after improving ζ estimation. Table 4.2 illustrates the performance comparison between block based Doppler compensation, time varying Doppler shift compensation and its improvements. The achieved BER decreases significantly in the improved system compared with the block based approach. Likewise, there are additional improvements in the BERs of 83.8 % compared with the proposed technique. This is shown in Fig. (4.13)(a), where the BER of packet 6 is reduced compared with Fig. (4.7)(a). Additionally, the error statistics of packet 6, shown in Fig. (4.7)(b) and Fig. (4.13)(b), confirm that estimating multi-lags contributes to an increase in the accuracy of the speed estimation.

As demonstrated in Fig. (4.13)(c), the experimental results show that the investigation was also successful with 512 sub-carriers, as it was able to improve perfor-

Table 4.2: Performance of the experimental results between the improved and block-based Doppler shift techniques for N_c=1024

Packet index	1	2	3	4	5	6	7	8	9	10
Block	0	119	423	347	3	44	11	505	39	2443
Proposed	0	0	3	6	0	33	0	6	9	0
improved	0	0	0	0	0	3	0	0	0	5
Packet index	11	12	13	14	15	16	17	18	1 9	20
Block	24	0	33	178	21	1702	21	0	471	119
Proposed	0	0	6	14	5	0	0	0	23	0
improved	0	0	0	0	9	0	0	0	0	0

mance by about 86%. This was an expected result, because reducing the symbol length entails increasing the sub-carrier spacing and reducing the sensitivity to the Doppler shift. Additionally, reducing the symbol length enables more frequent tracking of the Doppler shift. However, severe consequences accompany this reduction in the symbol time, since it mitigates immunity against ISI, in addition to reducing the available bandwidth. This performance reveals that improving the synchronization and adopting smoothing produces low BER. Furthermore, compensating residual Doppler shift or CFO preserves the orthogonality of the sub-carriers and ultimately contributes towards mitigating decoding errors.

However, it is worthwhile mentioning that this approximation of the CFO cannot be extrapolated to all cases, as in the case of higher acceleration where a special signal processing method, such as an adaptive weighting coefficients selection and/or iterative-based estimation of the Doppler shift, should be adopted due to the effect of the time varying Doppler shift and the inherent ISI on the correlation peak. Another problem with this approach is that it fails to compensate for an abrupt change in the direction of velocity, as it needs at least two symbols to self-adapt to this sudden variation which causes a decoding error. In terms of the achieved data rate, Table 4.4 presents two types of OFDM sub-carrier allocation that account for the transmission overhead due to pilots, channel coding, and guard period.

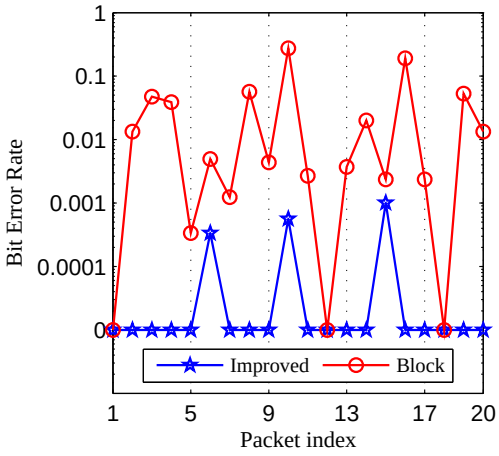

(a) BER for each packer over 1000 m range

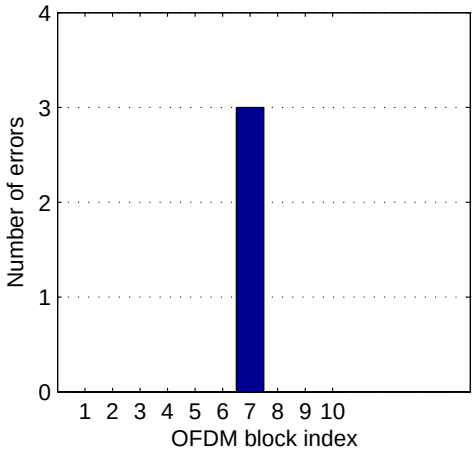

(b) Packet 6; symbol 7 error statistics

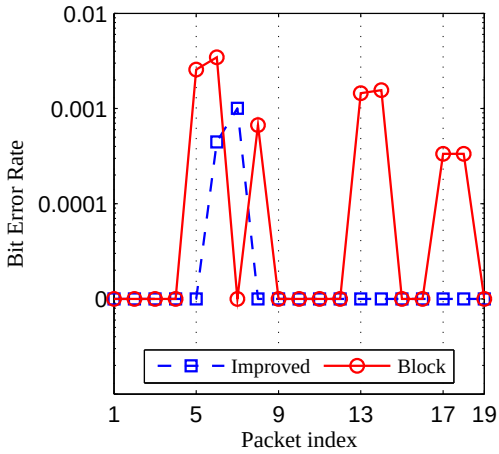

(c) BER for each packer over 1000 m range at 512 sub-carriers.

Figure 4.13: Performance of the improved proposed system.

4.6 Simulation results

Fig. (4.14) shows, in terms of BERs, the performance comparison between the block-based approach and the proposed technique obtained by simulations. For the block-based approach, two scenarios of the transmitted packet structure are investigated. The first structure includes 20 ms chirp, followed by a silent period then 10 CP-OFDM symbols. The second structure comprises only a single CP-OFDM frame. The former structure is investigated in the experiment; therefore the second structure is considered here for the purpose of the simulation. It can be seen that the performance of the block approach is poor in the case of multi-scale Doppler within the OFDM symbol. When the speed is low, as shown in the OFDM symbols indices

Table 4.3: Performance of the experimental results between the improved and block-based Doppler shift techniques for N_c=512

Packet index	1	2	3	4	5	6	7	8	9	10	11	12	13	14	15	16	17	18	19
Block	0	0	0	0	23	31	0	6	0	0	0	0	13	14	0	0	3	3	0
Improved	0	0	0	0	0	4	9	0	0	0	0	0	0	0	0	0	0	0	0

Table 4.4: OFDM symbol structure and the corresponding data rates

N_c	N_d	N_p	N_b	data rates (kb/s)
512	448	64	20	3.0833
1024	896	128	10	3.2794

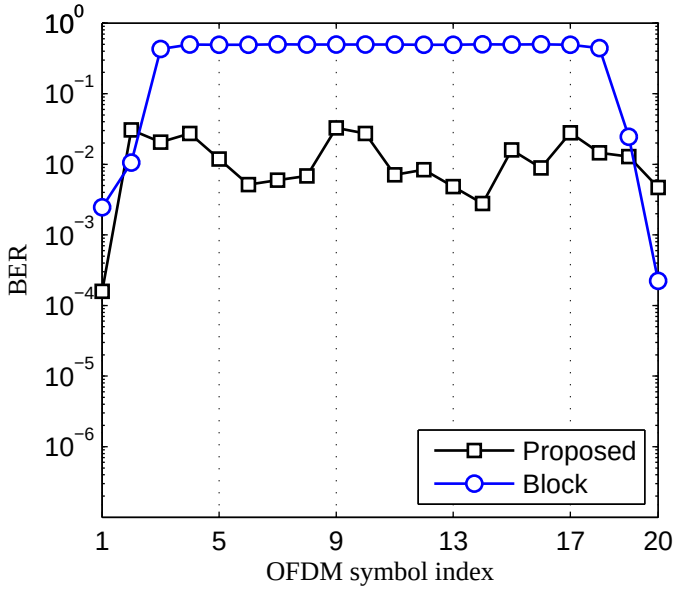

Figure 4.14: Performance comparison of block based and proposed techniques.

1 and 20, the block algorithm performance is approximately identical to that of the proposed scheme. However, as the speed increases, the BER also increases in the block-based approach, whereas the proposed algorithm demonstrates less performance error despite an escalation in speed. The degradation in the BERs in the proposed algorithm is due to the effect of the acceleration on the CP correlation.

4.7 Chapter summary

The performance of time-varying Doppler shift compensation for an OFDM-based UWA communication system has been investigated. The algorithm accommodates for channels with linear acceleration during a packet of multiple OFDM frames. Unlike existing Doppler compensation methods, the proposed scheme is more pragmatic, as it considers the notion that the speed is changing linearly during the OFDM symbol time. Additionally, under the assumption of linear speed during the packet time, it has been shown that using the linear equation approach to predict the first order Doppler shift as a reinforcement parameter leads to acceptable performance over other techniques. Furthermore, it has been shown that employing weighted coefficients improves the performance as it fine tunes the estimated parameters. However, an approach to fine tuning these parameters adaptively and in accordance with the acceleration is required and will be discussed in the next chapter.

Chapter 5

Adaptive time varying Doppler shift compensation

This chapter presents an adaptive approach to address the two main problems associated with the time varying Doppler shift, the first being the acceleration effects on the CP correlation and the second, the effect of a sudden change in the velocity direction between packets on the entire OFDM symbols. In addition, this chapter considers the residual Doppler shift or CFO that was estimated iteratively within a range according to a design based on the sub-carrier spacing using pilots, which are basically utilized for the purpose of channel estimation. Furthermore, the proposed receiver adopts three estimations of the symbol timing offset. These estimations are centroid-based localization, first order expectation and autocorrelation of the received cyclic-prefix with its replica. Subsequently, a penalization algorithm is applied in order to drop the anomalous parameter among them. Therefore, the consequences of the inflection point that accompanies the abrupt change in the velocity are mitigated and a reliable time varying Doppler shift is obtained. This Doppler shift is fine tuned in an iterative manner. The proposed receiver was evaluated through simulations and sea trials conducted over 500 m and 1000 m channel ranges. In simulations, a model was designed to imitate the time varying Doppler shift with two scenarios (expansion/compression) in combination with a multipath.

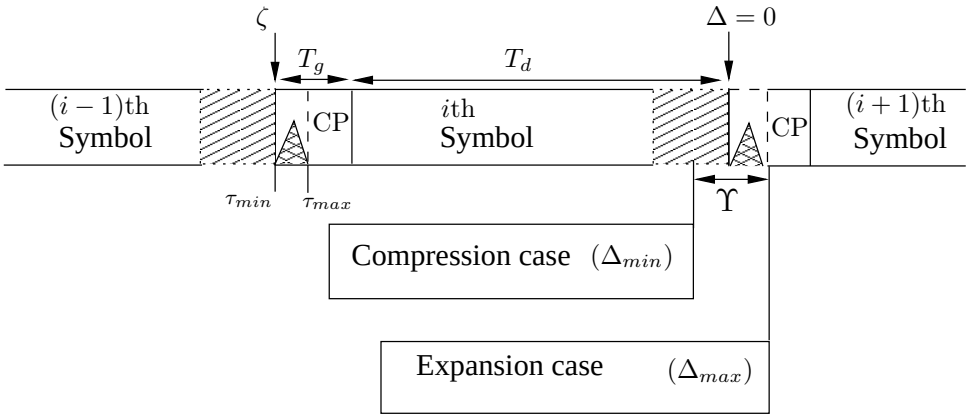

Figure 5.1: OFDM symbol structure due to Doppler effects.

5.1 Acceleration effects

A pragmatic underwater communication system which adopts Doppler shift estimation and compensation should consider the change of speed with time, which is called acceleration (a). The effect of acceleration as a result of the mobility of the transmitter and/or receiver and causes time-varying Doppler shift. Therefore, this type of Doppler shift can be modelled [8] as

$$\Delta(t) = \Delta_0 + \frac{a(t)t}{c}, \tag{5.1}$$

where Δ_0 is the initial Doppler shift which accompanies the platform velocity and $a(t)$ is time varying acceleration. The acceleration effects can be twofold. First, an effect on the chirp signal detection, particularly when the change in velocity during the chirp period is greater in magnitude than the platform velocity. Consequently, this mismatch affects the correlation peak of the chirp when detecting the start of the packet. A more significant effect of acceleration to be considered is its effect over the whole symbol or packet. In this case, the cyclic prefix and its replica undergo different Doppler-shifts. This results in uncertainty of the correlational behaviour and consequently adds an error to the first order moment estimate $\hat{\phi}_l$.

There are three different cases of an OFDM symbol subject to Doppler shift as shown in Fig. (5.1). The first case is when there is no Doppler shift. In this case, the OFDM symbol coincides with the exact timing, preserving the orthogonality among sub-carrier frequency components. In the compression case, the symbol time is reduced and the sampling frequency must be increased to compensate for the Doppler shift whereas in the expansion case, the symbol time is increased and the sampling

frequency is reduced. In addition, the received signal within the FFT window contains a part of the current OFDM symbol and part of the next one. This causes an ISI and an ICI, which implies that the orthogonality has been compromised.

Let us assume without loss of generality that the initial velocity in (5.1) is zero, therefore, the Doppler shift at the end of the packet is:

$$\Delta = \frac{aT_{\text{pac}}}{c}. \tag{5.2}$$

In addition, it is mentioned in [8] that the Doppler shift estimation error is related to the acceleration and the chirp duration. In the proposed CP-based Doppler shift compensation, this error is modelled as

$$\epsilon'_{\Delta} = \frac{aT_g}{c}. \tag{5.3}$$

Therefore, for practical acceleration levels (1 m/s^2), reducing the length of the cyclic prefix is more useful. However, this reduces the sensitivity to low acceleration. The other crucial implication of acceleration over the symbol length to be considered is the residual Doppler shift. In the case of constant acceleration, this effect is dealt with by adaptive equalization in a single carrier transmission, which can not be used with OFDM. In addition, for constant acceleration, the estimated Doppler represents the average velocity, i.e, the maximum residual Doppler shift at the symbol ends is given as [8]

$$\max(\Delta_{residual}) = \mp\frac{aT_u}{2c}. \tag{5.4}$$

It can be inferred that, to mitigate the residual Doppler shift, the symbol length should be reduced, and hence, the sub-carrier spacing is increased. However, in OFDM system design, reducing the symbol length entails reducing the immunity against the ISI.

5.2 Adaptive OFDM receiver structure

The receiver structure is comprised of an acquisition stage, an estimation of the cyclic prefix position (symbol timing), an adaptive Doppler shift estimation and compensation, and channel decoding. The receiver block diagram is presented in Fig. (5.2). In open-loop receivers, the Doppler shift is approximated based on one-shot esti-

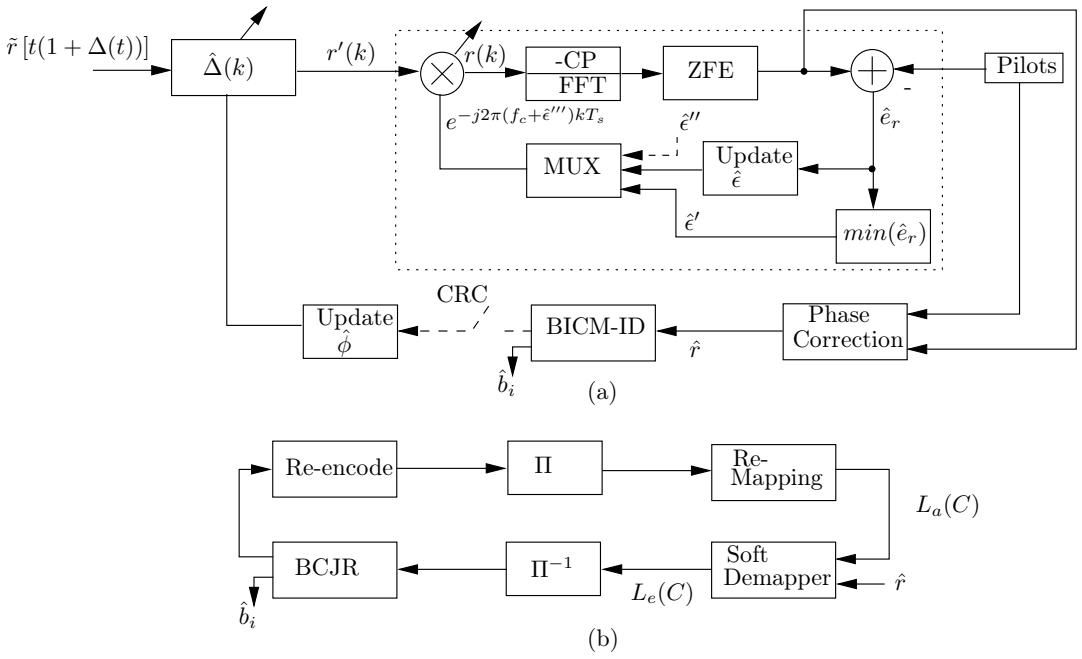

Figure 5.2: Receiver structure

mation. The iterative receiver, instead of depending on a single estimation of the centroid-based localization and linear prediction to estimate the Doppler shift, combines conventional autocorrelation and then averaging based on three estimations. Furthermore, the pilot has been utilized for phase error detection and correction in addition to channel estimation. The proposed system adopts an iterative estimation of the first order moment that results in minimum phase and decoding errors. In a practical communication system, there is a CRC to detect bit errors after decoding and an action such as retransmission or repeat decoding is taken. Additionally, the iterations rely on the criteria of minimum phase error estimation to compensate the residual Doppler shift. In the proposed technique, the estimation errors are subject to penalization by enabling a *learning and punishment* (LP) action to fine tune ϕ iteratively. Only the minimum phase error which accompanies the ith iteration is chosen with its associated ϕ, therefore, an accurate Doppler shift is obtained. In *learning mode* (LM), the acceleration of the previous packet is observed to designate an adaptive *expectation range* (ER), whereas the *punishment mode* (PM) drops an out of range estimation.

5.2.1 Estimation of Symbol timing expansion/compression

In this chapter, instead of a single estimation of the first order moment, it has been estimated by the collaboration of centroid-based localization ϕ_l, auto correlation of

the cyclic prefix with its Doppler-shifted replica ϕ_{yy} and first order expectation ϕ_E. In such a case, the conditional expectation of ϕ is given

$$\hat{\phi} = E(\phi/\tilde{\phi}) = E\left[\phi/\tilde{\phi}(0), \phi/\tilde{\phi}(1), \phi/\tilde{\phi}(2)\right], \tag{5.5}$$

where the symbol E denotes the expectation operator and $\tilde{\phi} = \left[\tilde{\phi}_l, \tilde{\phi}_{yy}, \tilde{\phi}_E\right]$ is a row vector of scalar real values noisy measurements. For the first OFDM symbol j, the estimation of the first order moment $\hat{\phi}_j$ is based on averaging $\tilde{\phi}_l$ and $\tilde{\phi}_{yy}$. However an additional parameter is added which is based on the linear expectation $\tilde{\phi}_E$ as mentioned in chapter 4, therefore

$$\bar{\phi}_j = \frac{\tilde{\phi}_l + \tilde{\phi}_{yy} + \tilde{\phi}_E}{3}, \quad \text{for } j > 2 \tag{5.6}$$

5.2.1.1 Control range and PM algorithms

The parameter $\tilde{\phi}_E$ can only be considered reliable with increasing or decreasing gradient, i.e., when the speed change is unidirectional during a packet time. However, this is an unrealistic condition, where the speed could be steepening and levelling off during the packet time. Therefore, it is crucial to govern the estimation within a specific range to detect anomalous situations. This range is the first part of the PM and it is built on the assumption that the speed is increasing with the packet time at constant acceleration.

Based on that, the system is capable of predicting the drift in samples in the next symbol. Let us define a new variable ϕ_a to buffer the absolute difference between $\hat{\phi}_c$ and $\hat{\phi}_p$

$$\phi_a = |\hat{\phi}_c - \hat{\phi}_p|, \tag{5.7}$$

where $\hat{\phi}_c$ and $\hat{\phi}_p$ represent the current and previous estimation at time j and $j-1$, respectively; determining the mean value $\bar{\phi}_a$ of (5.7) over the OFDM blocks. Accordingly, we formulate a general expected range in samples $\hat{\phi}_C$ and it can be written as

$$\hat{\phi}_C \leftarrow \hat{\phi}_{j-1} \pm 2|\bar{\phi}_a|, \tag{5.8}$$

where the (+) sign indicates an acceleration in the expansion of the signal since the distance is increased and vice versa. Algorithm 2 is developed to deal with these scenarios.

input : Parameters $\bar{\phi}_a$, $\hat{\phi}_{j-1}$
output: Range for $\hat{\phi}_{CP}$, $\hat{\phi}_{CN}$

1 **if** $Flag > 10$ **then** // <Flag represents the symbol index>
2 $\quad \hat{\phi}_{CP} \leftarrow \hat{\phi}_{j-1} + 2|\bar{\phi}_a|$
3 $\quad \hat{\phi}_{CN} \leftarrow \hat{\phi}_{j-1} - 2|\bar{\phi}_a|$
4 $\quad$ **else**
5 $\quad \hat{\phi}_{CP} \leftarrow \hat{\phi}_{j-1} + 4$
6 $\quad \hat{\phi}_{CN} \leftarrow \hat{\phi}_{j-1} - 4$
7 **end**

Algorithm 2: Range algorithm

It can be noticed from algorithm 2 that $\hat{\phi}_{CP}$ and $\hat{\phi}_{NP}$ ranges are assigned for the positive and negative acceleration, respectively. Particularly, if $\hat{\phi}_{j-1} = 5$ samples and the average drift in samples of the the previous 10 OFDM blocks were $\bar{\phi}_a = 2$ samples, therefore, it is expected $\hat{\phi}$ to be $\hat{\phi}_{j-1} \mp 2$. Accordingly, in algorithm (2), lines 2 and 3, we expand the range to a square half of this coefficient. In this case the range is expressed as $[\hat{\phi}_{j-1} - 2|\bar{\phi}_a|, \hat{\phi}_{j-1} + 2|\bar{\phi}_a|]$ instead of $[\hat{\phi}_{j-1} - |\bar{\phi}_a|, \hat{\phi}_{j-1} + |\bar{\phi}_a|]$. In lines 5 and 6 on the other hand, $\hat{\phi}_{j-1} \mp 4$ is based on the assumption that $a = 1\text{m/s}^2$. In this case the speed will change ∓ 0.25m/s in each OFDM symbol and this can be interpreted in terms of samples to ∓ 2 samples. As in lines 2 and 3, the tolerance is also increased by 2.

The second step in the PM is to set the conditions that are needed to make an action to correct the estimation. There are three cases adopted here to perform the PM. In each case, two out of three parameters are considered and the third one is dropped. This procedure is resorted to in order to accommodate the abrupt change in the direction of the velocity, hence, the range control detects this perturbation in the speed while the PM applies the appropriate action by ignoring the nuisance parameter. Consequently, the average of the reliable parameters are considered and utilized in the search. This procedure of PM is shown in algorithm (3).

5.2.2 Early termination search algorithm

In this algorithm, we are trying to estimate and compensate the time varying Doppler shift recursively. An adaptive step-size is formulated in accordance with a number of iterations to obtain an optimal search that results in minimum errors. The criteria of optimality is adopted here in the sense of performance investigation,

input : Parameters $\tilde{\phi}(i)$, $\hat{\phi}_{CN}$, $\hat{\phi}_{CP}$
output: Parameters within the expected range

```
for i = 1 : 3 do
    if (φ̃(i) < φ̂_CN || φ̃(i) > φ̂_CP) then
        switch (i) do
            case (1)
                φ̃(1) ← 0.5(φ̃(2) + φ̃(3))
            case (2)
                φ̃(2) ← 0.5(φ̃(1) + φ̃(3))
            case (3)
                φ̃(3) ← 0.5(φ̃(1) + φ̃(2))

        endsw
        else
        φ̃(i) ← φ̄
    end
end
```

Algorithm 3: PM Algorithm

therefore, the CRC is employed to terminate the search swiftly once there is zero decoding errors. On the other hand, this search algorithm reveals the minimum phase error and their accompanied parameters that give the lowest BER to be utilized later in the outer iteration. This outer iteration is enabled when the search algorithm fails to produce zero decoding errors.

5.2.2.1 Selection of step-size (μ) and correction factor (K_i)

For a closed-form system that contains several instantaneous variables, the estimation of the required parameter is generally not possible [96]. An alternative solution to approximate the parameter is adopting an iterative approach. The estimation of the parameter at iteration i represents the initial expectation and then this estimation is resumed recursively to improve it. Based on this approach, the parameter $\hat{\phi}_{i-1}$ which is fine tuned earlier to produce minimum error among three estimation agents, is utilized. The adaptation factor is shown as

$$\mu = 0.33(\frac{sgn(i/2)\ \lfloor |i/2| \rfloor}{0.5\ \ell})^n, \tag{5.9}$$

where n is a positive integer exponent and ℓ represents the search points. It should be stressed that equation (5.9) is empirically obtained. The search is chosen to converge

the correction term given in (5.10) towards minimizing the phase error and reliable estimation of $\hat{\phi}$. This correction term is initialized to 1 and then approximated iteratively. The idea behind selecting a cubic exponent step size is to search in a convergent manner as the cardinality of estimation is high at the beginning and once it diverges the estimation error is expected to be increased. In terms of complexity, this search algorithm is better than a linear approach, where it requires higher execution time. In addition, this type of search has an automatic early termination (AET) condition. This termination depends on:

1. The CRC results 0 errors,

2. Reaching the maximum search points.

Resorting to the iteration is to practice another step-size and correction term that should be selected closer to those at previous iteration. In this manner, it is devised that the search algorithm diverges one step per iteration around the range $[\ell/2]$ towards left and $[\ell/2]$ towards right. An action is taken in case of reaching the full range by considering the estimated $\hat{\phi}$ at iteration i.

$$K_i = \begin{cases} \mu + 1 & mod(i,2) = 0 \\ \mu - 1 & otherwise \end{cases} \tag{5.10}$$

As shown in Fig. (5.15), the exponent n of the step-size in (5.9) plays an important role on reducing the errors. Although a higher degree of exponent indicates that the estimation is reliable, there is a level at which no improvement gain is obtained.

It is shown in Fig. (5.3)(b) that at $n = 3$, the horizontal asymptote start smoothly during the first 10 candidate points of the search range, whereas, the smoothness period is smaller when $n = 2$. On the other hand, in a linear case $n = 1$, the step-size is constant.

The implications of the step-size in (5.9) are shown in Fig. (5.3)(a). In this figure, the correction factor K_i is changing in accordance with the step size to ultimately enforce $\hat{\phi}_c$ to converge. However, failing to attain an improvement and ultimately converging to AET condition 1 results in an increased estimation error, hence, the correction term in (5.10) diverges and then the search algorithm starts to choose a larger step-size.

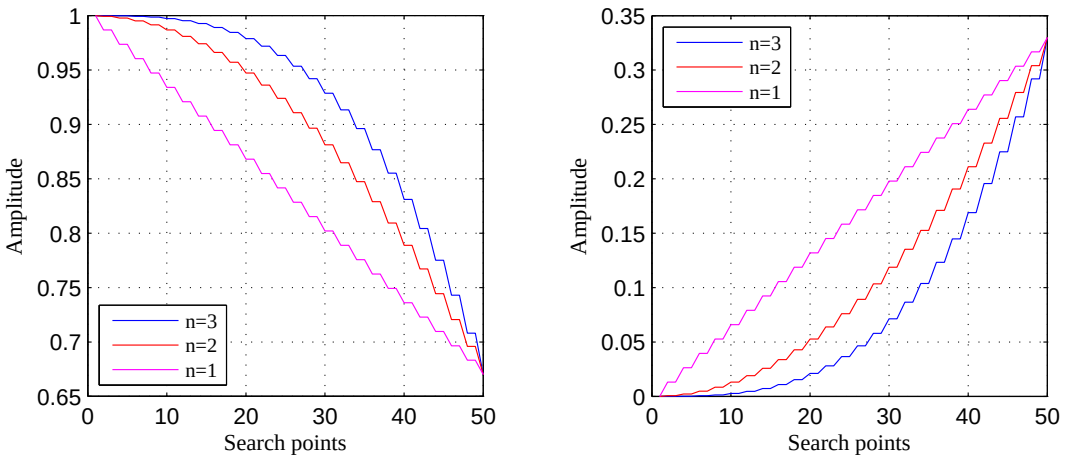

(a) Change of correction factor as a function of the exponents.

(b) Change of step-size as a function of the exponents.

Figure 5.3: Effect of exponents on step-size and correction factor convergence.

5.2.2.2 Time-varying Doppler shift estimation and tracking

In terms of performance, when $n = 3$, it can be inferred that the reliability of estimating $\hat{\phi}_c$ in (5.15) is high and is only needed to fine tune the approximation, thus it necessitates adjusting the step size closer towards the left or right around the middle of the search range. In this case fine tuned $\hat{\phi}_c$ is obtained. It represents the timing offset at the start of the OFDM symbol, which is approximated as

$$\hat{\phi}_c = \tilde{\phi} K_i. \tag{5.11}$$

The parameter $\hat{\phi}_c$ contributes to the improvement of other dependent parameters, particularly, the tracking step. Therefore, the iterative approach represented by the search is important to approximate the Doppler shift estimation. To be more specific, let us assume that the speed between the transmitter and receiver is 1 m/s, which is equivalent to 8 Hz for a carrier frequency of 12 kHz and sampling frequency $4f_c$, therefore, $\hat{\Delta}$ =1.0006 and the estimated ϕ should be 2.048 for 12288 FFT up-sampling. Actually, these calculations yield that there is a demand on estimating and compensating such Doppler shift that has a fraction of a variable time expansion and/or compression. Therefore, dealing with such time-varying Doppler shift needs to track this variation within the symbol time. In (4.14), this Doppler is dealt with by deriving a tracking step to estimate this variation based on dividing the time-varying Doppler shift into an integer part for re-sampling and its residual or CFO

is represented by the fractional part of the Doppler shift and smoother Doppler shift estimation is obtained. However, in the proposed adaptive system, recursive iteration to fine tune $\hat{\phi}_c$ is adopted and the time-varying Doppler shift contains the re-sampling factor with its residual. Furthermore, it has been dealt with CFO estimation separately hence, the Doppler shift is given as

$$\hat{\Delta}(k) = \frac{L_f - \hat{\Psi}(k)}{L_f}, \tag{5.12}$$

where $\Psi(k)$ is the sampling frequency offset initialized with $\hat{\phi}_s$ at k=1 and its update is approximated as

$$\Psi(k) = \Psi(k-1) + \hat{\phi}_{step}, \tag{5.13}$$

where $\hat{\phi}_{step}$ is given in (4.14).

Utilizing $4th$ order Lagrange interpolation polynomial [97] for re-sampling based upon the parameter $\hat{\Delta}(k)$ to produce $r'(k)$. This re-sampled signal can be mathematically written as

$$r'(k) = \sum_{i=0}^{N} \tilde{r}_{m'}[k(1+\Delta(k))]V_i(m'), \tag{5.14}$$

where

$$V_i(m') = \prod_{i=0, n\neq i}^{N} \frac{m' - m'_n}{m'_i - m'_n}, \tag{5.15}$$

where, $V_i(m')$ represents the polynomial of degree N associated with each node i. where $m' = m' + \hat{\Delta}(k)$ initiated with 3, $n \in \{1, 2, ...N\}$, $R = \lfloor m' \rfloor$ and $m'_i = R_{i-2}$. Therefore, for five points $N = 4$, the current point, the two previous points and next two points are considered to fit the interpolation curve.

5.2.2.3 Residual Doppler shift estimation

Post-FFT CFO estimation is adopted. When all angles of the received nth pilots $Y_p(n)$ are shifted by the same angle, the ZFE is capable of correcting the rotation. However, this is not the case where each sub-carrier is rotated depending on the residual Doppler shift. In order to estimate this residual, a range of these parameters are assumed. Start with $\hat{\epsilon}$ and for each candidate i, the phase error vector is

determined as

$$\hat{e}_i(n) = \sum_{n=0}^{N_p-1} \angle(Y_p(n)) - \angle(X_p(n)), \tag{5.16}$$

considering the mean phase error between the transmitted and received pilots that is given as

$$\bar{e}_i = \frac{\sum_{n=0}^{N_p-1} \hat{e}_i(n)}{N_p}, \tag{5.17}$$

therefore, the estimated residual phase error at the pilots sub-carriers indices can be formulated as

$$\hat{e}_r = \sum_{n=0}^{N_p-1} |\hat{e}_i(n) - \bar{e}_i|, \tag{5.18}$$

and the CFO can be approximated as a function of this pilot-based residual phase error estimation

$$\hat{\epsilon}' = \epsilon \left(\underset{min}{\hat{e}_r} \right). \tag{5.19}$$

This criteria denotes the CFO candidate that accompanies the lowest phase error. Hence, after re-sampling, the resulting received signal $r'(t)$ is then down-converted to baseband with the chosen $\hat{\epsilon}'$ and can be written as

$$r(t) = r'(t)e^{-j2\pi(f_c+\hat{\epsilon}')kT_s}. \tag{5.20}$$

After compensating the CFO in (5.20), the resulting signal $r(t)$ is converted to the frequency domain and delivered to the ZFE. To improve the receiver performance, post-FFT tracking is useful to mitigate the remaining CFO [86]. Although this residual is small, it degrades the receiver performance due to the accumulated phase rotation consequences along each OFDM symbol in the packet [98]. On the assumption that the CFO is compensated earlier, it is worth eliminating its phase rotation effect. Here in this proposed technique, we utilize the pilots to estimate the residual phase error of the current OFDM symbol which can be written as

$$\theta_i = \angle(Y(n)) - \bar{e}_i, \tag{5.21}$$

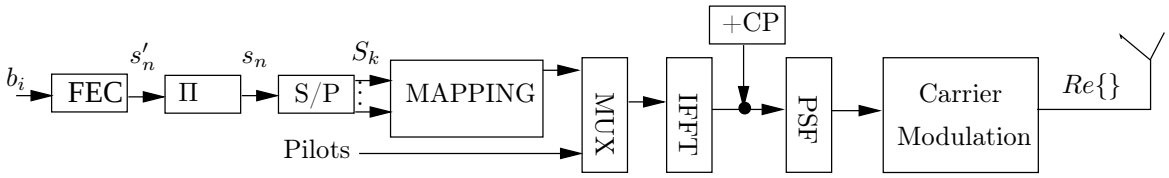

Figure 5.4: Structure of the transmitter used in simulation.

and the residual phase error correction is written as

$$\hat{r} = Y(n) = e^{j\theta_i}, \tag{5.22}$$

which is the OFDM signal after residual phase correction. This yields to deliver reliable information to the BICM-ID decoder.

Based on the CRC, a decision is made to terminate the search or resume the iteration. In Fig. (5.2), it can be seen that once the search points are completed and there is an error after performing the CRC, which is assigned a dashed line, the outer iteration is enabled as a final trial. To deal with this case, the phase error given in (5.16) is utilized to buffer the associated parameters $\hat{\phi}'_c$ and $\hat{\epsilon}''$ that result in minimum phase error during previous iterations. Exploiting $\hat{\phi}'_c$ updates the Doppler shift and produces a new interpolation factor whereas $\hat{\epsilon}''$ is utilized in compensating the CFO. In order to distinguish the CFO at each stage, we use the variable $\hat{\epsilon}'''$, which denotes the output of the multiplexer among three estimations.

5.3 System design, simulation, and experimental results

Fig. (5.4) depicts the structure of the transmitter used in simulation. For the sake of simplicity, it is assumed that the system under consideration does not account for the PAPR, as in the experiment. The binary information bits b_i of length K_d are applied to the FEC of type NSC to produce a codeword, s'_n, of length $K_c = K_d/R$ encoded bits, where $R \in (0, 1]$ is the coding rate. The coded bits are permuted by a random interleaver of length L_I to generate bit sequence c_n, then converted in groups of m successive bits into alphabet symbols of constellation size $M = 2^m$. This mapping operation induces a sequence of $N_u = K_c/m$: $\mathbf{s} = \{s_0....s_{N_u-1}\}$, where $s_i \in \mathbb{C}$ and $\mathbb{C}$ denotes the set of complex symbols. Subsequently, in the

OFDM symbol to be constructed, pilot symbols of phase shift keying (PSK) with unit amplitude are embedded with the data symbols in a comb method. These pilot symbols are multi-purpose. Firstly, they are used for the purpose of channel response estimation at the receiver and secondly, as a reference for phase correction. The resulting OFDM symbol containing pilots and data-bearing sub-carriers is then modulated by an IFFT of size N_c and the last samples are copied and preface the symbol to form the CP-OFDM frame. The resulting frame is pulse shaped using a PSF and then up-converted using carrier modulation. The passband model of the transmitted OFDM ithsymbol $x(t)$ is mathematically represented as

$$\begin{aligned} x_i(t) &= \Re\left\{ e^{j2\pi f_c t} \sum_{i=0}^{\infty} \frac{1}{\sqrt{N_{\mathrm{c}}}} \sum_{n\in\mathcal{J}} d_i(n) e^{j2\pi \frac{n}{T_d}(t-T_g-iT)} p_{\mathrm{rc}}(t-iT) \right\} \\ &= \Re\left\{ \sum_{i=0}^{\infty} \frac{1}{\sqrt{N_{\mathrm{c}}}} \sum_{n\in\mathcal{J}} d_i(n) e^{j2\pi f_n(t-T_g-iT)} p_{\mathrm{rc}}(t-iT) \right\}, \end{aligned} \tag{5.23}$$

where $d_i(n)$ is the symbol transmitted over the nth sub-carrier, $p_{rc}(t-iT)$ is the pulse shaping filter.

The transmitted signal $x(t)$ in (5.23) is passed through the channel model shown in Fig. (5.5). This model is adopted to imitate the case of the time varying Doppler shift with constant acceleration. Performing this type of simulation necessitates designing a packet structure which contains multiple OFDM symbols to accommodate the required acceleration. As mentioned earlier, the LFM signal is utilized for packet synchronization, however, the effect of acceleration on the chirp is not negligible with such a type of packet transmission. Therefore, the chirp also undergoes this effect in the simulation, hence it is involved in the acceleration and deceleration of the first and second packet, respectively. It should be stressed that there is an acceleration in the expansion case or in the compression, similarly for deceleration. This is illustrated in Fig. (5.6) where the uphill and downhill of the solid line mean there is a change in the direction of the velocity with time i.e., inflection point from acceleration to deceleration whereas the flat line means that the relative velocity between the transmitter and receiver is constant or zero acceleration over the duration of the packet. Likewise for the dotted line, in this case, the velocity increases towards the negative in the first packet then starts decreasing towards the positive in the second packet. Accordingly, the simulation uses two consecutive packets to imitate

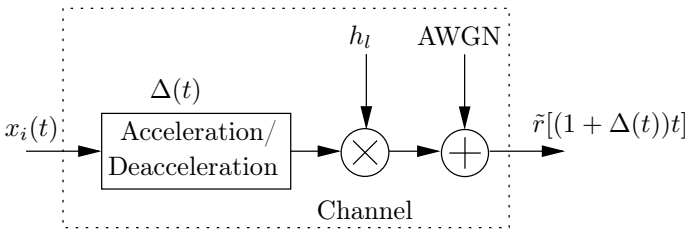

Figure 5.5: Simulation model.

the proposed system, namely packet 1 and packet 2. The first one was accelerated and the second one decelerated.

In simulating the time varying Doppler shift, the speed was assumed initially equal to zero and then the terminal speed of the packet is given as

$$\begin{aligned} V_{max}(t) &= \frac{a(t)\ L_{\text{pac}}}{f_s} \\ &= a(t) \cdot T_{\text{pac}}. \end{aligned} \tag{5.24}$$

Therefore, the associated Doppler shift at the end of the packet relative to the propagation speed can be written as

$$\Delta_{max}(t) = \frac{c - V_{max}(t)}{c}, \tag{5.25}$$

where $\Delta_{max}(t)$ represents the Doppler shift at $t = T_{pac}$. Based on the assumption that the speed is changing linearly during the packet duration, then at each sample time within the OFDM symbol, the first order Doppler shift is formulated as

$$\Delta_{step} = \frac{\Delta_{max}(t) - \Delta_0}{L_{\text{pac}}}, \tag{5.26}$$

where $t = T_{pac}$. Based on this step, the Doppler shift is speeding up until arriving at the last symbol in the first packet and then starts slowing down. It is well known that there are lots of UAC channels that have been characterized yet, however there are no standard as in the case of RF channels [99], therefore, channel A is adopted, hence the subsequent stage is convolving this time dispersion channel with the Doppler-shifted incoming signal and then adding the AWGN to investigate a

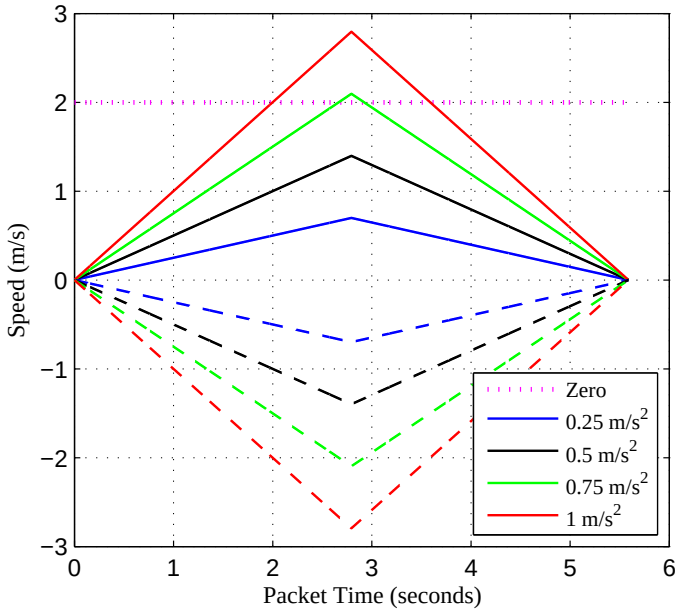

Figure 5.6: Scenarios of time-varying Doppler shift.

more realistic case.

5.3.1 System design parameters

5.3.1.1 Transmitted packet structure

The system bandwidth of 8 kHz (8 kHz- 16 kHz) is swept by a 50 ms chirp which prefixes a packet. The signal packet comprises 10 CP-OFDM frames of QPSK. The length of each QPSK OFDM frame plays an important role in controlling the performance of the Doppler shift estimation and compensation. In addition, required Doppler resolution and acceleration contribute in determining the OFDM frame and packet length, respectively.

5.3.1.2 Parameters of cyclic prefix

Due to the symmetry of the CP with its replica, there is a good correlation property of this guard interval denoted as cyclostationary because there is a cyclic convolution with the channel in the time domain. However, depending on the transmitted data, resulting envelops of the correlation peaks and their sidelobes are varied. Particularly, if the transmitted data are random, the peaks and side-lobes are variable whereas with symmetrical data (the start and end of the frame contain the same data) the peak-to-average power ratio is symmetrical. Since the Doppler is changing

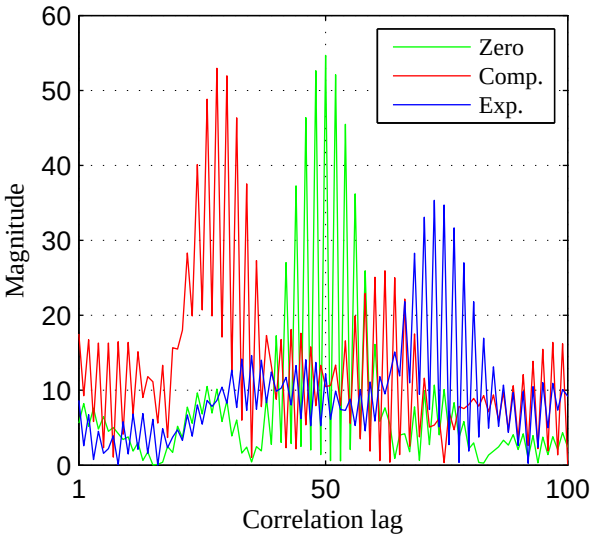

Figure 5.7: Correlation lag variation due to time scale expansion/compression at an acceleration of 1 m/s^2.

with time, there is a mismatch in the CP correlation, where the Doppler affects the first part of the CP by different amount of the second CP part. This mismatch appears in the position of the CP and this case is dealt with by searching within a specific window around the leading and trailing edge of the OFDM symbol as discussed in chapter 4. Furthermore, there is a mismatch in the length of the CP windows. To be more specific, let us assume the acceleration is 1 m/s^2 and the Doppler frequency shift at CP1 is F_d, then we expect $F_d \pm 2$Hz at CP2 when the symbol time is 0.25 s. This frequency shift is ignored relative to f_s and $N_g \cdot N_s$. Therfore, reducing the CP length could be useful in terms of its sensitivity to the Doppler shift and bandwidth.

The bandwidth of the cyclic prefix is chosen to accommodate the channel impairments and to minimize the loss of data rate. In this case, the coherence bandwidth lower bound is given as

$$B_c(\text{lower}) = \frac{N_c}{N_g}\delta f. \tag{5.27}$$

Furthermore, the BT product is subject to the required amount of gain to achieve reliable detection. A gain of (18 dB) (BT=64) was determined in accordance with the OFDM signal design to be sufficient, and therefore, the cyclic prefix is a 16 ms period.

5.3.2 Simulation results

In this section, we present the simulation results of the proposed system based on the simulation model described in Fig. (5.5). The CIR was $h(n) = 0.6708\delta(n)+0.5\delta(n-1)+0.3873\delta(n-2)+0.3162\delta(n-3)+0.2236\delta(n-4)$. In order to investigate the system performance, two scenarios are considered, acceleration (expansion) and deceleration (compression) up to 1.1 m/s^2. Fig. (5.7) shows the output of the centroid-based correlation. It can be seen in this figure that the length of the correlation window in the x-axis is 100 samples and the centre is 50 as in the case of zero Doppler shift, therefore, any drift relative to this centre due to an expansion or compression is exploited to estimate the timing offset. Fig. (5.8) shows a plot of the BERs at SNR=15 dB and a maximum delay spread of 10 ms for $N_c = 1024$. In order to assess the proposed system with the two scenarios, different accelerations and various CP lengths were used. For CP=32 or 8 ms, the system fails in all scenarios and at different accelerations. This is due to the severe ISI that introduces a delay spread greater than the CP length. However, for CP=64 and 128, the receiver achieves a satisfactory performance through all anticipated accelerations and scenarios. A clear benefit of increasing the CP length over shorter CP is in the low acceleration case. This is palpable in Fig. (5.8)(a) at $a = 0.3$ m/s^2. That means, at low accelerations we need to increase the resolution of the estimation by extending the CP length. In contrast, at higher accelerations, the impact of increasing the CP length on the performance is marginal as shown in Fig. (5.8)(b).

Fig. (5.9) shows the performance of the time varying Doppler shift compensation versus the delay spread of the channel. There was a significant reduction in the BER over a short delay spread. A possible explanation for this might be that shorter delay spread increases the certainty of the CP correlation peaks due to the increased area of the ISI free region; hence an accurate Doppler shift is obtained. Accordingly, these simulation results confirm a trade-off in the design of an OFDM frame structure between the spectral efficiency, the desired acceleration and ICI reduction. That means the guard time T_g should not only be chosen to achieve the condition $\geq \tau_{max}$, rather it should also consider what is the required maximum velocity that attain the optimal performance. Therefore, with the design parameters of $T_g = 16$ ms and $N_c = 1024$, it is verified from these simulation results that the system can attain a BER of 10^{-5} at $a = \pm 0.5$ m/s^2 and τ_{max}=5 ms.

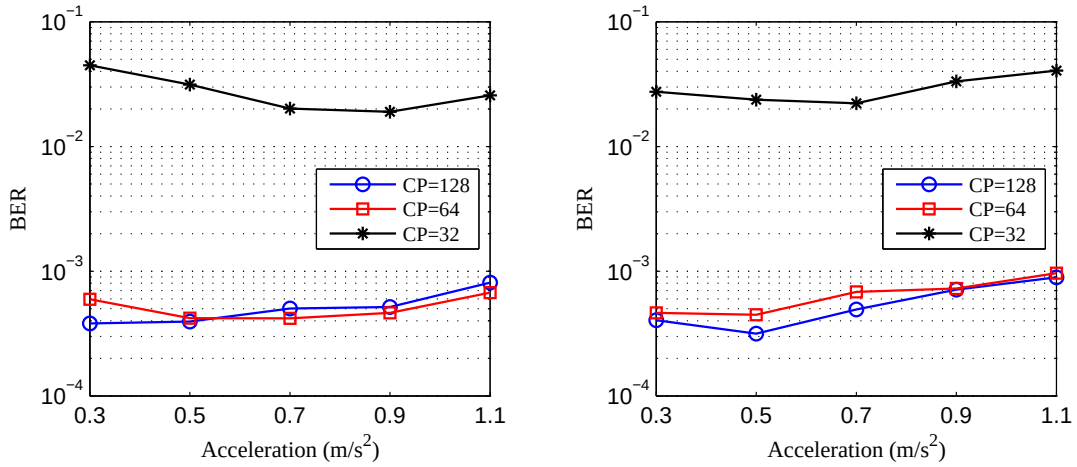

(a) Acceleration. (b) Deacceleration.

Figure 5.8: BERs performance for different acceleration and cyclic prefix lengths at SNR=15 dB, $\tau_{max} = 10$ ms, and $N_c = 1024$.

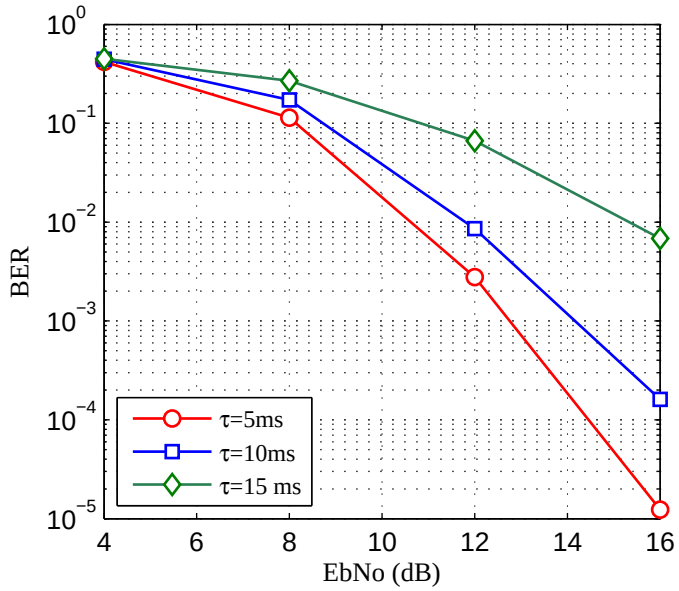

Figure 5.9: Effect of the maximum delay spread τ_{max} on the BER performance at $a = 0.5$ m/s^2 and $T_g = 16$ ms.

Fig. (5.10) depicts alternative scenarios when a higher acceleration is simulated. In order to investigate the system performance at higher acceleration, the simulation results are firstly obtained with AWGN at $a = \pm 1$ m/s^2 and then under the influence of the multipath channel. It can be shown that the performance of the proposed system in a combination of broadband time varying Doppler shift and multipath channels can achieve an acceptable performance. These results suggest that the proposed adaptive receiver can accommodate a multipath channel of τ_{max}=10

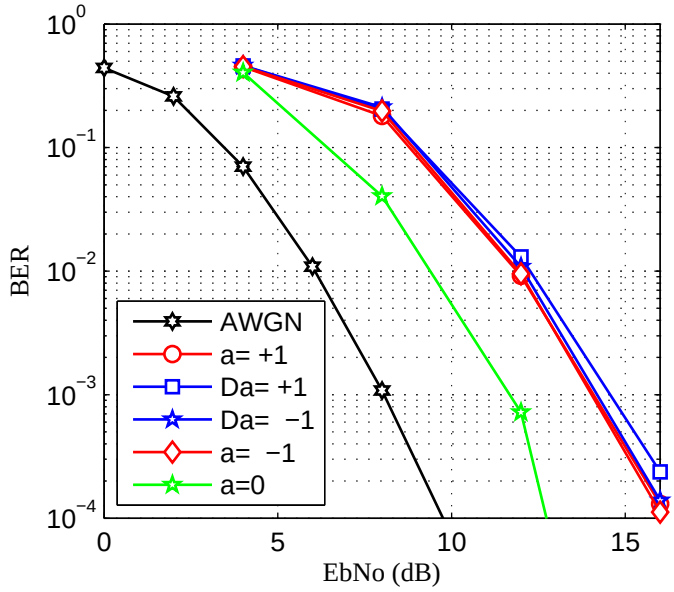

Figure 5.10: BER performance with the system parameters $T_g = 16$ ms, $N_c = 1024$ at τ_{max}=10 ms and $a = \pm 1$ m/s^2, where Da denotes deceleration case.

ms and time varying Doppler shift of $a = \pm 1$ m/s^2 in the case of expansion and compression with an acceptable BER. The maximum speed that associates this acceleration at the terminal (OFDM symbol number 10) of 272 ms packet duration is ± 2.72 m/s.

Table 5.1: Main system specifications

Parameter	**Value**
System bandwidth	4 kHz
Carrier frequency	12 kHz
Sampling frequency	48 kHz
Cosine roll-off factor	0.98
Code rate	1/2
Convolutional code polynomial	$[23, 35]_8$

5.3.3 Experimental results

5.3.3.1 Experimental setup and channel characteristics

This experiment was conducted by Newcastle University at the UK coast. The system parameters for each OFDM frame are summarized in Table 5.1. The transmission power was set at 108 dB 1μPa. It is known that in UAC, the multipath delay spread is inversly proportional to the distance between the transmitter and

receiver and the delay spread of the short range channel is usually long. Furthermore, the presence of the Doppler shift due to the transmitter/receiver pair motion increases the burden on the receiver due to the synchronization impairments' consequences. Fig. (5.11) and (5.12) show the detected channel profiles for the 100 and 500 m ranges, respectively. These figures depict the time varying CIR which is normalized to unity, the CIR of a single packet which is selected randomly and the time varying spectral before and after the BPF. The impulse response of the channels is determined by the FIR-correlator of the LFM chirp. It can be seen that the maximum delay spread is up to 11 and 6 ms, for 500 and 1000 m channel ranges respectively. However, upon a closer look to the CIR of 500 m range, it can be inferred that it is more severe as it exhibits longer delay spread and some of their paths have a comparable amplitude relative to the direct path. Consequently, synchronization impairments challenge the receiver performance, particularly, for the ZF estimator. Furthermore, in the case of 500 m range, it can be observed that the time difference of the arrival paths is quite significant; therefore, the CIR becomes larger [100]. Moreover, Fig. 5.11(c) and 5.12(c) show a visual representation of the received acoustic signal. It is noticeable throughout the spectrogram that the noise levels of the 500 m channel range are higher than the 1000 m channel range. The BPF is capable to mitigate these frequencies as shown in Fig. 5.11(d) and 5.12(d).

5.3.3.2 Performance evaluation of the proposed receiver

In addition to the simulation mentioned in the preceding section, this experiment is carried out to asses the system performance. The performance of the adaptive receiver is evaluated using the packet structure shown in Fig. (3.7) transmitted through the multipath channels described in Section 5.3.3.1. The chirp was used for the purpose of packet synchronization. This synchronization is achieved by correlating the LFM signal with its replica after the BPF. The highest correlation peak has been chosen to indicate the start of the packet. The performance of the proposed receiver is evaluated based on the criteria of the decoding BERs over 500 and 1000 m channel ranges and different OFDM data structures. CP-OFDM was used with a guard interval of $T_g = 16$ ms for each OFDM symbol. The number of sub-carriers used in the experiment were N_c =512, 1024 and 2048 with a sub-carrier spacing δf= 7.81, 3.906 and 1.9531 Hz, and OFDM symbol duration $T_u = 1/\delta f$=

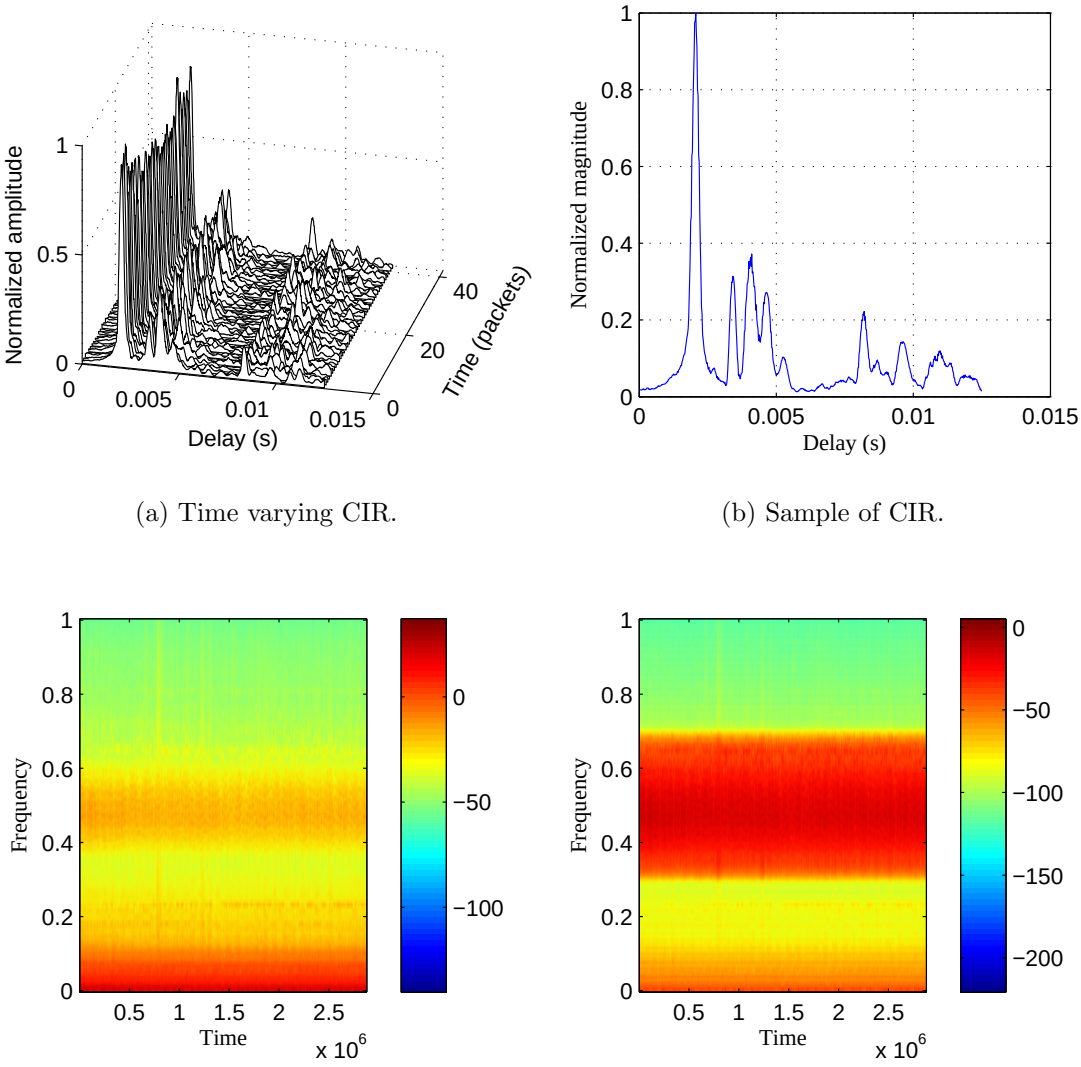

(a) Time varying CIR.

(b) Sample of CIR.

(c) Before BPF.

(d) After BPF.

Figure 5.11: Channel measurements for 1000 m range.

0.128 s, 0.256 s, and 0.512 s respectively. The code rate was 1/2 NSC and a QPSK modulation scheme was utilized. Each packet comprises respectively, 20, 10 and 5 OFDM frames N_f for N_c =512, 1024, and 2048 where the frame includes CP and OFDM symbol. The total number of information bits per packet are 8880, 8920 and 8940 for $N_c = 512$, 1024, and 2048 respectively. For $N_c = 512$, 19 packets were sent whereas 20 packets were sent for both cases of 1024 and 2048 sub-carriers. Each group of them was sent separately and at different time intervals over both channel ranges.

Fig. (5.13) presents the average BERs over each transmitted packet for 1000 m channel range and different sub-carriers spacing. It can be shown from this figure that the proposed scheme surpasses the block-based Doppler shift compensation

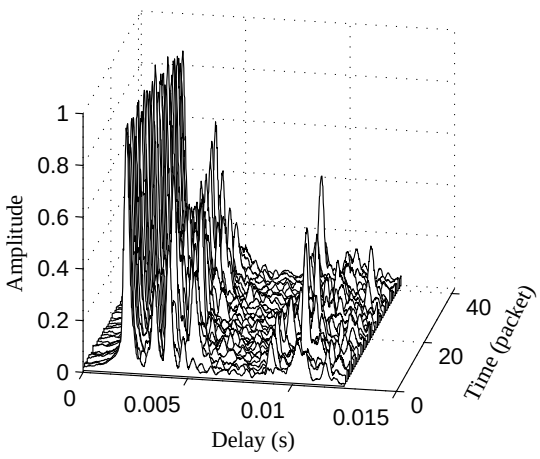

(a) Time varying CIR.

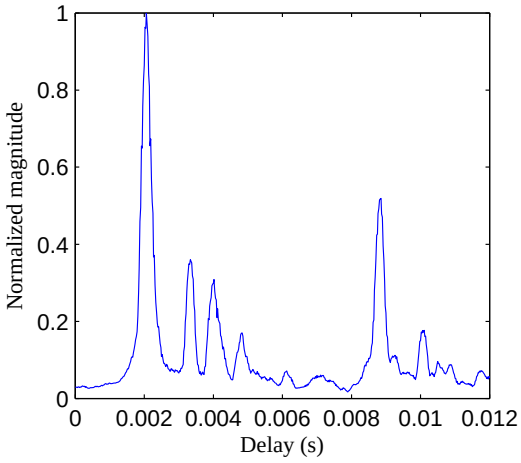

(b) Sample of CIR.

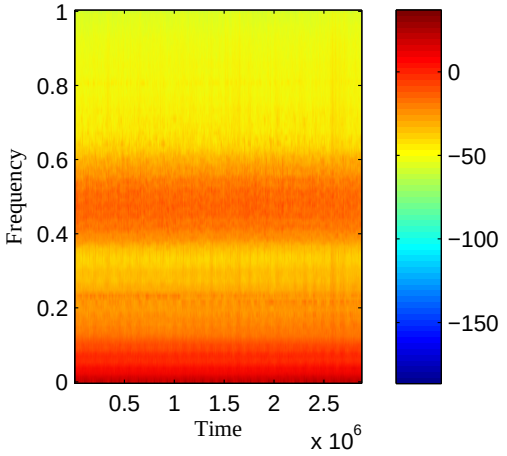

(c) Before BPF.

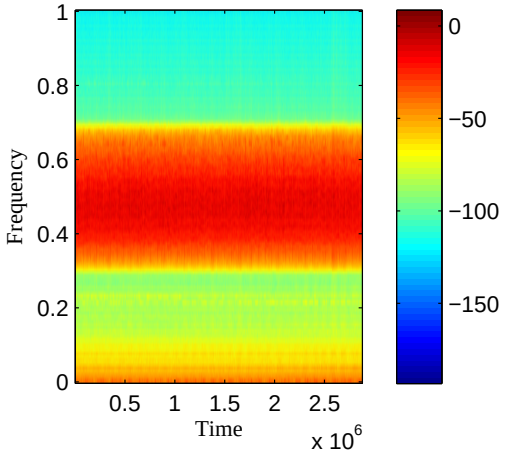

(d) After BPF.

Figure 5.12: Channel measurements for 500 m range.

in approximately all received packets. In total, 2 out of 20 packets have decoding errors in the case of 1000 m channel range and 1024 sub-carriers as shown in Fig. (5.13)(a). The number of errors in these packets were marginal and contributed by OFDM symbol number 2 and 6 of packets 8 and 19, respectively. This result is very encouraging, especially with 1000 m range and the consequences of the associated transmission loss. On the other hand, for 512 sub-carriers, 3 out of 19 packets have decoding errors as shown in Fig. (5.13)(b). This is an expected result, where the immunity of the OFDM sub-carriers against the ISI are proportional to the OFDM symbol length while the sensitivity to the Doppler shift is increased with symbol time.

Fig. (5.13)(c) presents the BER performance comparison of the proposed system

technique with a block-based approach for long OFDM symbol times. It can be observed that 13 out of 20 packets are error-free. It is evident that the adaptive system is capable of achieving satisfactory performance despite its tight sub-carrier bandwidth. Additionally, this result reveals that without a CFO compensation, the receiver deteriorates as in the case of a block-based method, therefore, estimating the coarse re-sampling factor is not enough to achieve reliable communication.

It can be seen in Fig. (5.13)(d), there is a recurrent high BERs in OFDM symbol index 1 for the whole transmitted packets in the case of 1000 m range and N_c =2048. The underlying reason for this case is due to the false alarm in detecting the maximum peak of the chirp signal which results in synchronization impairments. Furthermore, block error rates (BLERs) in this figure showed that the system capable of recovering the rest of the symbols within the packet and tracking the Doppler shift variations, where the errors are reduced dramatically with the packet time as shown in OFDM symbol 2 and 3. The reduction of the errors admit that the PM is working perfectly in the process of dropping the extraordinary parameters.

Turning now to the experimental evidence over 500 m channel range. Comparing the two results in the case of $N_c = 1024$ and 2048, it can be seen in Fig. (5.14) (a) and (b) that despite a significant reduction in the BERs with respect to the block-based technique, the performance of 1000 m range surpasses 500 m. These results are not surprising because it confirms that the associated ISI in a long distance is short due to the reduction in the delay spread length and vice versa. Through the effective contribution of the CP in estimating the Doppler shift, this delay spread of the channel will affect the certainty of the correlation peaks, therefore, room for CP correlation should be given. The suggestion here is to choose the CP longer than the channel dispersion time by at least 5 ms to achieve reliable communication, hence this revels a trade-off between the bandwidth efficiency and CP length. Furthermore, longer OFDM symbol time increases the immunity against the ISI, therefore, in the case of 500 m channel range and $N_c = 512$, the system fails. The aforementioned results confirm that the proposed scheme achieves near error-free transmission over 1000 m range with a sub-carriers length of $N_c = 1024$ or 512. In addition, although there is a narrow sub-carrier bandwidth, a satisfactory performance is achieved with $N_c = 2048$.

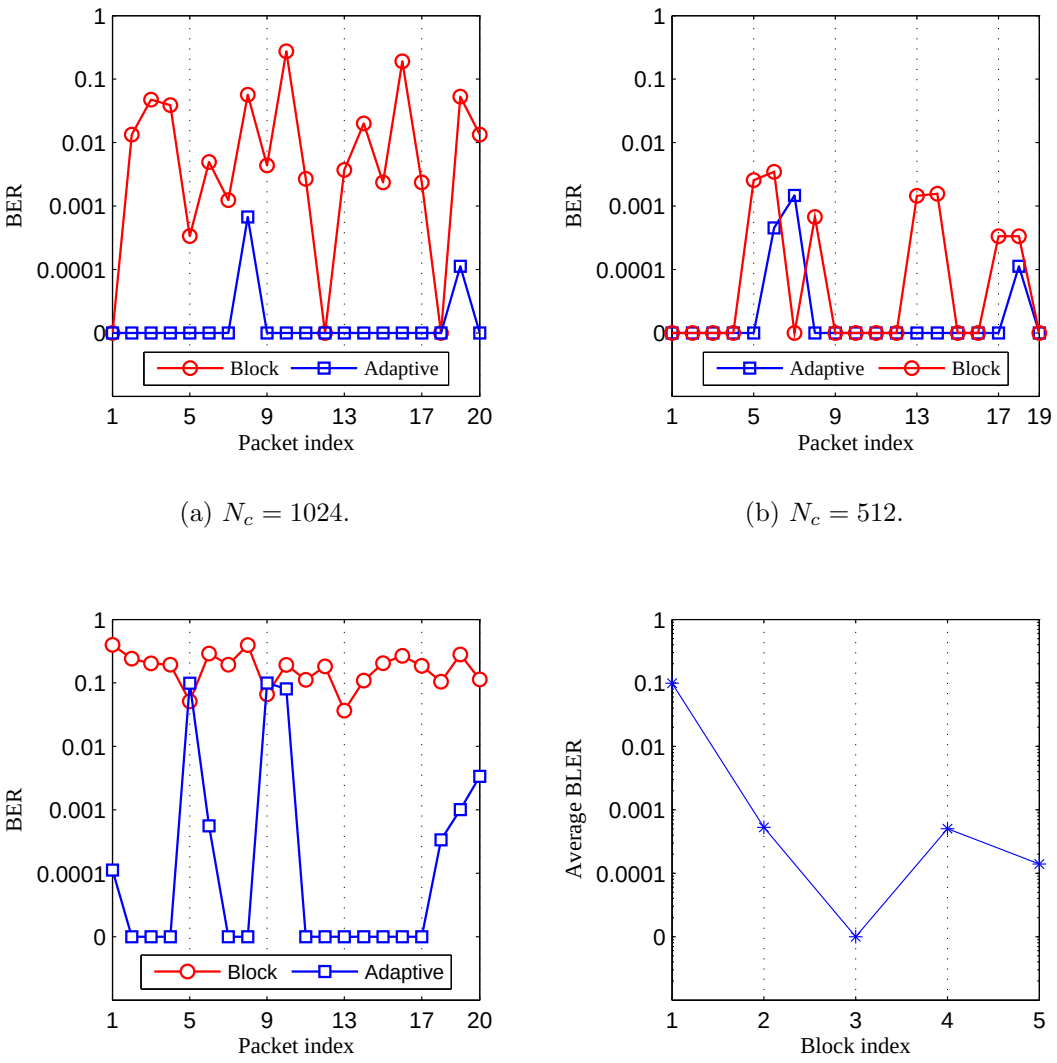

(a) $N_c = 1024$.

(b) $N_c = 512$.

(c) $N_c = 2048$.

(d) Average BER per symbol ($N_c = 2048$).

Figure 5.13: BER performance of adaptive time varying Doppler shift compensation receiver over 1000 m channel range for different sub-carriers length.

5.3.3.3 Search points, exponents and CFO range selection

The search points, exponents selection and CFO have a direct impact on the success of the receiver operation. In the search points, reducing the complexity of the receiver is crucial, and in such a case, a limited number of inner iterations is preferred. Consequently, we resort to early termination strategy in order to reduce the computation complexity. That is, the iterations are terminated once the BER of the current OFDM symbol attains zero error on the CRC output, otherwise, the receiver resumes to reach its predetermined iterations. At each iteration, two parameters are updated adaptively in accordance with the search points and the exponents. These parameters, μ_i and K_i fine tune ϕ_c and an accurate Doppler shift

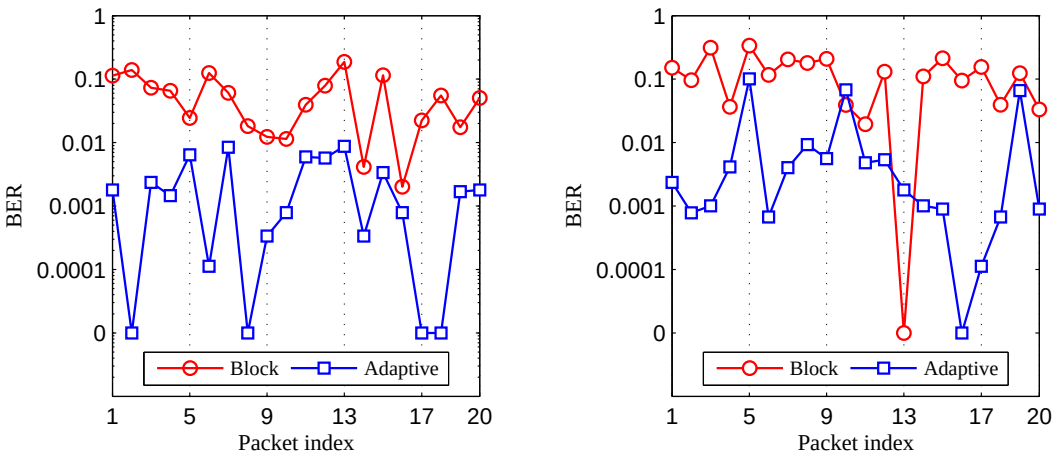

(a) $N_c = 1024$. (b) $N_c = 2048$.

Figure 5.14: BER performance of adaptive time varying Doppler shift compensation receiver over 500 m channel range for different sub-carriers length.

is obtained. Fig. (5.15)(a) demonstrates the adaptive change of the tracking parameters ϕ_c, ϕ_s, and ϕ_e of symbol index 8 of packet 6 with time. It is palpable from this figure that at the first iteration, the difference between them is big which results in a large tracking step. Accordingly, the CRC test does not indicate zero error, therefore the iterations are continuing to investigate the system with further fine tuned parameters. Obviously, the step size should be controlled to correct the values around the estimated parameters. However, as the iterations increase, the step size is diverged. This is shown in Fig. (5.15)(a), where ϕ_e starts to change its step size automatically after iteration 5.

This step size, through the use of exponents order n given in (5.9) will contribute to how large the correction term K_i at the next iteration is and will contribute ultimately to update the interpolation factor adaptively. In particular, Fig. (5.15)(b) shows two values of the exponents that have been chosen to investigate the performance of packet 6 over 1000 m channel range. In this figure, it can be seen that at $n = 2$, the system exhibits an acceleration of $\approx$1 m/s^2 due to the change of estimated speed, which is given as

$$v_r(t) = [\Delta(t) - 1] \times 1500, \tag{5.28}$$

during the symbol time that results in decoding errors in OFDM symbol 8 of packet 6 even with 10 inner iterations and 2 outer iterations. On the other hand,

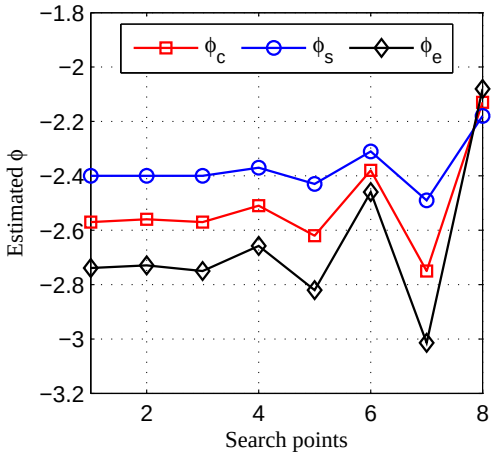

(a) Estimation of the parameter ϕ at $n = 3$.

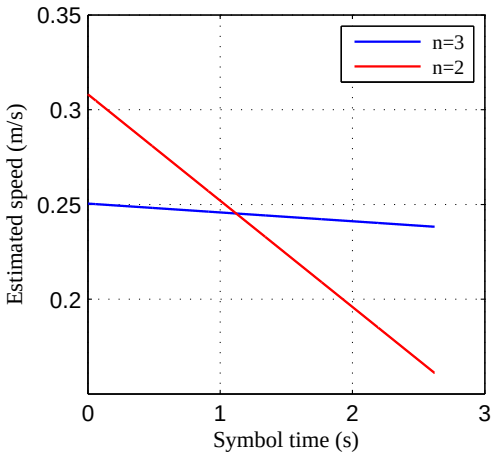

(b) Exponents effect on speed estimation of packet 6, symbol 8.

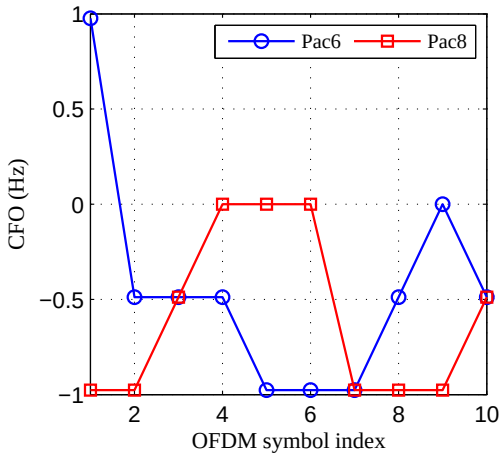

(c) CFO estimation for packets 6 and 8.

Figure 5.15: Effect of exponents on the estimation of μ_i and K_i, search points and smoothing the tracking step at $N_c = 1024$ over 1000 m channel range.

set $n = 3$ demonstrates the speed is changing very smoothly during the symbol time and the acceleration is almost zero, therefore, an evidence of the smoothness caused by the exponents order is interpreted in the resulting of zero error in packet 6 with 8 iterations as shown in Fig. (5.13)(a). It is worth mentioning that no specific rule has been adopted to choose the exponents order n in the proposed receiver. However, it has been noticed the order increases proportionally with the sub-carriers, therefore, n was set equal to 2, 3 and 4 for $N_c = 512$, 1024, and 2048, respectively. This is basically true on the assumption that it is likely the velocity changes with longer symbol time, especially with high acceleration, hence an adaptive step size is required.

The residual Doppler shift or CFO [12] destroys the orthogonality among sub-carrier frequency components. Consequently, in order to maintain the receiver performance, this CFO is estimated. As explained in Section 5.2, a range of CFO candidates are chosen based on the sub-carrier spacing for each OFDM symbol length and a CFO that results in minimum phase error is selected among the range. Starting with $\epsilon = \delta f f_c T_s = 0.25\delta f$, where $f_s = 1/T_s = 4f_c$, and for each candidate ϵ_i repeat

$$\hat{\epsilon} = \epsilon\epsilon_i, \tag{5.29}$$

where $\{\epsilon_i \in \mathbb{R} : -1 \leqslant \epsilon_i \leqslant 1\}$ for $N_c = 1024$ and 2048 and $\{\epsilon_i \in \mathbb{R} : -2 \leqslant \epsilon_i \leqslant 2\}$ for $N_c = 512$. To reduce the CFO search points, a step based on δf was employed and can be formulated as $\delta f/8$ in the case of $N_c = 1024$ and 2048, whereas the step was $\delta f/16$ for $N_c = 512$. Fig. (5.15)(c) illustrates how the CFO changes within the duration of packets 6 and 8. It can be inferred that there is no relation that governs the change in the residual Doppler shift between packet 6 and 8; the CFO changes randomly but sometimes constant. The residual Doppler shift is depending on the accuracy of estimating the re-sampling factor.

5.4 Chapter Summary

The focus of the chapter was on the Doppler effect caused by the acceleration due to the relative motion between the transmitter and receiver. This acceleration affects the correlation behaviour of the cyclic prefix and destroys the orthogonality of the sub-carriers due to the synchronization impairments. The proposed system is assessed through simulations at different scenarios and at different channel conditions to imitate the realistic case. Additionally, the suggested method is investigated with an off-line data that was recorded and processed from an experiment at the North Sea. This chapter presented a technique to tackle the effect of a broadband time varying Doppler shift in UWC. This technique adopted a *learning and punishment* approach to iteratively estimate the Doppler shift parameters. These parameters were estimated by the cooperation of a two point estimation of the normalized correlation of the first order moment in addition to the linear prediction of the speed change. This method is very robust when the relative velocity is changing linearly and capable of dealing with the velocity inflection. The suggested method is capable

of tackling an acceleration up to ± 1 m/s^2 during the packet time and correcting a speed up to 3 m/s.

Chapter 6

Conclusion and Future Work

Single carrier receivers for UWA that adopt high complexity algorithms such as beamformer achieve reliable communication over severe channel conditions. However, these types of receivers are highly complex. An alternative multicarrier receiver in the form of OFDM requires less complexity as far as real-time implementation is concerned. Furthermore, such types are attractive to combat channel impairments. This project was undertaken to design Doppler shift compensation algorithms for a single element multi-carrier receiver that would be applicable in real-time implementation and to evaluate the performance of utilizing the COFDM in the presence of this Doppler shift.

The present study, however, proposed several noteworthy contributions in order to track and compensate the time-varying Doppler shift. In order to accommodate this change, it was assumed that the speed is changing linearly within the OFDM symbol; therefore, a linear equation model was proposed to govern the first order Doppler shift. This linear prediction technique reinforces the cyclic prefix based Doppler shift estimation and an improvement in the BER was obtained. However, it was shown that as the acceleration increases, the accuracy of the Doppler shift estimation decreases, thus necessitating an advanced signal processing technique in order to tackle this challenge.

Therefore, an adaptive iterative receiver is suggested in this thesis to deal with time-varying acceleration during a period of 5.4 s. The suggested algorithm is capable of tackling the induced linear Doppler shift variation due to the acceleration and deceleration. In addition, the inflection point between them was dealt with by adopting a control range, which is derived based on the measured acceleration of

the previous two OFDM symbols and on the linearity of the speed change assumption. It has been shown through an extensive simulation and an experimental trial that the suggested algorithm is robust in the presence of a time-varying multipath channel and it can achieves an acceptable error performance.

The performance of the proposed Doppler compensation scheme was compared with a block-based technique, in both cases using a COFDM-based receiver. It was shown that the performance of the proposed receiver depends to a large extent on the delay spread of the channel and on the acceleration. The Doppler estimator accuracy affects the compensation of the residual Doppler shift which causes ICI and, in turn, affects the channel estimation, resulting in a reduction in the efficiency of decoding due to the resultant unreliable LLRs values. It was shown that weighting coefficients improve the Doppler shift estimation and accommodate the change in the speed between the OFDM symbols. The performance of the cyclic prefix correlation in estimating the Doppler shift depends on the range. Reducing the range entails increasing in the ISI and ultimately affects the correlation accuracy. Hence, adopting the weighting coefficients reduces the noise and channel effect on the Doppler shift estimation and a fine tuned re-sampling factor is obtained. The reason for the improvements is the weighting coefficients act as a smoothing filter which improves the estimation. The promising feature of the proposed receiver is its capability of delivering acceptable performance and a high data rate is achieved even with a tight sub-carrier spacing.

Although the research emphasis was to design a paradigm modem that is applicable for DSP-based real-time implementation, the effect of Doppler shift on the performance of the iterative receiver was also investigated. It is more pragmatic to consider the acceleration effects on the estimation of the Doppler shift; therefore, an adaptive compensation technique for time-varying was utilized to achieve reliable communication. It has been shown that with a linear velocity change, adopting *learning and punishment* approach provides a robust error performance. Results of simulations and experiments at various channel ranges reveal that the proposed adaptive time-varying technique is capable of tracking the Doppler shift with an acceleration range of ± 1 m/s^2 during the packet time and correcting a speed up to 3 m/s.

Future Work

It is recommended that further research be undertaken in the following areas:

1. Robust signal processing techniques are required to combat the Doppler effect at each path to deliver acceptable performance.

2. It is suggested that the association of the channel parameters is investigated in future studies, particularly the delay spread to improve predicting the Doppler shift.

3. Developing a channel model that fulfils the state of the art research in this field would be of great help in designing better algorithms.

4. Generalized deriving weighting coefficients adaptively.

5. Further experimental investigations are needed in order to consider more realistic model of the velocity with higher acceleration.

6. In the DSP-based real-time implementation, this research concentrated primarily on the decoding stage, which is represented by BCJR with iterative decoding, because it was the most restrictive in achieving on-line processing. Therefore, involving the rest of the system for the hardware implementation would be useful for future work in order to compare the multi-carrier system with a single carrier one in terms of performance and hardware implementation, where the code is written in c language.

References

[1] B. Kim and I. Lu., "Parameter study of ofdm underwater communications system," in *Proc. IEEE Oceans*, Providence, RI, Sep. 2000, pp. 1251–1255.

[2] R. J. Urick, *Principles of Underwater Sound*. McGraw-Hill, Inc., 3rd edition, 1983.

[3] L. Brekhovskikh and Y. Lysanov, *Fundamentals of Ocean Acoustics*. Springer, 1982.

[4] R. S. H. Istepanian and M. Stojanovic, *Underwater Acoustic Digital Signal Processing and Communication Systems*. Kluwer Academic Publisher, 2002.

[5] A. C. Singer, J. K. Nelson, and S. S. Kozat, "Signal processing for underwater acoustic communications," *IEEE Commun. Mag.*, vol. 47, pp. 90–96, Jan. 2009.

[6] M. Stojanovic, "Recent advances in high-speed underwater acoustic communications," *IEEE J. Ocean. Eng.*, vol. 21, pp. 125–136, Apr. 1996.

[7] ——, "Low-complexity ofdm detector for underwater channels," in *Proc. IEEE Oceans*, Sep. 2006, pp. 18–21.

[8] B. S. Sharif, J. Neasham, O. Hinton, and A. E. Adams, "A computationally efficient doppler compensation system for underwater acoustic communications," *IEEE J. Ocean. Eng.*, vol. 25, No. 1, pp. 52–61, Jan. 2000.

[9] J. G. Proakis, *Digital Communications*. McGraw Hill, Fifth edition, 2008.

[10] J. A. Neasham *et al.*, "Combined equalization and beamforming to achieve 20 kbits/s acoustic telemetry for rov's," in *Proc. IEEE Oceans*, Oct 1993, pp. 988–993.

[11] B. S. Sharif, J. Neasham, O. Hinton, A. E. Adams, and J. Davies, "Adaptive doppler compensation for coherent acoustic communication," *IEE Proceedings of Radar, Sonar and Navig.*, vol. 147, No. 1, pp. 239–246, Oct. 2000.

[12] B. Li, S. Zhou, M. Stojanovic, L. Freitag, and P.Willett, "Multicarrier communication over underwater acoustic channels with nonuniform doppler shifts," *IEEE J. Ocean. Eng.*, vol. 32, No.(2), pp. 198–209, 2008.

[13] S.Mason, C.Berger, S. Zhou, and P. Willett, "Detection, synchronization, and doppler scale estimation with multicarrier waveforms in underwater acoustic communication," *IEEE Journal on Selected Area on Communications*, vol. 26, No.(9), pp. 1638–1649, Dec. 2008.

[14] J. van de Beek, M. Sandell, and P. Borjesson, "Ml estimation of time and frequency offset in ofdm systems," *IEEE Transactions on Signal Processing*, vol. 45, No. 7, pp. 1800–1805, Jul. 1997.

[15] T. Kang and R. Iltis, "Fast-varying doppler compensation for underwater acoustic ofdm systems," in *Proc. IEEE Asilomar Conf. on Signals, Systems and Computers*, 2008, pp. 933 – 937.

[16] J. Armstrong, "Analysis of new and existing methods of reducing intercarrier interference due to carrier frequency offset in ofdm," *IEEE Trans. Comm.*, vol. 47, pp. 365– 369, mar. 1999.

[17] S. Ahmed and H. Arslan, "Estimation and compensation of doppler effect using variable sub-carrier spacing in multiband uac ofdm systems," in *Proc. IEEE Oceans*, Sep. 2010, pp. 1–4.

[18] A. B. Salberg and A. Swami, "Doppler and frequency-offset synchronization in wideband ofdm," vol. 4(6), pp. 2870–2881, Nov. 2005.

[19] A. Y. Kibangou, C. Siclet, and L. Ros, "Joint channel and doppler estimation for multicarrier underwater communications," in *Proc. IEEE ICASSP*, MARCH 2010, pp. 5630–5633.

[20] P. et. al, "Symbol by symbol doppler rate estimation for highly mobile underwater ofdm," in *Proc. WUWNET*, Nov. 2009.

[21] S. Yerramalli and U. Mitra, "Optimal resampling of ofdm signals for multiscale multilag underwater acoustic channels," *IEEE J. Ocean. Eng.*, vol. 36, No.(1), pp. 126–138, Jan. 2011.

[22] G. S. Howe, P. D. Tarbit, O. Hinton, B. S. Sharif, and A. E. Adams, "Sub-sea acoustic remote communications utilising an adaptive receiving beamformer for multipath suppression," in *Proc. IEEE Oceans*, 1994, pp. 313–316.

[23] C. P. Shah, C. C. Tsimenidis, B. S. Sharif, and J. A. Neasham, "Low complexity iterative receiver design for shallow water acoustic channels," *EURASIP Journal on Advances in Signal Processing*, vol. 2010, Article ID 590458,13 pages, 2010.

[24] M. Stojanovic, J. Catipovic, and J. Proakis, "Phase-coherent digital communication for underwater acoustic channels," *IEEE J. Ocean. Eng.*, vol. 19, pp. 100–111, Jan. 1994.

[25] M. Johnson, D. Herold, and J. Catipovic, "The design and performance of a compact underwater acoustic network node," in *Proc. IEEE Oceans*, 1994, pp. 467–471.

[26] M. Stojanovic and L. Freitag, "Multichannel detection for wideband underwater acoustic cdma communications," *IEEE J. Ocean. Eng.*, vol. 31, No.(3), pp. 685– 695, 2006.

[27] M. Stojanovic, "Design and capacity analysis of cellular-type underwater acoustic networks," *IEEE J. Ocean. Eng.*, vol. 33, No.(2), pp. 171– 181, 2008.

[28] L. Linton, P. Conder, and M. Faulkner, "Multiuser communication for underwater acoustic networks using mimo-ofdm-idma," in *Proc. International Conference on signal Processing and Communication systems ICSPCS*, Dec. 2008, pp. 1–8.

[29] J. H. Z. Yan and C. He, "Implementation of an ofdm underwater acoustic communication system on an underwater vehicle with multiprocessor structure," *Frontiers of Electrical and Electronic Engineering, China*, vol. 2, No. 2, pp. 151 – 155, Jan. 2007.

[30] M.R.Solaimani, Y. Gao, and U. Vilaipornsawai, *Turbo Coding for satellite and wireless Communications*. Springer, 2002.

[31] L. Kaizhuo, Y. Zhenhua, H. Jing, and H. Jianguo, "Design and implementation of underwater ofdm acoustic communication transmitter," in *ICALIP*, July 2008, pp. 609 – 613.

[32] R.Kothandaraman and M. Lopez, "An efficient implementation of turbo decoding on adi tigersharc ts201 dsp," in *IEEE SPCOM International Conference*, 2004, pp. 344– 348.

[33] H. Yan, S. Zhou, Z. Shi, and B. Li, "A dsp implementation of ofdm acoustic modem," in *Proc. WUWNet*, September 14 2007.

[34] H. Yan, L. Wan, S. Zhou, Z. Shi, J. Cui, J. Huang, and H. Zho, "Dsp based receiver implementation for ofdm acoustic modems," *Elsevier Journal on Physical Communication*, vol. 5, No. 1, pp. 22 – 32, Sep. 2011.

[35] H. Yan, S. Zhou, Z. Shi, J. Cui, L. Wan, J. Huang, and H. Zho, "Dsp implementation of siso and mimo ofdm acoustic modem," in *Proc. IEEEOcean*, May 2010.

[36] K. Zhong, S. Q. Swee, A. K. Tiong, and A. T. Bien, "A real-time coded ofdm acoustic modem in very shallow underwater communications," in *Proc. IEEE Oceans*, Asia-Pacific, May 2007, pp. 1 – 5.

[37] S. M. Kuo and B. H. Lee, *Real-time digital signal processing implementations, applications and experiments with the TMS320C55X*. John wiley and sons, LTD, 2001.

[38] J. G. Proakis, "Coded modulation for digital communications over rayleigh fading channels," *IEEE J. Ocean. Eng.*, vol. 16, pp. 66–73, Jan. 1991.

[39] G. Ungerboeck, "Channel coding with multi-level/phase signals," *IEEE Trans. Inf. Theory*, vol. 28, pp. 55–67, Jan. 1982.

[40] D. Divsalar and M. K. Simon, "The design of trellis coded mpsk for fading channels: performance criteria," *IEEE Trans. Commun.*, vol. 36, pp. 1004–1012, Sep. 1988.

[41] E. Zehavi, "8-psk trellis codes for a rayleigh fading channel," *IEEE Trans. Commun.*, vol. 40, pp. 873–883, May 1992.

[42] E. M. Sozer, J. G. Proakis, and F. Blackmon, "Iterative equalization and decoding techniques for shallow water acoustic channels," in *Proc. IEEE Oceans*, Nov. 2004, pp. 2201–2208.

[43] S. L. Goff, A. Glavieux, and C. Berrou, "Turbo codes and high spectral efficiency modulation," in *Proc. IEEE ICC*, New Orleans, LA, May 1994, pp. 645–649.

[44] S. L. Goff, K. B. Kien, C. C. Tsimenidis, and B. S. Sharif, "Constellation shaping for bandwidth-efficient turbo-coded modulation with iterative receiver," *IEEE Wireless Communications*, vol. 6, pp. 2223–2233, June 2007.

[45] F. Schreckenbach, N. Gortz, J. Hagenauer, and G. Bauch, "Optimized symbol mappings for bit-interleaved coded modulation with iterative decoding," in *Proc. IEEE Globecom Conference*, Dec. 2003, pp. 3316–3320.

[46] X. Li, A. Chindapol, and J. A. Ritcey, "Bit-interleaved coded modulation with iterative decoding and 8 psk signalling," *IEEE Transactions on Communication*, vol. 50, No.(5), pp. 1250–1257, Aug. 2002.

[47] K. Pelekanakis, "Exploiting space-time-frequency diversity with mimo-ofdm for underwater acoustic communications," *IEEE J. Ocean. Eng.*, vol. 36, No.(4), pp. 502–513, Oct. 2011.

[48] T. Jiang and Y. Wu, "An overview: peak-to-average power ratio techniques for ofdm signals," *IEEE Transactions on Broadcasting*, vol. 54, No. 2, pp. 257–268, June 2008.

[49] S. Han and J. Lee, "An overview of peak-to-average power ratio reduction techniques for multicarrier tranmission," *IEEE Wireless Communications*, vol. 12, No. 2, pp. 56–65, Feb. 2005.

[50] R. W. Bauml, R. F. H. Fisher, and J. B. Huber, "Reducing the peak-to-average power ratio of multicarrier modulation by selected mapping," *Electronic Letter*, vol. 32, No. 22, pp. 2056–2057, 1996.

[51] A. Devices, "Digital pulse-shaping filter basics AN-922," Jun. 2009. [Online]. Available: http://www.analog.com/en/processors-dsp/sharc/processors/application-notes/resources/index.html

[52] P. Tan and B. N.C, "A novel pulse-shaping for reduced ici in ofdm systems," in *Proc. IEEE VTC*, Sep. 2004, pp. 456 – 459.

[53] B. Muquet, Z. Wang, G. Giannakis, and M. Courville, "Cyclic prefixing or zero padding for wireless multicarrier transmission?" *IEEE Transactions on Communications*, vol. 50, pp. 2136–2148, Dec. 2002.

[54] A. Peled and A. Ruiz, "Frequency domain data transmission using reduced computational complexity algorithms," in *Proc. IEEE ICASSP*, 1980, pp. 964–967.

[55] W. S. Burdic, *Underwater Acoustic System Analysis*. Prentice Hall, 1991.

[56] J. A. Catipovic, "Performance limitations in underwater acoustic telemetry," *IEEE J. Ocean. Eng.*, vol. 15, pp. 205–216, 1990.

[57] R. F. W. Coates, *Underwater acoustic systems*. Macmillan, 1990.

[58] F. Hlawatsch and G. Matz, *Wireless Communications Over Rapidly Time-Varying Channels*. Elsevier Ltd., 2011.

[59] A. F. Molisch, *Wireless Communications*. John Wiley, 2005.

[60] G. Caire, G. Taricco, and E. Biglieri, "Bit-interleaved coded modulation," *IEEE Trans. Inf. Theory*, vol. 44, pp. 927–946, May 1998.

[61] A. Goldsmith, *Wireless Communications*. Cambridge University Press, 2005.

[62] X. Li and J. A. Ritcey, "Bit-interleaved coded modulation with iterative decoding," *IEEE Commun. Lett.*, vol. 1, pp. 169–171, Nov. 1997.

[63] A. Chindapol and J. A. Ritcey, "Design, analysis, and performance evaluation for bicm-id with square qam constellations in rayleigh fading channels," *IEEE J. Sel. Areas Commun.*, vol. 19, pp. 944–957, May 2001.

[64] X. Li and J. A. Ritcey, "Trellis-coded modulation with bit interleaving and iterative decoding," *IEEE Journal on Selected Area on Communications*, vol. 17, pp. 715–724, Apr. 1999.

[65] ——, "A soft-input soft-output app module for iterative decoding of concatenated code," *Electronic Letter*, vol. 34, pp. 942–943, May 1998.

[66] L. Hanzo, C. H. Wong, and M. S. Yee, *Adaptive Wireless Transceivers: Turbo-Coded, Turbo-Equalized and Space-Time Coded TDMA, CDMA, and OFDM Systems*. Wiley-IEEE Press, 2002.

[67] S. ten Brink, J. Speidel, and R. Yan, "Iterative demapping and decoding for multilevel modulation," in *Proc. IEEE Globecom Conference*, Nov. 1998, pp. 579–584.

[68] L. Bahl, J. Cocke, F. Jelinek, and J. Raviv, "Optimal decoding of linear codes for minimizing symbol error rate," *IEEE Trans. Inf. Theory*, vol. 20, pp. 284–287, Mar. 1974.

[69] J. P. Woodard and L. Hanzo, "Comparative study of turbo decoding techniques: An overview," *IEEE Journal on Vehicular Technology*, vol. 49, pp. 2208–2233, Nov. 2000.

[70] H. Malepati, *Digital media processing DSP algorithms using c*. Elsevier Ltd., 2010.

[71] B. Sklar, *Digital communications Fundamentals and Applications*. Prentice Hall P T R, Second edition, 2001.

[72] A. S. Alvarado, L. Agrell, and E. Svensson, "On bicm-id with multiple interleavers," in *14th European Wireless Conf.*, Sep. 2010.

[73] X. Zou, M. Wang, and G. Feng, "A new interleaver design for iteratively decoded bit-interleaved coded modulation," *IJSC*, vol. 3, pp. 338–343, 2008.

[74] S. Smith, *The Scientest and Engineer's Guide to Digital Signal Processing*. Analog Device, 1998.

[75] W. H. Park, M. H. Sunwoo, and S. K. Oh, "Efficient dsp architecture for viterbi decoding with small trace back latency." *IEICE Transactions*.

[76] P. Lapsley and G. Blalock, "How to estimate dsp processor performance," *IEEE Spectrum Magazine*, vol. 33, No. 7, pp. 74–78, Jul. 19962.

[77] T. Pollet, P. Spruyt, and M. Moeneclaey, "The ber performance of ofdm systems using non-synchronized sampling," in *Proc. IEEE Globecom Conference*, 1994, pp. 253–257.

[78] J. B. et al., "Weighted centroid localization in zigbee-based sensor networks," in *IEEE WISP*, 2007, pp. 1–6.

[79] F. Reichenbach and D. Timmermann, "Indoor localization with low complexity in wireless sensor networks," in *Proc. IEEE International Conf.Industrial Informatics*, Aug. 2006, pp. 1018–1023.

[80] A. Jadbabaie, J. Lin, and A. Morse, "Coordination of groups of mobile autonomous agents using nearest neighbor rules," *IEEE Transactions on Automatic Control*, vol. 48, No. 6, pp. 988–1001, June 2003.

[81] F. S. Cattivelli, C. Lopes, and A. H. Sayed, "Diffusion recursive least-squares for distributed estimation over adaptive networks," *IEEE Transactions on Signal Processing*, vol. 56, No. 5, pp. 1865– 1877, May 2008.

[82] B. Li, S. Zhou, J. Huang, and P. Willett, "Scalable ofdm design for underwater acoustic communications," in *Proc. IEEE ICASSP*, Las Vegas, 2008, pp. 5304–5307.

[83] A. Devices, "Adsp-21364 ez-kit lite evaluation system manual," Jul. 2007. [Online]. Available: http://www.analog.com

[84] Y. Or, G. Kutz, A. Chass, A. Gubeskys, and E. Pollak, "Iterative decoding algorithms for real time software implementation in wireless communication systems," in *IEEE Conf., VTS*, Jun. 2001, pp. 1884–1888.

[85] B. Li, S. Zhou, M. Stojanovic, L. Freitag, and P. Willett, "Non-uniform doppler compensation for zero-padded ofdm over fast-varying underwater acoustic channels," in *Proc. IEEE Ocean*, Aberdeen, 2007, pp. 1–6.

[86] M. Speth, S. Fechtel, G. Fock, and H. Meyr, "Optimum receiver design for wireless broad-band systems using ofdm-part ii," *IEEE Trans. Comm.*, vol. 49(4), pp. 571–578, 2001.

[87] B. Yang, K. B. Letaief, R. Cheng, and Z. Cao, "Timing recovery for ofdm transmission," *IEEE SA. Comm.*, vol. 49, pp. 467–479, Nov. 2000.

[88] M. K. Ozdemir, L. B. wireless solutions INC., and H. Arslan, "Channel estimation for wireless ofdm systems," *IEEE Comm. surveys*, vol. 9, No. 2, 2nd quarter 2007.

[89] V. de Beek, J. J., O. Edfords, and M. Sandell, "On channel estimation in ofdm system," in *Proc. IEEE VTC*, 1995, pp. 815–819.

[90] S. Coleri, M. Ergen, A. Puri, and A. Bahai, "Channel estimation techniques based on pilot arrangement in ofdm systems," *IEEE Transactions on Broadcasting*, vol. 48, No. 3, pp. 223–229, Sep. 2002.

[91] M. Hsieh and C. Wei, "Channel estimation for ofdm systems based on comb-type pilot arrangement in frequency selective fading channels," *IEEE Transactions on Consumer Electronic*, vol. 44, pp. 217–225, Feb. 1998.

[92] C. P. Shah, C. C. Tsimenidis, B. S. Sharif, and J. A. Neasham, "Low-complexity iterative receiver structure for time-varying frequency-selective shallow underwater acoustic channels using bicm- id:design and experimental results," *IEEE J. Ocean. Eng.*, vol. 36, pp. 406–421, 2011.

[93] A. E. Abdelkareem, B. S. Sharif, C. C. Tsimenidis, J. A. Neasham, and O. Hinton, "Low-complexity doppler compensation for ofdm-based underwater acoustic communication systems," in *Proc. IEEE Oceans*, Jun. 2011, pp. 1–6.

[94] A. E. Abdelkareem, B. S. Sharif, C. C. Tsimenidis, and J. A. Neasham, "Time varying doppler-shift compensation for ofdm-based shallow underwater acoustic communication systems," in *Proc. IEEE MASS*, Oct. 2011, pp. 885–891.

[95] S. K. Mitra, *Digital signal processing A computer based approach.* McGraw-Hill, 3rd edition,2006.

[96] A. H. Sayed, *Adaptive Filters.* Wiley-IEEE Press, 2008.

[97] M. Abramowitz and I. A. Stegun, *Handbook of Mathematical Functions with Formulas, Graphs, and Mathematical Tables.* New York: Dover,, 1972.

[98] W. Kim and D. C. Cox, "Residual frequency offset and phase compensation for ofdm systems," in *Proc. IEEE VTC*, 2007, pp. 2209–2213.

[99] R. Otnes, T. Jenserud, J. E. Voldhaug, and C. Solberg, "A roadmap to ubiquitous underwater acoustic communications and networking," in *3rd UAM: Technologies and Results*, Nafplion, Greece, Jun. 2009.

[100] A. Zielinski, Y. H. Yoon, and L. Wu, "Performance analysis of digital acoustic communication in a shallow water channel," *IEEE J. Ocean. Eng.*, vol. 20, pp. 293–299, Oct. 1995.